

**HOPF BIFURCATIONS IN A POWER SYSTEM SUSCEPTIBLE TO
SUBSYNCHRONOUS RESONANCE AND A NOVEL CONTROLLER
FOR DAMPING TORSIONAL OSCILLATIONS**

**Ph.D. Thesis by
Yaşar KÜÇÜKEFE**

Department: Electrical Engineering

Programme: Electrical Engineering

JUNE 2009

**HOPF BIFURCATIONS IN A POWER SYSTEM SUSCEPTIBLE TO
SUBSYNCHRONOUS RESONANCE AND A NOVEL CONTROLLER
FOR DAMPING TORSIONAL OSCILLATIONS**

**Ph.D. Thesis by
Yaşar KÜÇÜKEFE
(504032005)**

Date of submission : 23 October 2008

Date of defence examination: 16 June 2009

Supervisor (Chairman) : Prof. Dr. Adnan KAYPMAZ (ITU)
Members of the Examining Committee: Prof. Dr. Ömer Usta (ITU)
Assoc. Prof. Dr. Alper KONUKMAN
(GYTE)
Assoc. Prof. Dr. M. Turan SÖYLEMEZ
(ITU)
Assis. Prof. Dr. Bülent BİLİR
(Bahçeşehir Ü.)

JUNE 2009

İSTANBUL TEKNİK ÜNİVERSİTESİ ★ FEN BİLİMLERİ ENSTİTÜSÜ

**SENKRONALTI REZONANSA DUYARLI BİR GÜÇ SİSTEMİNDE
HOPF ÇATALLANMALARI VE BURULMA SALINIMLARININ
SÖNÜMLENDİRİLMESİ İÇİN YENİ BİR KONTROLÖR**

**DOKTORA TEZİ
Yaşar KÜÇÜKEFE
(504032005)**

Tezin Enstitüye Verildiği Tarih : 23 Ekim 2008

Tezin Savunulduğu Tarih : 16 Haziran 2009

**Tez Danışmanı : Prof. Dr. Adnan KAYPMAN (İTÜ)
Diğer Jüri Üyeleri : Prof. Dr. Ömer USTA (İTÜ)
Doç. Dr. Alper KONUKMAN (GYTE)
Doç. Dr. M. Turan SÖYLEMEZ (İTÜ)
Yrd. Doç. Dr. Bülent BİLİR
(Bahçeşehir Ü.)**

HAZİRAN 2009

FOREWORD

Firstly, I would like to thank my advisor Prof. Dr. Adnan Kaypmaz for his continuous support and guidance throughout my Ph.D. program. I am grateful to my wife, Bige, my daughter, Elif, and my son, Ufuk, for their patience and understanding. I'm indebted to Assis. Prof. Dr. İstemihan Genç for his valuable contributions. I also thank my colleagues Musa Tüfekci and Turgut Güçyener for their encouragement. Finally, I would like to express my gratitude to Serdar Tüfekçi, Neil Cave and Jim Haggan.

June 2009

Yaşar KÜÇÜKEFE

TABLE OF CONTENTS

| | <u>Page</u> |
|---|-------------|
| TABLE OF CONTENTS | v |
| ABBREVIATIONS | vii |
| LIST OF TABLES | ix |
| LIST OF FIGURES | xi |
| LIST OF SYMBOLS | xiii |
| SUMMARY | xv |
| ÖZET | xvii |
| 1. INTRODUCTION | 1 |
| 1.1 Statement of the Problem | 1 |
| 1.2 Objectives of the Dissertation | 2 |
| 1.3 Literature Review | 3 |
| 1.4 Outline of the Dissertation | 7 |
| 2. REVIEW OF BIFURCATION THEORY | 9 |
| 2.1 Stability of Equilibrium Solutions..... | 9 |
| 2.2 Bifurcation Mechanisms | 10 |
| 2.3 Hopf Bifurcation | 10 |
| 2.3.1 Subcritical Hopf Bifurcation | 11 |
| 2.3.2 Supercritical Hopf Bifurcation | 12 |
| 2.4 Center Manifold Theorem | 13 |
| 2.5 Lyapunov Coefficients | 13 |
| 2.5.1 The First Lyapunov Coefficient | 14 |
| 2.5.2 The Second Lyapunov Coefficient..... | 15 |
| 2.6 Torus Bifurcation | 16 |
| 3. SYSTEM DESCRIPTION AND MODELING | 19 |
| 3.1 Electrical System..... | 19 |
| 3.1.1 Electrical System d-axis Equivalent Circuit | 21 |
| 3.1.2 Electrical System q-axis Equivalent Circuit | 22 |
| 3.1.3 Electrical System State Equations..... | 22 |
| 3.2 Mechanical System | 23 |
| 3.3 Complete Mathematical Model..... | 25 |
| 3.4 Bifurcation Analysis..... | 26 |
| 3.4.1 Equilibrium Solutions | 26 |
| 3.4.2 Stability of the Equilibrium Points..... | 27 |
| 3.4.3 Oscillatory Modes | 28 |
| 3.5 Time Domain Simulations | 33 |
| 3.6 Parameter Dependency of the First Lyapunov Coefficient..... | 38 |
| 4. SSR WITH AUTOMATIC VOLTAGE REGULATOR | 43 |
| 4.1 Excitation System with AVR | 43 |
| 4.2 Complete Mathematical Model with AVR | 44 |
| 4.3 Bifurcation Analysis..... | 45 |

| | | |
|-----------|--|-----------|
| 4.3.1 | Equilibrium Solutions | 45 |
| 4.3.2 | Stability of Equilibrium Solutions in SMIB Power System with AVR... .. | 46 |
| 4.3.3 | Oscillatory Modes | 46 |
| 4.3.4 | Time Domain Simulations | 49 |
| 4.3.5 | Impact of the AVR Gain on $I_f(0)$ | 52 |
| 5. | DELAYED FEEDBACK CONTROLLER..... | 55 |
| 5.1 | Delayed Feedback Controller | 55 |
| 5.2 | The DFC Performance | 56 |
| 5.3 | Optimization of the DFC Parameters | 62 |
| 5.4 | DFC Performance at Different Operating Conditions..... | 67 |
| 5.4.1 | DFC Optimum Time Delay Depending on the Loading Level..... | 67 |
| 5.4.2 | DFC Optimum Time Delay Depending on the AVR Reference Voltage | 69 |
| 6. | THE EFFECT OF LIMITERS ON THE DFC PERFORMANCE | 73 |
| 6.1 | AVR and DFC with Limiters | 73 |
| 6.2 | The DFC Performance with Limiters..... | 74 |
| 7. | CONCLUSION..... | 81 |
| | REFERENCES..... | 85 |
| | APPENDICES | 91 |
| | CURRICULUM VITAE..... | 95 |

ABBREVIATIONS

| | |
|-------------|---|
| AVR | : Automatic Voltage Regulator |
| D | : Damping Coefficient |
| DFC | : Delayed Feedback Controller |
| EMTP | : Electromagnetic Transient Program |
| FACT | : Flexible AC Transmission |
| FBM | : First Benchmark Model |
| GH | : Generalized Hopf Bifurcation |
| HP | : High Pressure |
| IEEE | : Institute of Electrical and Electronics Engineers |
| IGE | : Induction Generator Effect |
| IP | : Intermediate Pressure |
| J | : Jacobian Matrix |
| K | : Stiffness Coefficient |
| LP | : Low Pressure |
| M | : Moment of Inertia |
| ODE | : Ordinary Differential Equation |
| PSD | : Power Spectral Density |
| PSS | : Power System Stabilizer |
| SBM | : Second Benchmark Model |
| SMES | : Superconducting Magnetic Storage |
| SMIB | : Single Machine Infinite Busbar |
| SSR | : Subsynchronous Resonance |
| TDAS | : Time Delay Auto-Synchronization |
| TIE | : Torsional Interaction Effect |
| TTE | : Transient Torque Effect |
| UPO | : Unstable Periodic Orbit |

LIST OF TABLES

| | <u>Page</u> |
|---|-------------|
| Table 3.1: Computed Eigenvalues for $\mu=0.5184$ and $\mu=0.7283$ | 32 |
| Table 3.2: Complex vectors p and q for $\mu=0.5184$ and $\mu=0.7283$ | 32 |
| Table 4.1: Computed Eigenvalues for $\mu=0.5197$ and $\mu=0.7345$ | 48 |
| Table 4.2: Complex vectors p and q for $\mu=0.5197$ and $\mu=0.7345$ | 49 |

LIST OF FIGURES

| | <u>Page</u> |
|---|-------------|
| Figure 2.1 : Subcritical Hopf Bifurcation | 11 |
| Figure 2.2 : Supercritical Hopf bifurcation..... | 12 |
| Figure 2.3 : Real part of imaginary eigenvalues w.r.t. λ ($\lambda_H=1.684$)..... | 16 |
| Figure 2.4 : Three dimensional projection for $\lambda=1.85$ (Supercritical Hopf)..... | 17 |
| Figure 2.5 : Three dimensional projection for $\lambda=2.02$ (Torus bifurcation) | 17 |
| Figure 3.1 : The SMIB power system (System-1, IEEE SBM for SSR studies) | 19 |
| Figure 3.2 : Equivalent Impedance (Z_{eq}) w.r.t. the compensation factor (μ)..... | 20 |
| Figure 3.3 : Electrical system d-axis equivalent circuit..... | 21 |
| Figure 3.4 : Electrical system q-axis equivalent circuit..... | 22 |
| Figure 3.5 : Schematic diagram of the mechanical system..... | 23 |
| Figure 3.6 : Generator rotor angle ($T_m=0.91$, $Efd=2.2$ and $V_0=1.0$)..... | 27 |
| Figure 3.7 : Relative rotational speeds (RSS) representing the mode shapes..... | 28 |
| Figure 3.8 : The flowchart for Bifurcation Analysis..... | 30 |
| Figure 3.9 : Oscillation modes of the system..... | 31 |
| Figure 3.10 : Real parts of the torsional mode eigenvalues | 31 |
| Figure 3.11 : Generator rotor speed (ωr) response ($\mu = \mu_{H1}=0.5184$)..... | 34 |
| Figure 3.12 : PSD estimation of the generator rotor speed, (a) $10s < t < 20s$ and (b) $20s < t < 30s$ | 34 |
| Figure 3.13 : Generator rotor speed (ωr) response, $\mu=0.52$ ($\mu_H=0.5184$)..... | 35 |
| Figure 3.14 : Generator load angle ($\mu=0.52$) (Subcritical Hopf bifurcation)..... | 35 |
| Figure 3.15 : Generator rotor speed response ($\mu=0.55$)..... | 36 |
| Figure 3.16 : Generator rotor speed response ($\mu=0.80$)..... | 37 |
| Figure 3.17 : Generator rotor speed response ($\mu=0.82$)..... | 37 |
| Figure 3.18 : Hopf Bifurcation points for varying values of T_m | 39 |
| Figure 3.19 : The first Lyapunov coefficients for varying values of T_m | 39 |
| Figure 3.20 : Hopf Bifurcation points for varying values of V_0 | 40 |
| Figure 3.21 : The first Lyapunov coefficients for varying values of V_0 | 40 |
| Figure 3.22 : Hopf Bifurcation points for varying values of Efd | 41 |
| Figure 3.23 : The first Lyapunov coefficients for varying values of Efd | 42 |
| Figure 4.1 : Block diagram of the excitation system with AVR..... | 43 |
| Figure 4.2 : Generator rotor angle ($T_m=0.91$, $K_A=250$, $V_0=1.0$ and $V_{ref}=1.0953$)..... | 46 |
| Figure 4.3 : Oscillation modes of the model with AVR | 47 |
| Figure 4.4 : Real parts of the torsional mode eigenvalues of the model with AVR . | 47 |
| Figure 4.5 : Generator rotor speed response ($\mu=\mu_{H1}=0.5197$) | 50 |
| Figure 4.6 : PSD of the generator rotor speed, (a) $10s < t < 20s$ and (b) $20s < t < 30s$.. | 50 |
| Figure 4.7 : Generator rotor speed ($\mu = 0.525$) (Supercritical Hopf bifurcation) | 51 |
| Figure 4.8 : Generator load angle ($\mu = 0.525$) (Supercritical Hopf bifurcation)..... | 51 |
| Figure 4.9 : Two-dimensional projections of the phase portrait onto the ωr - δr plane from $t=190s$ to $t=200s$ ($\mu = 0.525$) (Supercritical Hopf bifurcation) | 52 |
| Figure 4.10 : Variation of Hopf bifurcation point with the AVR Gain | 53 |

| | |
|---|----|
| Figure 4.11 : Variation of the first Lyapunov coefficients with AVR gain, K_A | 53 |
| Figure 5.1 : Delayed Feedback Controller (DFC)..... | 55 |
| Figure 5.2 : Excitation System with AVR and DFC..... | 56 |
| Figure 5.3 : Generator rotor speed response without the DFC ($\mu=0.55$)..... | 57 |
| Figure 5.4 : Generator rotor speed response with DFC ($\mu=0.55$, $\tau = 0.0185s$, $K_{DFC}=76$) | 57 |
| Figure 5.5 : Generator rotor speed with the DFC ($\mu=0.75$, $\tau = 0.0175s$)..... | 58 |
| Figure 5.6 : Generator rotor speed with the DFC ($\mu=0.85$, $\tau=0.0135s$)..... | 58 |
| Figure 5.7 : The DFC output ($\mu=0.55$, $\tau=0.0185s$, $K_{DFC}=76$)..... | 59 |
| Figure 5.8 : The DFC output ($\mu=0.75$, $\tau = 0.0175s$, $K_{DFC}=76$)..... | 60 |
| Figure 5.9 : The DFC output ($\mu=0.85$, $\tau = 0.0135s$, $K_{DFC}=76$)..... | 60 |
| Figure 5.10 : Generator terminal voltage with the DFC ($\mu=0.55$, $\tau=0.0185s$)..... | 61 |
| Figure 5.11 : Generator voltage with DFC ($\mu=0.75$, $\tau=0.0175s$, $K_{DFC}=76$) | 61 |
| Figure 5.12 : Generator voltage with the DFC ($\tau=0.0135s$, $K_{DFC}=76$)..... | 62 |
| Figure 5.15 : OPI vs DFC time delay. $\tau_{opt}=0.0185s$ ($\mu=0.55$, $K_{DFC}=76$) | 63 |
| Figure 5.16 : OPI vs DFC time delay. $\tau_{opt}=0.0175s$ ($\mu=0.75$, $K_{DFC}=76$) | 64 |
| Figure 5.19 : OPI vs DFC time delay. $\tau_{opt}=0.0135s$ ($\mu=0.85$, $K_{DFC}=76$) | 64 |
| Figure 5.18 : OPI vs DFC gain ($\mu=0.55$, $\tau=0.0185s$)..... | 65 |
| Figure 5.19 : OPI vs DFC gain ($\mu=0.75$, $\tau=0.0175s$)..... | 66 |
| Figure 5.20 : OPI vs DFC gain ($\mu=0.85$, $\tau=0.0135s$)..... | 66 |
| Figure 5.21 : DFC time delay optimum values ($T_m=0.91$, $V_{ref}=1.0953$, $K_{DFC}=76$) .. | 67 |
| Figure 5.22 : Generator rotor speed ($\mu=0.55$, $T_m=0.60$, $V_{ref}=1.09$, $\tau = 0.022s$)..... | 68 |
| Figure 5.23 : Generator rotor speed ($\mu=0.55$, $T_m=0.75$, $V_{ref}=1.09$, $\tau = 0.020s$)..... | 68 |
| Figure 5.24 : Generator rotor speed ($\mu=0.55$, $T_m=0.91$, $V_{ref}=1.0657$, $\tau = 0.0185s$).. | 69 |
| Figure 5.25 : Generator rotor speed ($\mu=0.55$, $V_{ref}=1.0657$, $\tau=0.0160s$, $K_{DFC}=76$)... | 70 |
| Figure 5.26 : Generator rotor speed ($\mu=0.55$, $V_{ref}=1.0657$, $\tau=0.0160s$, $K_{DFC}=45$)... | 70 |
| Figure 6.1 : AVR and DFC with limiters..... | 73 |
| Figure 6.2 : Generator rotor speed with DFC and AVR limiters ($\mu=0.55$)..... | 74 |
| Figure 6.3 : Generator rotor angle with DFC and AVR limiters ($\mu=0.55$)..... | 75 |
| Figure 6.4 : (a) DFC output, VS and (b) Regulator output, VR ($\mu=0.55$)..... | 75 |
| Figure 6.5 : (a) Exciter output, Efd and (b) Terminal voltage, Vt ($\mu=0.55$) | 76 |
| Figure 6.6 : Generator rotor speed with DFC and AVR limiters ($\mu=0.75$)..... | 77 |
| Figure 6.7 : Generator rotor angle with DFC and AVR limiters ($\mu=0.75$)..... | 77 |
| Figure 6.8 : (a) DFC output, VS and (b) Regulator output, VR ($\mu=0.75$)..... | 78 |
| Figure 6.9 : (a) Exciter output, Efd and (b) Terminal voltage, Vt ($\mu=0.75$) | 78 |
| Figure 6.10 : Generator rotor speed with DFC and AVR limiters ($\mu=0.85$)..... | 79 |
| Figure 6.11 : (a) DFC output, VS and (b) Regulator output, VR ($\mu=0.85$)..... | 80 |
| Figure 6.12 : (a) Exciter output and (b) Generator terminal voltage ($\mu=0.85$)..... | 80 |

LIST OF SYMBOLS

| | |
|-------------------|--|
| B, C | : Multilinear Vector Functions for two and three coordinates |
| D, E | : Multilinear Vector Functions for four and five coordinates |
| d | : Subscript for d-axis Quantities |
| D | : Damping Coefficient |
| e_c | : Series Capacitor Voltage |
| f | : Subscript for Field Circuit Quantities |
| i | : Current |
| J | : Jacobian Matrix |
| k | : Subscript for Generator Damper Windings Quantities |
| K | : Spring Constant |
| $l_1(\mathbf{0})$ | : The First Lyapunov Coefficient |
| $l_2(\mathbf{0})$ | : The Second Lyapunov Coefficient |
| M | : Moment of Inertia |
| q | : Subscript for q-axis Quantities |
| R | : Resistance |
| T_e | : Electro-mechanical Torque |
| T_m | : Mechanical Torque |
| v | : Voltage |
| ω | : Rotor Angular Velocity |
| ω_r | : Generator Rotor Angular Velocity |
| X | : Reactance |
| W^c | : Center Manifold |
| Ψ | : Flux Linkage |
| θ | : Rotor Angle |
| δ | : Load Angle |
| λ | : Eigenvalue |
| p, q | : Complex Vectors |

HOPF BIFURCATIONS IN A POWER SYSTEM SUSCEPTIBLE TO SUBSYNCHRONOUS RESONANCE AND A NOVEL CONTROLLER FOR DAMPING TORSIONAL OSCILLATIONS

SUMMARY

In this study, bifurcation theory is employed for the analysis of torsional oscillations in a power system, which consists of a synchronous generator connected to an infinite busbar through two parallel transmission lines, one of which is equipped with a series compensation capacitor. The first system of the IEEE Second Benchmark Model for Subsynchronous Resonance studies has been used. Damper windings of the synchronous generator are included in the nonlinear model.

Synchronous generators connected to transmission lines with series capacitor compensation are potentially subject to the interaction between the subsynchronous electrical mode and torsional oscillation modes of the turbine generator shaft system. This phenomenon is called Subsynchronous Resonance (SSR). Hopf bifurcation occurs at certain values of the series compensation factor. Instead of employing the Floquet multipliers method reported in the literature, the first Lyapunov coefficients are computed analytically to determine the type of Hopf bifurcation (subcritical or supercritical) existing in the power system under study. The impact of mechanical torque input, network voltage level and field voltage on the Hopf bifurcation point and the first Lyapunov coefficient is also explored.

Moreover, an automatic voltage regulator (AVR) is included into the model. It is shown that subcritical Hopf bifurcations in the model without AVR changes to supercritical Hopf bifurcation if the AVR is added to the model.

In addition, a novel controller based on the delayed feedback control theory has been developed for damping the unstable torsional oscillations caused by SSR. The proposed Time Delay Auto-Synchronization controller has two set parameters to be tuned and uses the state variable synchronous generator rotor angular speed as the only input. The optimal values of the controller time delay and gain parameters have been determined by computing a performance index evaluating the dynamic responses in time domain. The effectiveness of the proposed controller is demonstrated via time-domain simulations in MATLAB-Simulink.

Finally, the impact of AVR and TDAS controller limiters on the damping performance is also investigated. It is demonstrated that the controller is effective even in the presence of limiters within the practical operating ranges of series capacitor compensation.

SENKRONALTI REZONANSA DUYARLI BİR GÜÇ SİSTEMİNDE HOPF ÇATALLANMALARI VE BURULMA SALINIMLARININ SÖNÜMLENDİRİLMESİ İÇİN YENİ BİR KONTROLÖR

ÖZET

Bu çalışmada, bir elektrik güç sistemindeki burulma salınımlarının analizi için çatallanma teorisinden yararlanılmıştır. Modellenen elektrik güç sistemi, birinde seri kapasitör kompanzasyonu bulunan iki paralel iletim hattı üzerinden sonsuz baraya bağlı bir senkron makine içermektedir. Senkronaltı rezonans araştırmaları için geliştirilen IEEE İkinci Gösterge Modelinin birinci sistemi kullanılmıştır. Senkron makinenin amortisör sargıları doğrusal olmayan modele dahil edilmiştir.

Seri kompanzasyon kapasitör tesis edilmiş olan iletim hatlarına bağlı senkron makineler, potansiyel olarak senkronaltı elektrik modunun, türbin-generatör şaft sisteminin burulma salınım modları ile etkileşimine maruz kalabilirler. Bu olay senkronaltı rezonans (SSR) olarak isimlendirilir. Belirli seri kompanzasyon değerlerinde Hopf çatallanması meydana gelir. Modellenen elektrik güç sisteminde meydana gelen Hopf çatallanmalarının hangi tip olduğu (kritik-altı veya kritik-üstü), literatürde yaygın biçimde kullanılan Floquet çarpanları yöntemi yerine, birinci Lyapunov katsayılarının analitik olarak hesaplanması ile belirlenmiştir. Mekanik tork değeri, şebeke gerilim seviyesi ve uyarı geriliminin Hopf çatallanma noktaları ile birinci Lyapunov katsayısının değeri üzerindeki etkileri araştırılmıştır.

Ek olarak, Otomatik Gerilim Düzenleyicisinin (AVR) Hopf çatallanması üzerindeki etkisi de incelenmiş ve AVR içermeyen modelde kritik-altı olan Hopf çatallanmasının, AVR ilave edildiği zaman kritik-üstü Hopf çatallanmasına dönüştüğü gösterilmiştir.

Ayrıca, SSR sonucu ortaya çıkan kararsız burulma salınımlarını söndürmek için, zaman gecikmeli geri besleme teorisine dayanan bir kontrolör tasarlanmıştır. Önerilen Zaman Gecikmeli Otokronizasyon Kontrolörünün iki adet ayar değeri mevcuttur ve girdi olarak kullandığı tek durum değişkeni, senkron makine rotorunun açısal hızıdır. Kontrolörün zaman gecikme ve kazanç parametreleri için uygun değerler, sistemin dinamik cevabını değerlendiren bir performans endeksi hesaplanarak belirlenmiştir. Önerilen kontrolörün etkili sonuçlar verdiği, MATLAB-Simulink kullanılarak gerçekleştirilen simülasyonlar ile gösterilmiştir.

Son olarak, AVR ve kontrolör çıkış sınırlayıcılarının söndürme performansı üzerindeki etkileri de araştırılmış ve seri kapasitör kompanzasyonun pratik değerleri için, sınırlayıcıların mevcut olduğu durumda da kontrolörün etkili olduğu gösterilmiştir.

1. INTRODUCTION

Series capacitor compensation of AC transmission lines is an effective way of increasing load carrying capacity and enhancing transient stability in electric power systems [1]. However, potential danger of interaction between torsional oscillation modes of the turbine generator shaft system and the subsynchronous electrical mode may arise in electric power systems consisting of turbine-generators connected to transmission lines with series compensation capacitors. This phenomenon is called Subsynchronous Resonance (SSR). Unless adequate measures are implemented, SSR can lead to turbine-generator shaft failures as occurred at the Mohave Power Plant in Southern Nevada in the USA in 1970 [2].

1.1 Statement of the Problem

The SSR condition due to the interaction between the electrical subsynchronous mode and turbine-generator torsional modes occurs through a Hopf bifurcation. The determination of the type of Hopf bifurcation (i.e. subcritical or supercritical) is important to identify the stability of limit cycles arising out of the Hopf bifurcation. The rigorous method of computing the first Lyapunov coefficient is well suited for this task because of the analytic techniques involved in the process. Moreover, the impact of Automatic Voltage Regulator and dynamic parameters on the first Lyapunov coefficient, thereby on the stability of limit cycles is an area requiring further research.

Furthermore, it is crucial to mitigate the risk of a catastrophic failure of turbine-generator shafts due to SSR. In recent years, the delayed feedback control theory has been widely applied to improve damping in dynamic systems. The development of a delayed feedback controller for damping the torsional oscillations caused by SSR can bring substantial benefits including the further utilization of series capacitor compensation and mitigating the fatigue deformation on turbine-generator shafts due to torsional oscillations.

1.2 Objectives of the Dissertation

In this dissertation, the first system of the IEEE SBM for SSR studies is used to analyze Hopf bifurcations occurring in a power system experiencing SSR. The single-machine-infinite-busbar (SMIB) power system, which consists of a synchronous generator connected to an infinite busbar through two parallel transmission lines, one of which is equipped with an adjustable series capacitor, is modeled using autonomous ordinary differential equations. The inherently nonlinear model representing the dynamics of the turbine-generator shaft system and network components is analyzed by employing the bifurcation theory. The oscillation modes and their stability at various operating conditions are studied taking the series compensation factor as the bifurcation parameter. The interaction between the subsynchronous electrical mode and the torsional modes of the turbine-generator mechanical system and the resulting effect on the stability are also investigated.

The existence of Hopf bifurcations in the SMIB power system under study is verified. The first Lyapunov coefficient is computed analytically to determine the type of Hopf bifurcation (i.e. supercritical or subcritical) through which the system stability of equilibrium is lost. The impacts of the mechanical torque input, field voltage, network voltage and the automatic voltage regulator (AVR) on the first Lyapunov coefficient thereby on the characteristic of Hopf bifurcation are studied separately. Time domain simulations are used to validate the analytic findings. Transition from subcritical Hopf bifurcation to supercritical Hopf bifurcation is also explored.

In addition, a novel controller based on the Delayed Feedback Control theory has been developed for damping the unstable torsional oscillations due to the SSR. With only two parameters to be optimally set, the proposed Time Delay Auto-Synchronization (TDAS) controller requires the measurement of the synchronous generator rotor angular speed, an easily accessible state variable. The TDAS controller output is then combined into the automatic voltage regulator (AVR) as the stabilizing signal. Time domain simulations in MATLAB-Simulink demonstrate that the proposed TDAS controller is very effective for damping the unstable subsynchronous oscillations.

Determining the optimum set values for time delay and gain parameters of the TDAS controller involves evaluation of time domain simulations at various operating conditions in the absence of a practical method for this purpose. This is mainly because of the fact that the analysis of delay-differential systems is extremely complex. Moreover, it is found that the controller effectiveness is not reduced with the inclusion of AVR limiters in the range of practical operational levels of series capacitor compensation.

1.3 Literature Review

Following the shaft failure incidents at the Mohave Power Plant in 1970, considerable effort by researchers and industry professionals has been devoted to the analysis of SSR phenomenon. Walker et al. [3] found that torsional fatigue caused the shaft failures at Mohave. Farmer et al. [4] identified three types of SSR: induction generator effect, torsional interaction effect, and transient torque effect.

The induction generator effect (IGE) occurs as a result of self excitation of the synchronous generators when the resistance of the rotor circuits to the subsynchronous current, viewed from the armature terminal, is negative [5]. If this negative resistance of the generator is greater in magnitude than the positive resistance of the network at the natural frequencies, then the electrical system becomes self-excited.

Oscillations of the generator rotor speed at natural frequencies of the torsional modes result in the modulation of the generator terminal voltage. The torsional interaction effect (TIE) occurs if the frequency of the produced voltage component is close to one of natural frequencies of the electric network. The resulting armature currents produce a magnetic field which is phased to produce a torque which reinforces the aforementioned generator rotor oscillations [6]. Turbine-generator shaft damage can occur due to severe torque amplification.

Contrary to IGE and TIE, the transient torque effect (TTE) is not self-excited. Following a significant system disturbance, natural modes of the turbine-generator shaft system are excited, subjecting shaft segments to torsional stresses [7] which can cause catastrophic shaft damage.

IEEE SSR Working Group has constructed three benchmark models for computer simulation of the SSR [8, 9]. Analytical tools for studying the SSR involve frequency scanning technique [10, 11], eigenvalue technique [12-13], the complex torque coefficient method [14, 15] and time domain simulation programs [16-18]. The first three techniques are linear and the fourth one is nonlinear.

In the frequency scanning method, the equivalent resistance and reactance looking into the network from a point behind the stator winding of a generator are computed as a function of frequency. The eigenvalue technique provides both the oscillation frequencies and the damping values for each frequency using the linearized system of differential equations representing the electric power system. The eigenvalue method is very useful in the analysis of small systems. On the other hand, it is difficult to apply in large power systems. In the complex torque coefficient method, transfer function of the mechanical system is obtained using the linearized equations of the multi-mass shaft system of a turbine generator. Then the resulting mechanical transfer function is combined with the electrical transfer function, which represent the effect of damping and synchronizing torques in order to identify torsional modes and evaluate their stabilities.

Time domain simulation programs are used to avoid the disadvantages associated with the linearization of the ordinary differential equations. Numerically integrating the set of nonlinear ODEs representing a dynamic system, time domain simulation programs enable detailed and accurate modeling and therefore are extremely useful for the analysis of SSR problems. Among widely used ones are Electromagnetic Transient Program (EMTP) and MATLAB-Simulink. Exponential growth observed in the linearized methods does not occur in the nonlinear analysis performed using the time domain simulation programs.

SSR countermeasures and mitigation techniques have been an active area of research over decades. Hingorani [19] developed the NGH SSR damping scheme which consists of a linear resistor and an anti-parallel thyristor combination across a series compensation capacitor segment with measuring equipment and appropriate controls. Zhao and Chen [20] proposed an improved NGH SSR damping scheme, adding SSR detection and pre-firing functions to the original NGH scheme. The use of static synchronous compensator (STATCOM), a flexible AC transmission system (FACT)

device, for damping of subsynchronous oscillations was analyzed in [21-22]. Damping of torsional oscillations using excitation controllers and static VAR compensators was studied in [23-24] and [25], respectively. Wang and Tseng [26] proposed a damping scheme utilizing a superconducting magnetic storage (SMES) unit to stabilize torsional oscillations. Wang [27] studied the first system of the IEEE Second Benchmark Model by employing the modal control theory. Linear and nonlinear state feedback controllers are proposed in [28] to control the bifurcation in a power system susceptible to SSR.

Hopf bifurcation is defined as the birth of a limit cycle from equilibrium in a nonlinear dynamical system governed by autonomous ODEs under variation of one or more parameters on which the system is dependent. Hopf bifurcations associated with the voltage stability in power systems were widely investigated by researchers [29-34]. In the SSR area, Zhu et al. [35] demonstrated the existence of Hopf bifurcations in a SMIB experiencing SSR and reported a limited oscillation behavior at the Hopf bifurcation point. Iravani et al. [36] investigated Hopf bifurcation phenomenon of the torsional dynamics. Harb [37] employed the bifurcation theory to investigate the complex dynamics of SSR. The effect of the machine saturation on SSR was also studied by Harb et al [38].

Floquet theory is widely used to study the stability of limit cycles. The procedure involves the calculation of steady-state solutions, Hopf bifurcation points and the branches of periodic orbits which emanate from the Hopf bifurcation points [32]. Then by tracing the evolution of the Floquet multipliers, one can observe the stability of these solutions. One of the multipliers is always unity for an autonomous system. If all the other multipliers are inside the unit circle in the complex plane, then the limit cycle is orbitally stable. A multiplier crossing the unit circle is called a *critical multiplier*. If only one multiplier crosses the unit circle along the positive real axis then cyclic fold occurs. Period doubling, on the other hand, occurs when the critical multiplier leaves the unit circle along the negative real axis. Only one pair of complex conjugate multipliers crossing the unit circle indicates occurrence of a torus bifurcation [39].

Another method to analyze Hopf bifurcations is to compute the first and second Lyapunov coefficients [40]. Negative sign of the first Lyapunov coefficient

corresponds to the occurrence of supercritical Hopf bifurcations through which an orbitally stable limit cycle is born, whilst the first Lyapunov coefficient with positive sign implies that a subcritical Hopf bifurcation occurs and an unstable limit cycle bifurcates from equilibrium after loss of stability. If the first Lyapunov coefficient vanishes with a nonzero second Lyapunov coefficient, then generalized Hopf bifurcation occurs [41]. Kucukefe and Kaypmaz [42] investigated the Hopf bifurcations occurring in the first system of the IEEE Second Benchmark Model for SSR studies by computing the first Lyapunov coefficient.

In this dissertation, the emphasis is given to determining the type of Hopf bifurcation by computing the first Lyapunov coefficient. Moreover, the impact of the operating parameters other than the series compensation level on the first Lyapunov coefficient, thereby on the type of Hopf bifurcation, has been investigated. From this point of view, the dissertation differs from the studies of Zhu [35], who verified the occurrence of SSR on the Boardman generator model, and Harb [37], who studied the bifurcations depending on the variations in the series compensation level and also determined the amplitudes of the limit cycles emanating from the Hopf bifurcation on the Boardman and CHOLLA#4 generator models. Furthermore, both Zhu and Harb employed the Floquet multipliers method to determine the type of Hopf bifurcation.

Delayed feedback control [43] is a simple and efficient method to stabilize both unstable periodic orbits (UPO) embedded in the strange attractors of chaotic systems [44] and unstable steady states [45]. Also known as Time Delay Auto-Synchronization (TDAS), this control scheme makes use of the current state of a system and its state τ -time unit in the past to generate a control signal. In the case with UPOs, the most efficient control performance of TDAS scheme can be obtained if time delay (τ) corresponds to an integer multiple of the minimal period of the unstable orbit. The method works best if τ is set a value related to intrinsic characteristic time scale given by the imaginary part of the system's eigenvalue in the case of unstable steady states [46]. Successful implementations of TDAS algorithm are reported in diverse experimental systems including mechanical pendulums [47], chemical systems [48], helicopter rotor blades [49], a cardiac system [50], trajectory tracking [51], and absorption of mechanical vibrations [52].

1.4 Outline of the Dissertation

The dissertation is organized as follows. Chapter 2 gives a review of the bifurcation theory and describes the procedures for computing the Lyapunov coefficients. In Chapter 3, the first system of the IEEE SBM is described and its complete nonlinear model is obtained. Furthermore, bifurcation analysis of the nonlinear model is performed and the occurrence of Hopf bifurcations is verified. The first Lyapunov coefficients are computed to determine the type of Hopf bifurcations. The AVR is included into the model in Chapter 4 and its effect on the Hopf bifurcations is investigated. Chapter 5 introduces the novel controller based on the Delayed Feedback Control theory to stabilize the unstable torsional oscillations. Optimization performance index to determine the optimal values of the controller is also described. In Chapter 6, the effect of AVR and TDAS controller limiters is investigated.

2. REVIEW OF BIFURCATION THEORY

Bifurcation theory deals with qualitative changes in dynamical systems. As a matured branch of mathematics, the theory offers useful tools in the analysis of dynamical systems, particularly nonlinear ones. By definition, a nonlinear system is a system which does not satisfy the superposition principle. The most common way to define a continuous-time nonlinear dynamical system is to represent the system in the form of autonomous ordinary differential equations (ODEs). Consider a continuous-time nonlinear system depending on a parameter vector.

$$\dot{x} = f(x, \alpha), \quad x \in \mathbb{R}^n, \quad \alpha \in \mathbb{R}^m \quad (2.1)$$

where f is smooth with respect to x and α . If varying the parameter vector α results in qualitative changes in the system dynamic behavior in a way that different behaviors (aperiodic, periodic, chaotic, etc.) and stability conditions are introduced, these changes are called *bifurcations* and the parameter vector values at which the changes occur are called *bifurcation (critical) values*.

2.1 Stability of Equilibrium Solutions

Suppose that nonlinear dynamical system (2.1) has an equilibrium at x^0 (i.e. $f(x^0, \alpha^0) = 0$) and \mathbf{J} denotes the Jacobian matrix of $f(x)$ evaluated at the equilibrium. The Jacobian matrix is defined as follows:

$$\mathbf{J} = \begin{bmatrix} \frac{\partial f_1}{\partial x_1} & \dots & \frac{\partial f_1}{\partial x_n} \\ \vdots & \ddots & \vdots \\ \frac{\partial f_n}{\partial x_1} & \dots & \frac{\partial f_n}{\partial x_n} \end{bmatrix} \quad (2.2)$$

The eigenvalues of \mathbf{J} provides information about the local stability of the equilibrium solution. If all the eigenvalues $\lambda_1, \lambda_2, \dots, \lambda_n$ of \mathbf{J} satisfy $Re(\lambda_i) < 0$ for $i=1, 2, \dots, n$, then the system $f(x^0, \alpha^0)$ is asymptotically stable.

2.2 Bifurcation Mechanisms

There are different types of bifurcations. Among the most important ones are fold bifurcation, pitchfork bifurcation, transcritical bifurcation, period doubling and Hopf bifurcation [53]. Fold bifurcations are associated with dynamic systems which have Jacobian matrix with a single zero eigenvalue while all the other eigenvalues remain in the left half plane. This type of bifurcation has also other names such as saddle-node bifurcation and turning point. Transcritical bifurcation is characterized by the intersection of two bifurcation curves. Pitchfork bifurcations often occur in systems with some symmetry, as a manifestation of symmetry breaking. Period doubling bifurcation, as its name implies, is a bifurcation in which the dynamic system switches to a new behavior with twice the period of the previous system. The bifurcation corresponding to the presence of distinct pair of purely imaginary eigenvalues ($\lambda_{1,2} = \pm i\omega_0$, $\omega_0 > 0$) of the Jacobian matrix $f_x(x^0, \alpha^0)$ is called a Hopf (or Andronov-Hopf) bifurcation. A Hopf point is called transversal if the real part of the parameter dependent complex eigenvalues creating the Hopf bifurcation condition has non-zero derivative with respect to the bifurcation parameter (i.e. $d(\text{Re}(\lambda(\alpha)))/d\alpha \neq 0$ at $\alpha = \alpha_0$). Transversality condition is usually met.

2.3 Hopf Bifurcation

Hopf bifurcation is the birth of limit cycles from equilibrium in dynamical systems generated by ODEs, when the equilibrium changes stability via a purely imaginary eigenvalues [54]. Limit cycles are periodic orbits that represent regular motions in a dynamical system. Hopf bifurcations generate limit cycles from equilibrium. Supercritical Hopf bifurcation results in a stable limit cycle and exists after the bifurcation point, whereas an unstable limit cycle emanates from subcritical Hopf bifurcation and is present before the critical value. In both cases, loss of stability of the equilibrium occurs.

Floquet theory is widely employed in order to study the stability of limit cycles. Floquet multipliers give information about the stability of a limit cycle. One multiplier is always unity. A periodic orbit (i.e. limit cycle) is stable if the remaining Floquet multipliers are smaller than unity in modulus. If all the other multipliers are inside the unit circle in the complex plane, then the limit cycle is orbitally stable. A

multiplier crossing the unit circle is called a *critical multiplier*. If only one multiplier crosses the unit circle along the positive real axis then cyclic fold occurs. Period doubling, on the other hand, occurs when the critical multiplier leaves the unit circle along the negative real axis. Only one pair of complex conjugate multipliers crossing the unit circle indicates occurrence of a torus bifurcation. The Floquet multipliers are the eigenvalues of the monodromy matrix. Various algorithms for calculating the monodromy matrix can be found in [54].

In this dissertation, we compute the first Lyapunov coefficient instead of obtaining the Floquet multipliers in order to study the stability of limit cycles in a SMIB power system susceptible to SSR. The type of Hopf bifurcation (i.e. Supercritical or subcritical) is determined by computing the first Lyapunov coefficient at Hopf bifurcation point. The first Lyapunov coefficient is negative if a supercritical Hopf bifurcation occurs. On the other hand, positive sign of the first Lyapunov coefficient corresponds to the occurrence of a subcritical Hopf bifurcation [40].

2.3.1 Subcritical Hopf Bifurcation

A subcritical Hopf bifurcation occurs when a stable equilibrium point and an unstable limit cycle coalesce [55]. Consider the following nonlinear system of two differential equations depending on one parameter [40]:

$$\begin{aligned} \dot{y}_1 &= \beta y_1 - y_2 + y_1(y_1^2 + y_2^2) \\ \dot{y}_2 &= y_1 + \beta y_2 + y_2(y_1^2 + y_2^2) \end{aligned} \quad (2.3)$$

Fig. 2.1 depicts the subcritical Hopf bifurcation occurring in the nonlinear system.

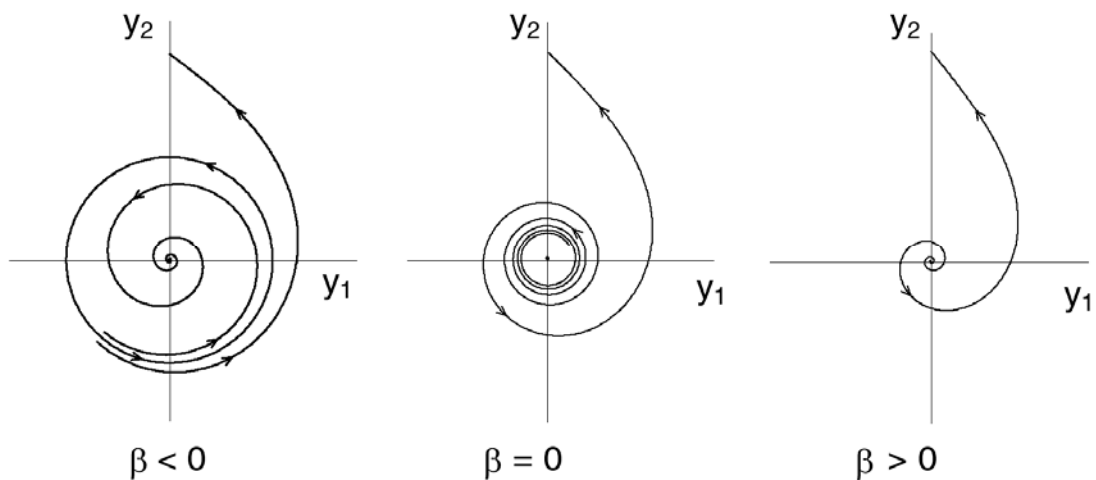


Figure 2.1 : Subcritical Hopf Bifurcation

The system (2.3) is stable for $\beta < 0$ and unstable for $\beta > 0$. The loss of stability of the equilibrium occurs at $\beta=0$ through Hopf bifurcation. The first Lyapunov coefficient for the system (2.3) has a positive sign ($l_1(0) = 2.0$), indicating that the Hopf bifurcation is subcritical. Therefore, there exists an unstable limit cycle.

The region of attraction of the equilibrium point is bounded by the unstable cycle, which shrinks as the control parameter approaches its critical value and disappears. Thus, the system is pushed out from a neighborhood of the equilibrium, giving a sharp or catastrophic loss of stability. In this case, resetting the control parameter to a negative value may not result in stable equilibrium since it may have left its stability of attraction.

2.3.2 Supercritical Hopf Bifurcation

The supercritical Hopf bifurcation corresponds to the coalescing of an unstable equilibrium point and a stable limit cycle [55].

As an example, consider the following system with two dimensions depending on one parameter [40]:

$$\begin{aligned} \dot{y}_1 &= \beta y_1 - y_2 + y_1(y_1^2 + y_2^2) \\ \dot{y}_2 &= y_1 + \beta y_2 + y_2(y_1^2 + y_2^2) \end{aligned} \quad (2.4)$$

The loss of stability of equilibrium occurs at $\beta=0$ through a Hopf bifurcation. Contrary to (2.3), there is a stable limit cycle. All orbits starting inside or outside the cycle for $\beta > 0$ tend to the cycle as $t \rightarrow +\infty$. The first Lyapunov coefficient has a negative sign ($l_1(0) = -2.0$), revealing that the Hopf bifurcation is supercritical.

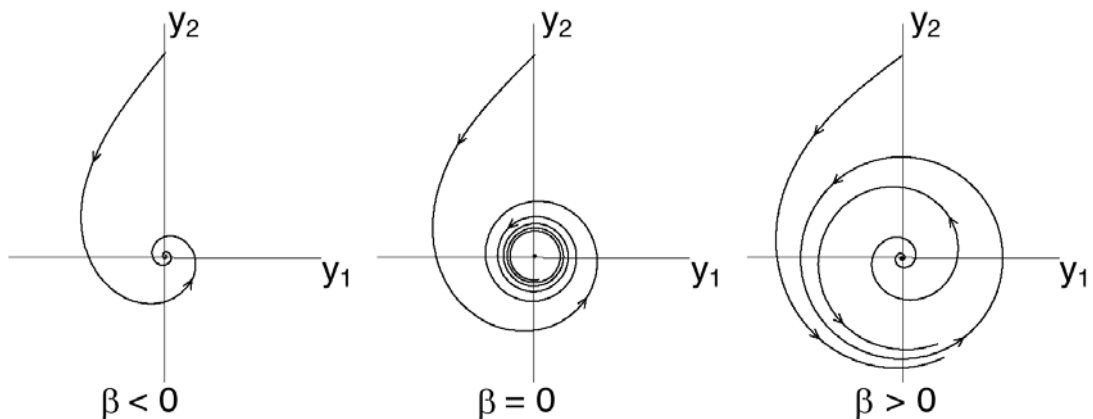


Figure 2.2 : Supercritical Hopf bifurcation

2.4 Center Manifold Theorem

Center Manifold Theorem allows reducing the dimension of multidimensional systems near a local bifurcation. The center manifold is an invariant manifold of the differential equations which is tangent at the equilibrium point to the eigenspace of the neutrally stable eigenvalues [56]. The complicated asymptotic behavior is isolated by locating an invariant manifold tangent to the subspace spanned by the eigenspace of eigenvalues on the imaginary axis.

The analysis of bifurcations of equilibria and fixed points in multidimensional systems reduces to that for the differential equations restricted to the invariant W_α^c . Since these bifurcations are determined by the normal form coefficients of the restricted systems at the critical parameter value α^0 , one is able to compute the center manifold $W^c=W_{\alpha^0}^c$ and ODEs restricted to this manifold up to sufficiently high-order terms.

2.5 Lyapunov Coefficients

This section presents methods to compute the Lyapunov coefficients found in [39]. Unknown coefficients of the Taylor expansion of a function representing the center manifold W^c can be computed either by a recursive procedure or a projection method. The former involves solving a linear system of algebraic equations at each step whilst the latter uses eigenvectors corresponding to the critical eigenvalues of \mathbf{J} and to “project” the system into the critical eigenspace and its complement. The projection procedure is based on the Fredholm Alternative Theorem and avoids the transformation of the system into its eigenbasis.

Suppose the system (2.1) has the form

$$\dot{x} = \mathbf{J}x + F(x), \quad x \in \mathbb{R}^n \quad (2.5)$$

where $F(x) = O(\|x\|^2)$ is a smooth function. We write its Taylor expansion near $x = 0$ as

$$F(x) = \frac{1}{2}B(x, x) + \frac{1}{6}C(x, x, x) + \frac{1}{24}D(x, x, x, x) + \frac{1}{120}E(x, x, x, x, x) + O(\|x\|^6) \quad (2.6)$$

where B, C, D and E are multilinear vector functions. In coordinates, we have

$$B_i(x, y) = \sum_{j,k=1}^n \frac{\partial^2 f_i(\xi, \alpha^0)}{\partial \xi_j \partial \xi_k} \Big|_{\xi=0} x_j y_k \quad (2.7)$$

$$C_i(x, y, z) = \sum_{j,k,l=1}^n \frac{\partial^3 f_i(\xi, \alpha^0)}{\partial \xi_j \partial \xi_k \partial \xi_l} \Big|_{\xi=0} x_j y_k z_l \quad (2.8)$$

$$D_i(x, y, z, u) = \sum_{j,k,l,m=1}^n \frac{\partial^4 f_i(\xi, \alpha^0)}{\partial \xi_j \partial \xi_k \partial \xi_l \partial \xi_m} \Big|_{\xi=0} x_j y_k z_l u_m \quad (2.9)$$

$$E_i(x, y, z, u, v) = \sum_{j,k,l,m,p=1}^n \frac{\partial^5 f_i(\xi, \alpha^0)}{\partial \xi_j \partial \xi_k \partial \xi_l \partial \xi_m \partial \xi_p} \Big|_{\xi=0} x_j y_k z_l u_m v_p \quad (2.10)$$

for $i=1,2, \dots, n$.

In case of a Hopf bifurcation, the Jacobian matrix \mathbf{J} has a simple pair of complex eigenvalues on the imaginary axis, $\lambda_{1,2} = \pm i\omega_0$, $\omega_0 > 0$, and these eigenvalues are the only eigenvalues with $\text{Re}(\lambda) = 0$. Let $q \in C^n$ be a complex eigenvector corresponding to λ_1 :

$$\mathbf{J}q = i\omega_0 q, \quad \mathbf{J}\bar{q} = -i\omega_0 \bar{q} \quad (2.11)$$

Introduce also the adjoint eigenvector $p \in C^n$ having the properties:

$$\mathbf{J}^T p = i\omega_0 p, \quad \mathbf{J}^T \bar{p} = -i\omega_0 \bar{p} \quad (2.12)$$

The procedure for obtaining q and p complex eigenvectors is given in Appendix-A.

2.5.1 The First Lyapunov Coefficient

After normalization of (2.9) and (2.10) according to $\langle p, q \rangle = 1$, where $\langle p, q \rangle = \sum_{i=1}^n \bar{p}_i q_i$ is the standard scalar product in C^n , the following invariant expression gives the first Lyapunov coefficient, $l_1(0)$:

$$l_1(0) = \frac{1}{2\omega_0} \text{Re}[\langle p, C(q, q, \bar{q}) \rangle - 2\langle B(q, \mathbf{J}^{-1} B(q, \bar{q})) \rangle + \langle p, B(\bar{q}, (2i\omega_0 I_n - \mathbf{J})^{-1} B(q, q)) \rangle] \quad (2.13)$$

Whether a Hopf bifurcation is supercritical or subcritical can be found from the sign of the first Lyapunov coefficient. Negative sign of $l_1(0)$ indicates a supercritical Hopf bifurcation and positive $l_1(0)$ corresponds to a subcritical Hopf bifurcation. A *Hopf bifurcation of codimension 2* is a Hopf point where $l_1(0)$ vanishes, provided that the second Lyapunov coefficient is nonzero [57].

2.5.2 The Second Lyapunov Coefficient

After normalization of (2.9) and (2.10) according to $\langle p, q \rangle = 1$, the procedure for deriving the expression for the second Lyapunov coefficient is as follows:

$$\begin{aligned}
l_2(0) = & \frac{1}{12\omega_0} \text{Re}[\langle p, E(q, q, q, \bar{q}, \bar{q}) + D(q, q, q, \bar{h}_{20}) + 3D(q, \bar{q}, \bar{q}, h_{20}) + 6D(q, q, \bar{q}, h_{11}) \\
& + C(\bar{q}, \bar{q}, h_{30}) + 3C(q, q, \bar{h}_{21}) + 6C(q, \bar{q}, h_{21}) + 3C(q, \bar{h}_{20}, h_{20}) + 6C(q, h_{11}, h_{11}) \\
& + 6C(\bar{q}, h_{20}, h_{11}) + 2B(\bar{q}, h_{31}) + 3B(q, h_{22}) + B(\bar{h}_{20}, h_{30}) \\
& + 3B(\bar{h}_{21}, h_{20}) + 6B(h_{11}, h_{21}) \rangle] \tag{2.14}
\end{aligned}$$

where

$$h_{20} = (2i\omega_0 I_n - J)^{-1} B(q, q) \tag{2.15}$$

$$h_{11} = -J^{-1} B(q, \bar{q}) \tag{2.16}$$

$$h_{30} = (3i\omega_0 I_n - J)^{-1} [C(q, q, q) + 3B(q, h_{20})] \tag{2.17}$$

$$h_{21} = (i\omega_0 I_n - J)^{-1} [C(q, q, \bar{q}) + B(\bar{q}, h_{20}) + 2B(q, h_{11}) - 2c_1 q] \tag{2.18}$$

$$c_1 = \frac{1}{2} \langle p, C(q, q, \bar{q}) \rangle - 2 \langle B(q, J^{-1} B(q, \bar{q})) \rangle + \langle p, B(\bar{q}, (2i\omega_0 I_n - J)^{-1} B(q, q)) \rangle \tag{2.19}$$

$$\begin{aligned}
h_{31} = & (2i\omega_0 I_n - J)^{-1} [D(q, q, q, \bar{q}) + 3C(q, q, h_{11}) + 3C(q, \bar{q}, h_{20}) \\
& + 3B(h_{20}, h_{11}) + B(\bar{q}, h_{30}) + 3B(q, h_{21}) - 6c_1 h_{20}] \tag{2.20}
\end{aligned}$$

$$\begin{aligned}
h_{22} = & -J^{-1} [D(q, q, \bar{q}, \bar{q}) + 4C(q, \bar{q}, h_{11}) + C(\bar{q}, \bar{q}, h_{20}) + C(q, q, \bar{h}_{20}) + 2B(h_{11}, h_{11}) \\
& + 2B(q, \bar{h}_{21}) + 2B(\bar{q}, h_{21}) + B(\bar{h}_{20}, h_{20}) - 4h_{11}(c_1 + \bar{c}_1)] \tag{2.21}
\end{aligned}$$

Obtaining the second Lyapunov coefficient analytically is extremely complex. Therefore, numerical methods available in the continuation and bifurcation software MATCONT [58] can be used to calculate $l_2(0)$.

2.6 Torus Bifurcation

It is important to note that various forms of bifurcations may occur in a nonlinear system, following the loss stability of equilibrium through a Hopf bifurcation, irrespective of birth of stable or unstable limit cycles.

Consider the following system [55] as an example:

$$\begin{aligned} \dot{y}_1 &= (\lambda - 3)y_1 - 0.25y_2 + y_1[y_3 + 0.2(1 - y_3^2)] \\ \dot{y}_2 &= 0.25y_1 + (\lambda - 3)y_2 + y_2[y_3 + 0.2(1 - y_3^2)] \\ \dot{y}_3 &= \lambda y_3 - (y_1^2 + y_2^2 + y_3^2) \end{aligned} \quad (2.22)$$

There is a Hopf bifurcation for $\lambda_H=1.684$ as illustrated in Fig. 2.3. The first Lyapunov coefficient has a negative sign ($l_1(0) = -1.55$). Hence, the type of Hopf bifurcation is supercritical. Stable limit cycles with angular frequency $\omega=0.25$ rad/s are born. On the other hand, a bifurcation into a torus occurs for $\lambda_0=2$. Fig. 2.4 shows three dimensional projection of the phase portrait for $\lambda=1.85$ at which a stable limit cycle exists. Bifurcation into torus for $\lambda=2.02$ is depicted in Fig. 2.5.

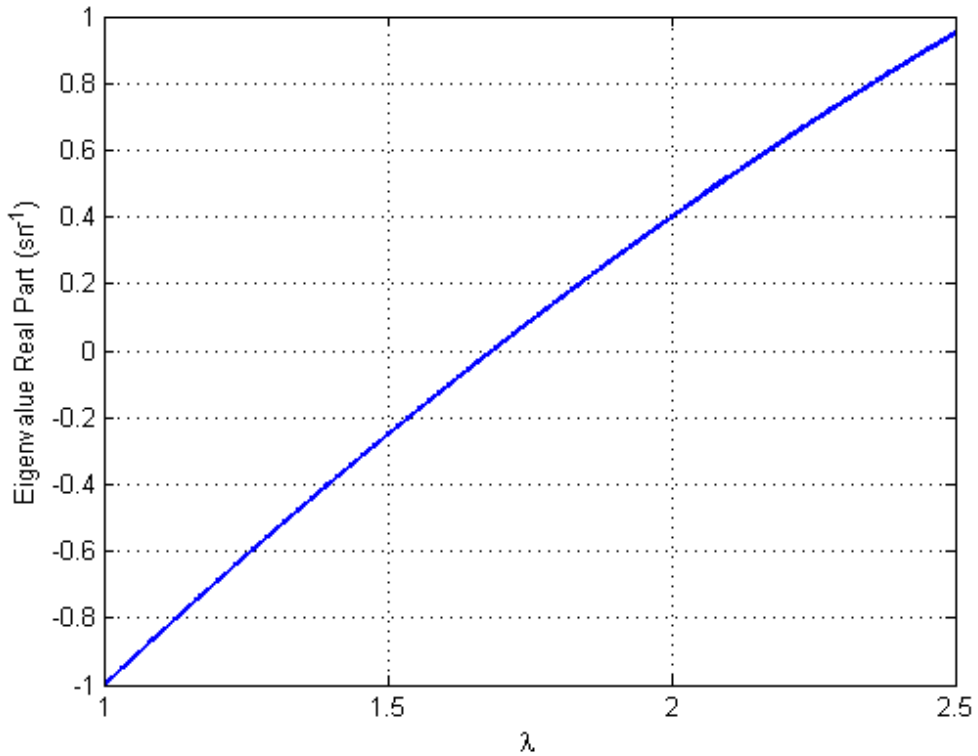


Figure 2.3 : Real part of imaginary eigenvalues w.r.t. λ ($\lambda_H=1.684$)

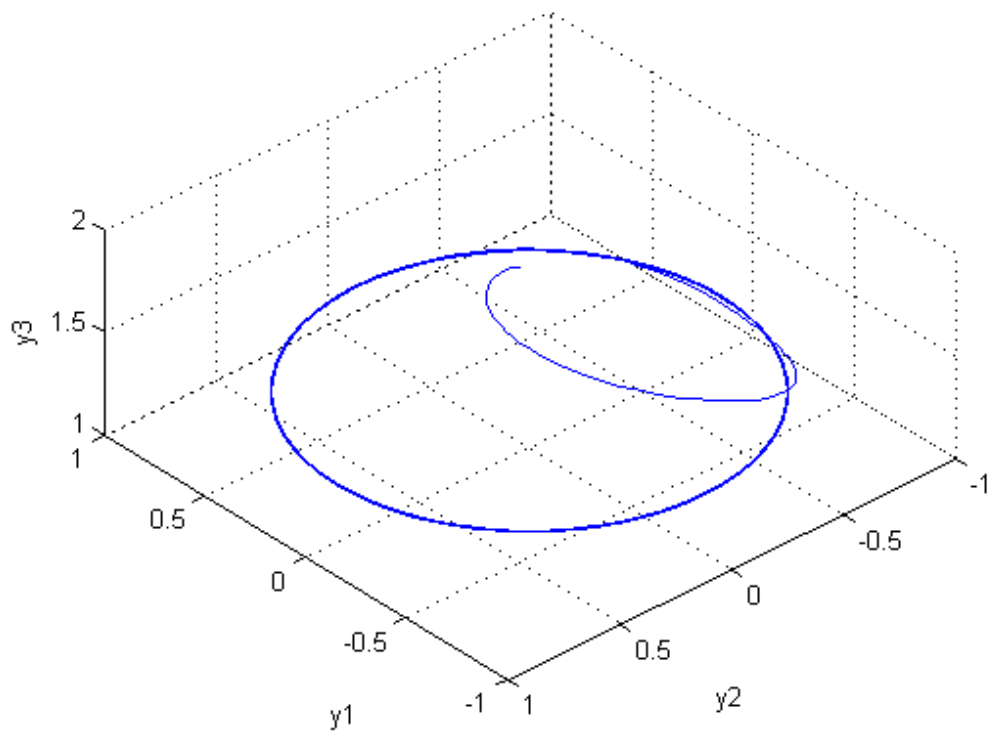


Figure 2.4 : Three dimensional projection for $\lambda=1.85$ (Supercritical Hopf)

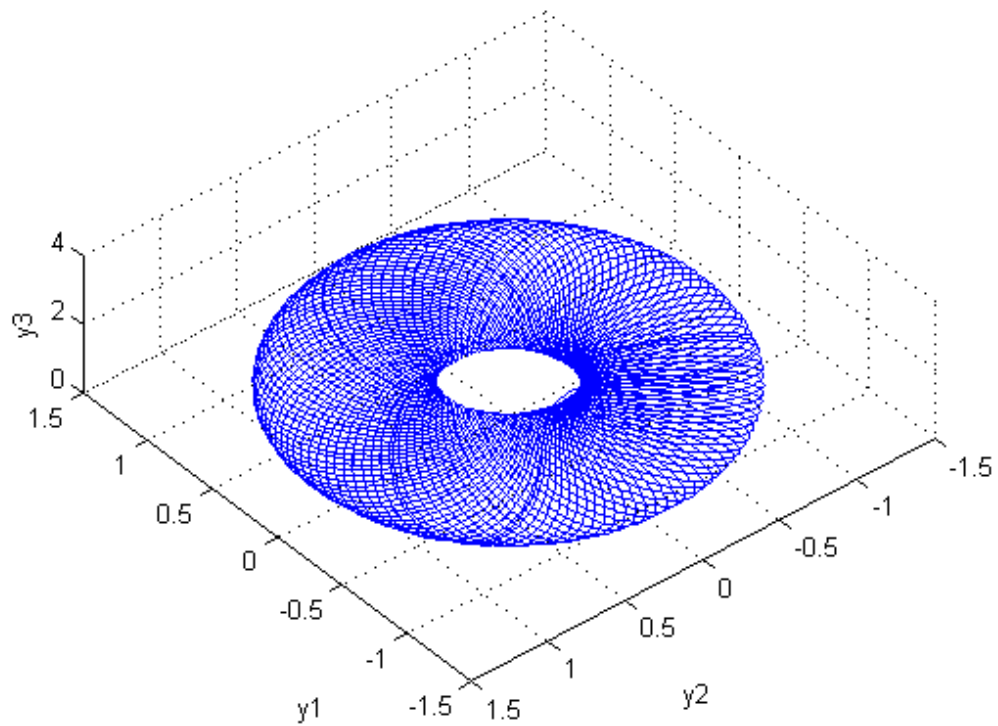


Figure 2.5: Three dimensional projection for $\lambda=2.02$ (Torus bifurcation)

3. SYSTEM DESCRIPTION AND MODELING

In this chapter, we construct a mathematical model of the first system of the IEEE Second Benchmark Model for SSR studies. The SMIB power system consists of a synchronous generator connected to an infinite busbar through two parallel transmission lines, one of which is equipped with an adjustable series compensation capacitor. We include the dynamics of the d-q axes generator damper windings in the model. The excitation system is modeled without AVR and it supplies constant field voltage. The turbine-governor dynamics and the effect of machine saturation are neglected in the model.

3.1 Electrical System

Fig. 3.1 shows the first system of the IEEE SBM for SSR studies.

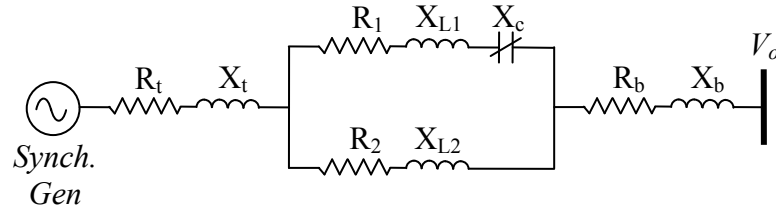


Figure 3.1 : The SMIB power system (System-1, IEEE SBM for SSR studies)

Series capacitor compensation in the transmission line-1 reduces the equivalent impedance between the synchronous generator and the infinite busbar. As a result, benefits such as improved transient stability [1] and increased load carrying capacity of the transmission system are achieved. The expression which gives the equivalent impedance of the network elements between the generator and the infinite busbar can be written as

$$Z_{eq} = (R_t + jX_t) + \left[\frac{R_1 + j(X_{L1} - \mu X_{L1})}{R_2 + jX_{L2}} \right] + (R_b + jX_b) \quad (3.1)$$

where μ is the series compensation factor defined as the ratio of X_c to X_{L1} (i.e. $\mu = X_c / X_{L1}$).

It follows from (3.1) that the equivalent impedance decreases as μ is increased. Fig. 3.2 shows that the equivalent impedance drops to 0.31 p.u. from 0.53 p.u. if the series compensation capacity is fully utilized.

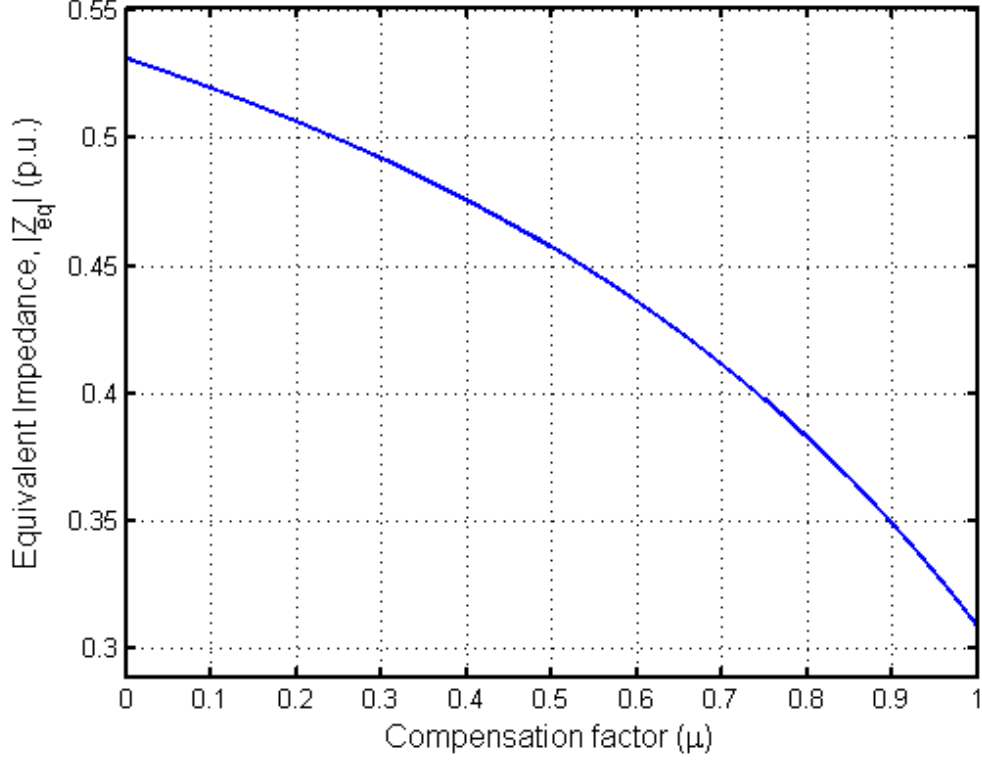


Figure 3.2 : Equivalent Impedance (Z_{eq}) w.r.t. the compensation factor (μ)

Park's transformation from three phase reference frame to direct and quadrature axes (d-q axes) is performed in order to obtain state equations describing the dynamics of the electrical system [59-62]. Before writing the equations for generator flux linkages and voltages of the d-q axes equivalent circuits, first we define the following parameters to represent the equations conveniently.

$$R_E = R_t + kR_{L1} + R_b \quad (3.2)$$

$$X_E = X_t + kX_{L1} + X_b \quad (3.3)$$

where

$$k = \frac{\sqrt{R_2^2 + X_{L2}^2}}{\sqrt{(R_1 + R_2)^2 + (X_{L1} + X_{L2} - \mu X_{L1})^2}}$$

Hereafter X_C will be represented as μX_{L1} .

3.1.1 Electrical System d-axis Equivalent Circuit

Fig. 3.3 shows the electrical system d-axis equivalent circuit.

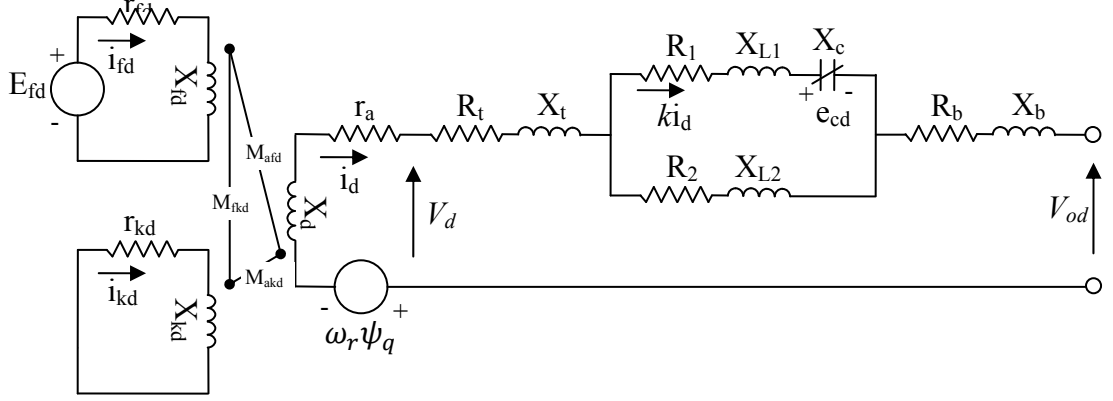


Figure 3.3 : Electrical system d-axis equivalent circuit

Using the basic circuit theory, the equations representing the flux linkages and voltages can be written as follows

Flux linkages in the d-axis:

$$\psi_d = -X_d i_d + X_{afd} i_{fd} + X_{akd} i_{kd} \quad (3.4)$$

$$\psi_{fd} = -X_{afd} i_d + X_{fd} i_{fd} + X_{fkd} i_{kd} \quad (3.5)$$

$$\psi_{kd} = -X_{akd} i_d + X_{fkd} i_{fd} + X_{kd} i_{kd} \quad (3.6)$$

d-axis voltage equations:

$$\frac{d\psi_d}{dt} = \omega_b (V_d + r_a i_d + \omega_r \psi_q) \quad (3.7)$$

$$\frac{d\psi_{fd}}{dt} = \omega_b (E_{fd} - r_{fd} i_{fd}) \quad (3.8)$$

$$\frac{d\psi_{kd}}{dt} = \omega_b (-r_{kd} i_{kd}) \quad (3.9)$$

$$V_d = R_E i_d - X_E i_q + \frac{X_E}{\omega_b} \frac{di_d}{dt} + e_{cd} + V_{od} \quad (3.10)$$

$$V_{od} = V_{0d} \sin \delta_r \quad (3.10)$$

$$e_{cd} = \mu X_{L1} k i_q - \frac{1}{\omega_b} \frac{de_{cq}}{dt} \quad (3.11)$$

3.1.2 Electrical System q-axis Equivalent Circuit

The electrical system q-axis equivalent circuit is shown in Fig. 3.3.

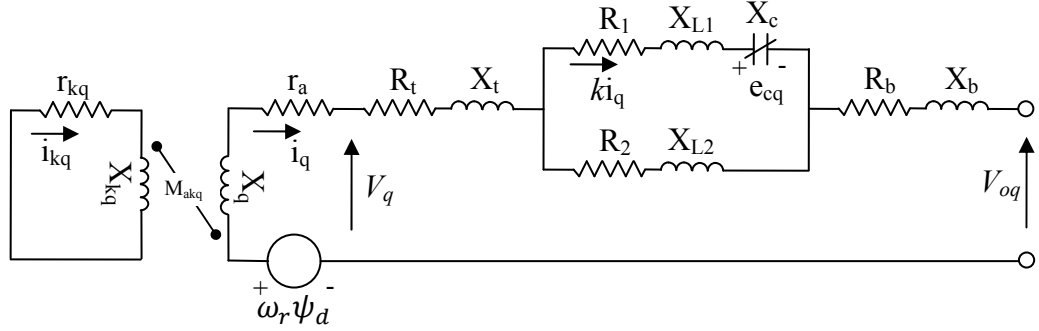


Figure 3.4 : Electrical system q-axis equivalent circuit

Flux linkages in the q-axis:

$$\psi_q = -X_q i_q + X_{akq} i_{kq} \quad (3.12)$$

$$\psi_{kq} = -X_{akq} i_q + X_{kq} i_{kq} \quad (3.13)$$

q-axis voltage equations:

$$\frac{d\psi_q}{dt} = \omega_b (V_q + r_a i_q - \omega_r \psi_d) \quad (3.14)$$

$$\frac{d\psi_{kq}}{dt} = \omega_b (-r_{kq} i_{kq}) \quad (3.15)$$

$$V_q = R_E i_q + X_E i_d + \frac{X_E}{\omega_b} \frac{di_q}{dt} + e_{cq} + V_{0q} \quad (3.16)$$

$$V_{0q} = V_{0q} \cos \delta_r \quad (3.17)$$

$$e_{cq} = \frac{1}{\omega_b} \frac{de_{cd}}{dt} - \mu X_{L1} k i_d \quad (3.18)$$

3.1.3 Electrical System State Equations

We define the state variables of the electrical system as $\mathbf{i}_g = [i_d \ i_q \ i_f \ i_{kq} \ i_{kd}]^T$, $\mathbf{i}_g \in \mathbb{R}^5$, and $\mathbf{e}_c = [e_{cd} \ e_{cq}]^T$, $\mathbf{e}_c \in \mathbb{R}^2$. Using (3.4)-(3.18), the state equations of the electrical system can be written as

$$\frac{d\mathbf{i}_g}{dt} = \mathbf{B}^{-1} \omega_b (\mathbf{C} \mathbf{i}_g + \mathbf{D}) \quad (3.19)$$

$$\frac{d\mathbf{e}_c}{dt} = \omega_b (\mathbf{E} \mathbf{i}_g + \mathbf{F} \mathbf{e}_c) \quad (3.20)$$

where:

$$B = \begin{bmatrix} -(X_d + X_E) & 0 & X_{afd} & 0 & X_{akd} \\ 0 & -(X_q + X_E) & 0 & X_{akq} & 0 \\ -X_{afd} & 0 & X_{fd} & 0 & X_{fkd} \\ 0 & -X_{akq} & 0 & X_{kq} & 0 \\ -X_{akd} & 0 & X_{fkd} & 0 & X_{kd} \end{bmatrix} \quad (3.21)$$

$$C = \begin{bmatrix} (r_a + R_E) & -(X_E + \omega_r X_q) & 0 & \omega_r X_{akq} & 0 \\ (X_E + \omega_r X_d) & (r_a + R_E) & -\omega_r X_{afd} & 0 & -\omega_r X_{akd} \\ 0 & 0 & -r_{fd} & 0 & 0 \\ 0 & 0 & 0 & -r_{kq} & 0 \\ 0 & 0 & 0 & 0 & -r_{kd} \end{bmatrix} \quad (3.22)$$

$$D = \begin{bmatrix} V_0 \sin(\delta_r) + e_{cd} \\ V_0 \cos(\delta_r) + e_{cq} \\ r_{fd} E_{fd} / X_{afd} \\ 0 \\ 0 \end{bmatrix}, \quad E = \begin{bmatrix} \mu k X_{L1} & 0 & 0 & 0 & 0 \\ 0 & \mu k X_{L1} & 0 & 0 & 0 \end{bmatrix}, \quad F = \begin{bmatrix} 0 & 1 \\ -1 & 0 \end{bmatrix} \quad (3.23)$$

The numerical parameters of the electrical system in p.u. are listed below.

$$\begin{aligned} X_d &= 1.65, & X_q &= 1.59, & X_{fd} &= 1.6286, & X_{kd} &= 1.642, & X_{kq} &= 1.5238, \\ X_{akd} &= 1.51, & X_{akq} &= 1.45, & X_{afd} &= 1.51, & X_{fkd} &= 1.51, & r_a &= 0.0045, \\ r_{fd} &= 0.00096, & r_{kd} &= 0.016, & r_{kq} &= 0.0116, & X_{TR} &= 0.12, & R_{TR} &= 0.0012, \\ X_{L1} &= 0.48, & R_1 &= 0.0444, & X_{L2} &= 0.4434, & R_2 &= 0.0402, & X_b &= 0.18, \\ R_b &= 0.0084 \end{aligned}$$

3.2 Mechanical System

The mechanical system consists of a high pressure (HP) turbine, a low pressure (LP) turbine, a generator and an exciter (Exc.). Fig. 3.4 shows the schematic diagram of the mechanical system.

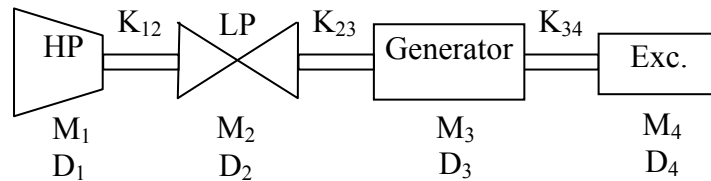


Figure 3.5 : Schematic diagram of the mechanical system

The equations governing dynamics of the mechanical system can be written as follows [62].

HP Turbine:

$$\frac{d\omega_1}{dt} = \frac{1}{M_1} [-D_1(\omega_1 - 1) - K_{12}(\theta_1 - \theta_2)] \quad (3.24)$$

$$\frac{d\theta_1}{dt} = \omega_b(\omega_1 - 1) \quad (3.25)$$

LP Turbine:

$$\frac{d\omega_2}{dt} = \frac{1}{M_2} [-D_2(\omega_2 - 1) + K_{12}(\theta_1 - \theta_2) - K_{23}(\theta_2 - \delta_r)] \quad (3.26)$$

$$\frac{d\theta_2}{dt} = \omega_b(\omega_2 - 1) \quad (3.27)$$

Generator:

$$\frac{d\omega_r}{dt} = \frac{1}{M_3} [T_m - T_e - D_3(\omega_r - 1) + K_{23}(\theta_2 - \delta_r) - K_{34}(\delta_r - \theta_4)] \quad (3.28)$$

$$\frac{d\delta_r}{dt} = \omega_b(\omega_r - 1) \quad (3.29)$$

Exciter:

$$\frac{d\omega_4}{dt} = \frac{1}{M_4} [-D_4(\omega_4 - 1) + K_{34}(\delta_r - \theta_4)] \quad (3.30)$$

$$\frac{d\theta_4}{dt} = \omega_b(\omega_4 - 1) \quad (3.31)$$

Defining the state variables as $\mathbf{R}_s = [\omega_1 \ \theta_1 \ \omega_2 \ \theta_2 \ \omega_r \ \delta_r \ \omega_4 \ \theta_4]^T$, $\mathbf{R}_s \in \mathbb{R}^8$, and using (3.24)-(3.31), we write the equations representing the mechanical system in state space form as follows:

$$\frac{d\mathbf{R}_s}{dt} = \mathbf{G} \mathbf{R}_s + \mathbf{H} \quad (3.32)$$

where

$$G = \begin{bmatrix} \frac{-D_1}{M_1} & \frac{-K_{12}}{M_1} & 0 & \frac{K_{12}}{M_1} & 0 & 0 & 0 & 0 \\ \omega_b & 0 & 0 & 0 & 0 & 0 & 0 & 0 \\ 0 & \frac{K_{12}}{M_2} & \frac{-D_2}{M_2} & \frac{-(K_{12}+K_{23})}{M_2} & 0 & \frac{K_{23}}{M_2} & 0 & 0 \\ 0 & 0 & \omega_b & 0 & 0 & 0 & 0 & 0 \\ 0 & 0 & 0 & \frac{K_{23}}{M_3} & \frac{-D_3}{M_3} & \frac{-(K_{23}+K_{34})}{M_3} & 0 & \frac{K_{34}}{M_3} \\ 0 & 0 & 0 & 0 & \omega_b & 0 & 0 & 0 \\ 0 & 0 & 0 & 0 & 0 & \frac{K_{34}}{M_4} & \frac{-D_4}{M_4} & \frac{-K_{34}}{M_4} \\ 0 & 0 & 0 & 0 & 0 & 0 & \omega_b & 0 \end{bmatrix} \quad (3.33)$$

$$H = \left[\frac{D_1}{M_1} \quad -\omega_b \quad \frac{D_2}{M_2} \quad -\omega_b \quad \frac{(T_m - T_e + D_3)}{M_3} \quad -\omega_b \quad \frac{D_4}{M_4} \quad -\omega_b \right]^T \quad (3.34)$$

In (3.34), T_e represents the electromechanical torque and it is expressed as

$$T_e = (X_q - X_d) i_d i_q + X_{afd} i_f i_q - X_{akq} i_{kq} i_d + X_{akd} i_{kd} i_q \quad (3.35)$$

The numerical parameters of the mechanical system in p.u. are as follows

$$D_1 = 0.0498, \quad M_1 = 0.498, \quad K_{12} = 42.6572$$

$$D_2 = 0.031 \quad M_2 = 3.1004 \quad K_{23} = 83.3823$$

$$D_3 = 0.1758 \quad M_3 = 1.7581 \quad K_{34} = 3.7363$$

$$D_4 = 0.0014 \quad M_4 = 0.0138$$

3.3 Complete Mathematical Model

The complete mathematical model of the nonlinear dynamical system in the state representation form is obtained by combining (3.19), (3.20) and (3.32). The dynamic system has 15 state variables: $i_d, i_q, i_f, i_{kq}, i_{kd}, e_{cd}, e_{cq}, \omega_1, \theta_1, \omega_2, \theta_2, \omega_r, \delta_r, \omega_4, \theta_4$. There are 4 control parameters: Mechanical torque input (T_m), Field voltage (E_{fd}), Infinite busbar voltage (V_0) and the series compensation factor (μ).

Defining the state vector $\mathbf{x} = [i_g^T \mathbf{V}_c^T \mathbf{R}_s^T]^T$, $\mathbf{x} \in \mathbb{R}^{15}$, we write

$$\dot{\mathbf{x}} = \begin{bmatrix} \mathbf{B}^{-1} \omega_b (\mathbf{C} \mathbf{i}_g + \mathbf{D}) \\ \omega_b (\mathbf{E} \mathbf{i}_g + \mathbf{F} \mathbf{e}_c) \\ \mathbf{G} \mathbf{R}_s + \mathbf{H} \end{bmatrix} \quad (3.36)$$

3.4 Bifurcation Analysis

We use the series compensation factor ($\mu=X_c/X_{L1}$) as the bifurcation parameter and perform bifurcation analysis by monitoring the real parts of the eigenvalues of the Jacobian matrix at the system equilibrium for values of μ from 0 to 1. The other three control parameters are kept constant at set values $T_m=0.91$, $E_{fd}=2.2$ and $V_0=1.0$.

3.4.1 Equilibrium Solutions

In order to obtain the equilibrium solutions for the model, standard methods for solving the initial value problems of the ordinary differential equations are employed. The equilibrium points for no series compensation case (i.e. $\mu=0$) are calculated first. To begin with, we set the angular speeds to the nominal value and the rotor angles to the load angle.

$$\omega_r = \omega_1 = \omega_2 = \omega_4 = 1 \quad (3.37)$$

$$\theta_1 = \theta_2 = \theta_4 = \delta_r \quad (3.38)$$

No current flows through the damper windings in the equilibrium condition.

$$i_{kq0} = i_{kd0} = 0 \quad (3.39)$$

Series capacitor d-q axes voltages are set to zero for $\mu=0$ at which the bifurcation analysis is started.

$$e_{cd0} = e_{cq0} = 0 \quad (3.40)$$

With known values of T_m , E_{fd} and V_0 , the load angle initial value is selected as p.u. value of the mechanical torque input.

$$\delta_{r0} = T_m \quad (3.41)$$

Using (3.19), initial values for the state variables \mathbf{i}_g can be written as

$$\mathbf{i}_{g0} = [i_{d0} \ i_{q0} \ i_{f0} \ i_{kq0} \ i_{kd0}]^T = -\mathbf{C}^{-1}\mathbf{D} \quad (3.42)$$

Having found the initial values of the state variables, the set of ordinary differential equations in (3.36) describing the dynamic model is solved using MATLAB. The

rest of the procedure is quite straightforward. The series compensation factor is increased to 1.0 at 0.001 incremental steps and at each step the equilibrium points are obtained by setting the previous step's equilibrium solutions as the initial values and solving the current ODEs.

3.4.2 Stability of the Equilibrium Points

The eigenvalues of the Jacobian matrix evaluated at the equilibrium points of the model for values of μ from 0 to 1 are determined. In a stable system, real parts of all eigenvalues are less than zero. Fig. 3.6 shows the generator rotor angle (δ_r) variation depending on the series compensation factor. Full use of the series compensation capacity enables the synchronous generator to operate at a power angle of 0.85 rad. instead of 1.05 rad., without the series capacitor. On the other hand, the system loses dynamic stability through a subcritical Hopf bifurcation at $\mu=0.5184$ due to the SSR as a result of interaction between the second torsional mode and the subsynchronous electrical mode. Even though the second torsional mode becomes stable again at $\mu=0.8110$, the first torsional mode stability is lost at $\mu=0.7283$ and therefore overall system stability is not regained.

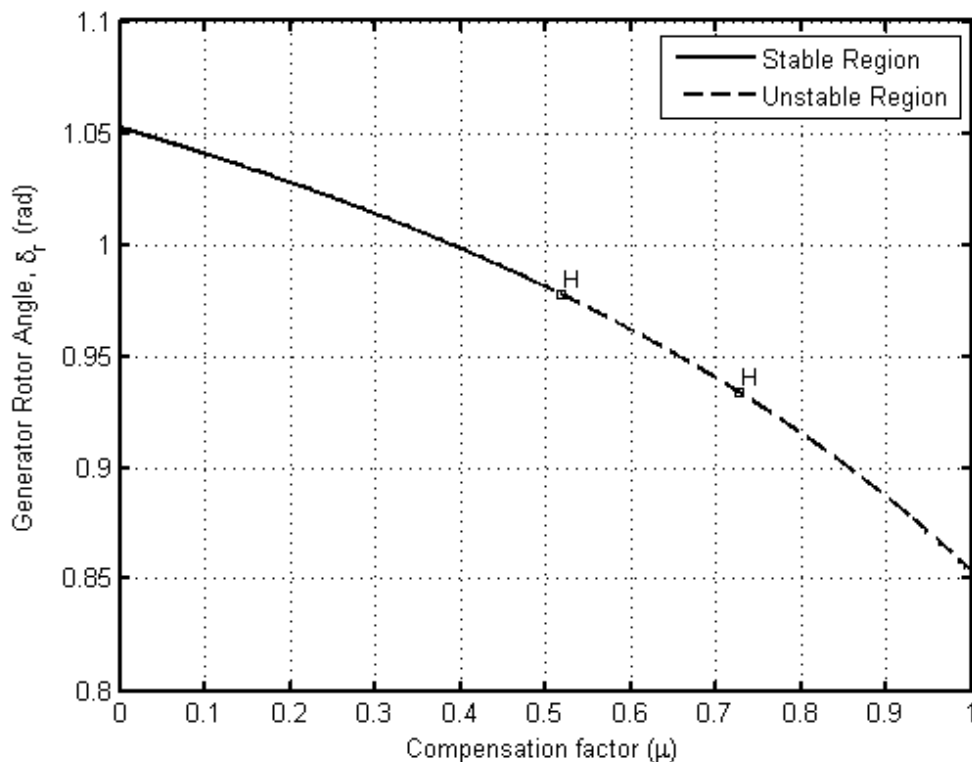


Figure 3.6 : Generator rotor angle ($T_m=0.91$, $E_{fd}=2.2$ and $V_0=1.0$)

3.4.3 Oscillatory Modes

The Jacobian matrix at the equilibrium condition has 6 pairs of complex conjugate eigenvalues. Hence, there are 6 modes of oscillation in the model. Supersynchronous and subsynchronous electrical modes have frequencies dependent on the series compensation level. The mechanical modes comprise one local swing mode and three torsional oscillation modes. Also called electro-mechanical mode, the local swing mode plays an important part in dynamic stability of a power system. In this mode, the turbine-generator shaft sections oscillate as a rigid rotating mass. In the model, the local swing mode has a frequency of 1.53 Hz. On the other hand, if the torsional modes are excited, some of the shaft masses oscillate against the others causing loss of fatigue life and eventually the shaft damage [63] in the absence of sufficient damping. In the model, there are three torsional oscillation modes with frequencies of 24.7, 32.4 and 51.1 Hz. Fig. 3.7 shows the relative rotation speed of shaft segments representing the mode shapes of the turbine-generator shaft system in the model.

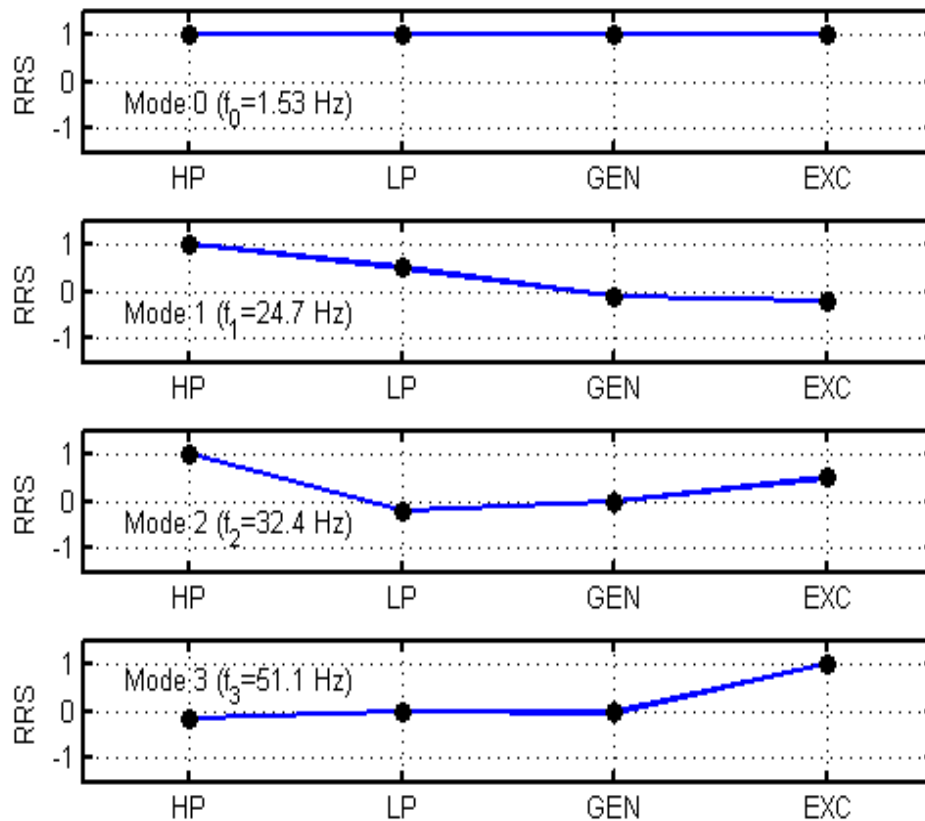


Figure 3.7 : Relative rotational speeds (RSS) representing the mode shapes

Relative rotation speeds have been determined by applying a small magnitude torque component with a frequency equal to one of the mechanical oscillation modes of the turbine-generator shaft system in order to excite the corresponding natural mode. The process is repeated for all four mechanical modes. At each step, rotor speeds of each shaft section are obtained. The rotational speed values are then converted into the relative quantities and scaled. From the view point of fatigue deformation on the shaft, the local swing mode oscillations do not result in any damage associated with torsional fatigue. Of primary interest are the modes with the polarity reversals along the shaft, which can be very dangerous if the damping is not sufficient or they are self excited due to the SSR.

The flowchart of the bifurcation analysis is depicted in Fig. 3.8. The equilibrium solution for $\mu=0$, $T_m=0.91$, $E_{fd}=2.2$ and $V_0=1.0$ is obtained by solving (3.36). Then, the Jacobian matrix eigenvalues at incremental values of μ are evaluated and at each step, zero-crossing of the eigenvalues real parts are checked to detect the occurrence of a bifurcation condition. The first Lyapunov coefficient is computed if Hopf bifurcation occurs at the corresponding value of μ .

Fig.3.9 shows the oscillatory modes of the system depending on the series compensation factor. As the compensation factor increases, the subsynchronous electrical mode frequency decreases and interacts with all three torsional modes. The interaction between the oscillatory modes results in movement of the real part of the corresponding eigenvalues towards to the zero-axis, as shown in Fig.3.10. The oscillatory modes other than the torsional modes are highly damped and therefore they are not shown in Fig. 3.10.

The interaction between the subsynchronous electrical mode and the third torsional mode occurs at $\mu=0.07$ without causing instability. The real part of the second torsional mode eigenvalue crosses the zero-axis at $\mu=0.5184$, as a result of interaction with the subsynchronous electrical mode, and the system stability of equilibrium is lost through a Hopf bifurcation. Even though the second torsional mode becomes stable again at $\mu=0.8110$, the overall system stability is not regained due to the Hopf bifurcation occurring at $\mu=0.7283$ in the first torsional mode which strongly interacts with the subsynchronous electrical mode.

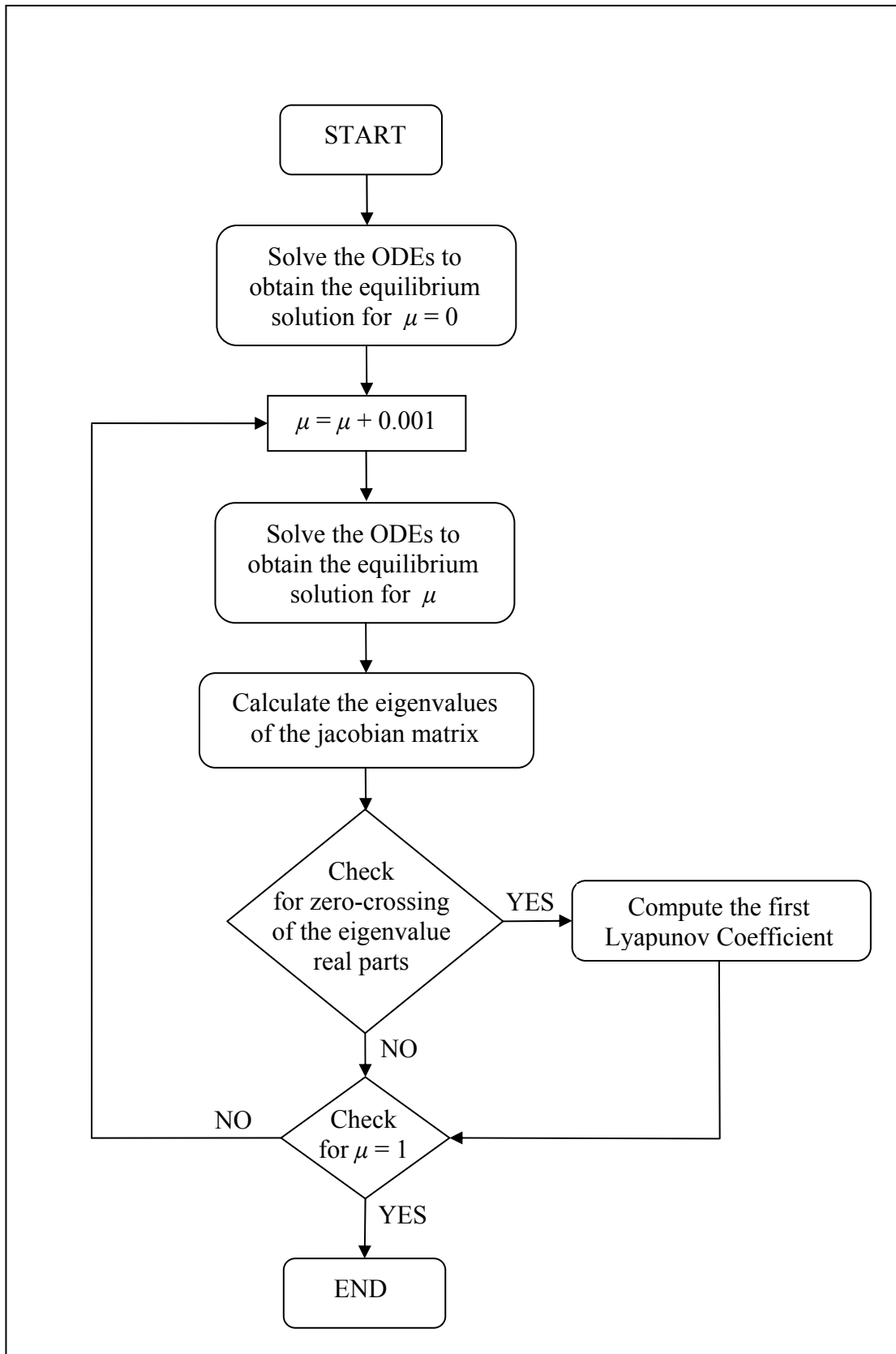


Figure 3.8 : The flowchart for Bifurcation Analysis

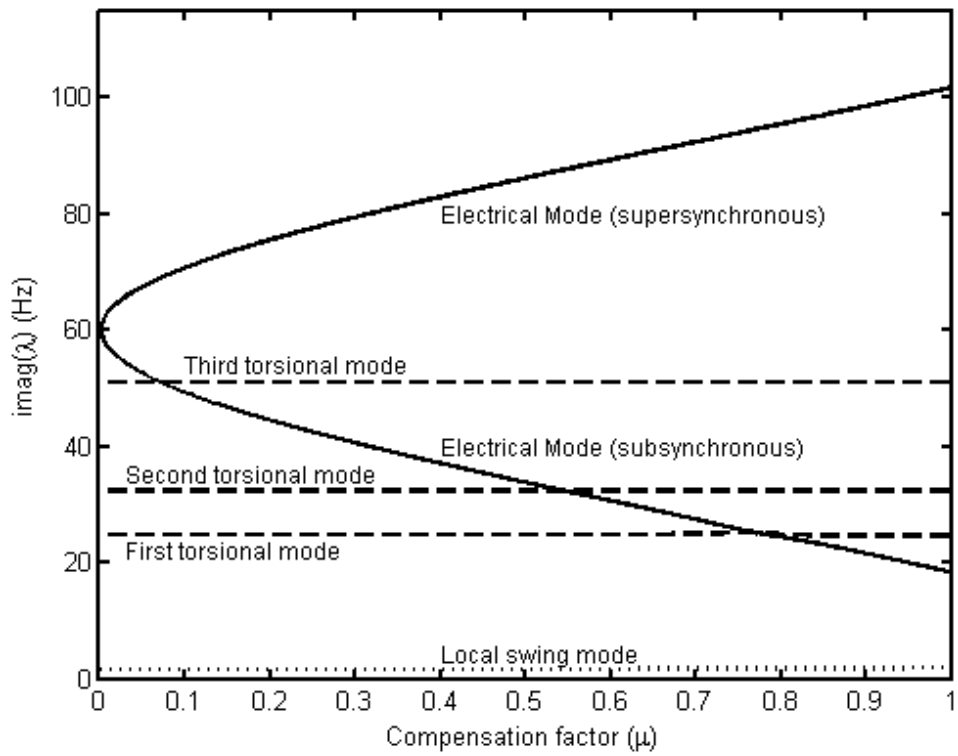


Figure 3.9 : Oscillation modes of the system

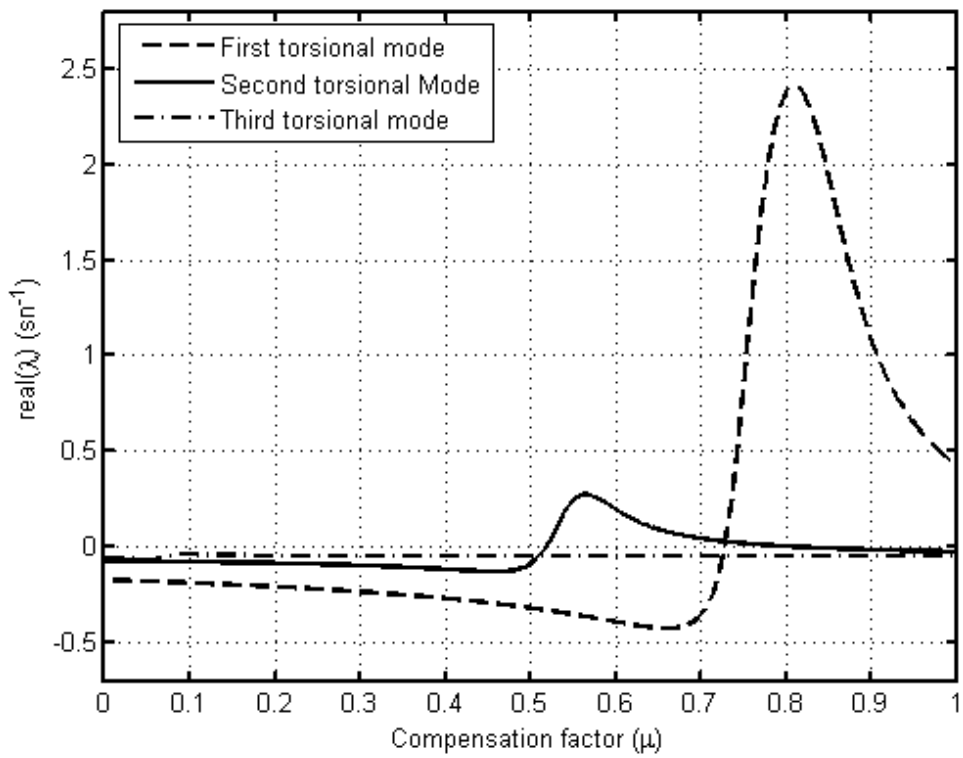


Figure 3.10 : Real parts of the torsional mode eigenvalues

Table 3.1: Computed Eigenvalues for $\mu=0.5184$ and $\mu=0.7283$

| Eigen- value Number | $\mu=0.5184$ | | | $\mu=0.7283$ | | |
|---------------------------|------------------------------------|------------------------------|---------------------------|------------------------------------|------------------------------|---------------------------|
| | Real Part (s ⁻¹) | Imaginary Part (Rad/s) | Imaginary Part (Hz) | Real Part (s ⁻¹) | Imaginary Part (Rad/s) | Imaginary Part (Hz) |
| 1, 2 | -10.403 | ± 544.841 | 86.714 | -10.920 | ± 585.699 | 93.217 |
| 3, 4 | -0.049 | ± 321.038 | 51.095 | -0.049 | ± 321.038 | 51.095 |
| 5, 6 | -8.375 | ± 208.336 | 33.158 | -8.599 | ± 166.123 | 26.439 |
| 7, 8 | 0 | ± 203.754 | 32.428 | 0.027 | ± 203.362 | 32.366 |
| 9, 10 | -0.332 | ± 155.645 | 24.772 | 0 | ± 157.301 | 25.035 |
| 11 | -27.703 | | | | | |
| 12, 13 | -0.956 | ± 10.317 | 1.642 | -1.111 | ± 10.807 | 1.720 |
| 14 | -0.288 | | | | | |
| 15 | -7.661 | | | | | |

Table 3.1 shows the eigenvalues of the SMIB power system at Hopf bifurcation points $\mu=0.5184$ and $\mu=0.7283$. In order to compute the first Lyapunov coefficient, computation of the complex vectors p and q satisfying (2.11) and (2.12) has been performed according to the procedure described in Appendix-A.1. Table 3.2 gives p and q complex vectors.

Table 3.2: Complex vectors p and q for $\mu=0.5184$ and $\mu=0.7283$

| $\mu=0.5184$ | | $\mu=0.7283$ | |
|---------------------|---------------------|---------------------|---------------------|
| Complex vector, p | Complex vector, q | Complex vector, p | Complex vector, q |
| -0.1568168987 | 0.0921782393 | -0.1992053453 | 0.4326843035 |
| -0.4726205366 | 0.0107718912 | -0.5046542364 | 0.2176372442 |
| -0.0608214353 | -0.0749905653 | -0.0766285818 | -0.3709173982 |
| -0.4487179858 | -0.0088150010 | -0.4786297979 | -0.1827961665 |
| -0.0914763745 | -0.0749384790 | -0.1169180864 | -0.3695424263 |
| -0.1603110936 | 0.0075350728 | -0.2228731617 | 0.0905822721 |
| 0.0446754154 | -0.0549391636 | 0.0758401959 | -0.1570033202 |
| -0.0302496636 | -0.1848909092 | 0.0143495701 | 0.3753247283 |
| -0.3648369095 | -0.8045114295 | 0.1427655113 | 1.1683608664 |
| 0.0087648208 | 0.3229436519 | 0.0033252031 | 0.5546827353 |
| 0.1041756487 | 1.4310469041 | 0.0333880582 | 1.6997876514 |
| -0.0072784961 | -0.1361024685 | -0.0104513585 | -0.9664520014 |
| -0.0824227770 | -0.6627130851 | -0.1040389355 | -3.1113374694 |
| -0.0122943119 | -0.0017954127 | -0.0138075703 | -0.0099981937 |
| -0.1389246074 | -0.0085128663 | -0.1373240889 | -0.0311432479 |

Using (2.13), $l_1(0)$ for the Hopf bifurcation occurring in the second torsional mode at $\mu=0.5184$ is computed as 1.44×10^{-5} . The positive sign of $l_1(0)$ reveals that the type of Hopf bifurcation is subcritical. Similarly, the first torsional mode undergoes a subcritical Hopf bifurcation at $\mu=0.7283$ with positive $l_1(0)$ ($=3.95 \times 10^{-5}$).

3.5 Time Domain Simulations

Time domain simulations using the software MATLAB-Simulink are carried out to verify the analytic findings of the bifurcation analysis. The set of ODEs representing the nonlinear dynamic model under study has been included into the Simulink model as embedded m-file. By this way, complexity of the model has been reduced significantly.

Fig. 3.11 shows the generator rotor angular speed response to a disturbance of 0.46 p.u. negative pulse torque (50% of the applied mechanical torque) on the generator shaft at $t=1$ s for a duration of 0.5s at the first Hopf bifurcation point ($\mu_{H1}=0.5184$). Following the disturbance, the generator rotor speed oscillates at decaying magnitudes but never reaches equilibrium state. Power Spectrum Density (PSD) estimation of the generator rotor angular speed confirms that small magnitude oscillations at the frequency of 32.4 Hz remain undamped as depicted in Fig. 3.12 in the PSD estimation. This is because of the fact that the real part of the second torsional mode eigenvalue is zero at $\mu = 0.5184$.

In a similar manner, the Hopf bifurcation occurring at $\mu=0.7283$ causes the first torsional mode oscillations to experience transition from damped to undamped condition. At the values of the series compensation factor from 0.7283 to 0.8110, two unstable oscillation modes with the frequencies of 32.4 Hz and 24.7 Hz co-exist in the dynamic model.

The simulation is repeated for $\mu=0.52$ by applying the same disturbance at $t=1$ s as in the simulations at Hopf bifurcation points. The initial response to the disturbance is similar to the cases with $\mu = \mu_H$ in a form that the magnitude of oscillations of the stable modes decays following the disturbance and becomes zero eventually. However, the unstable second torsional mode causes the oscillations with frequency 32.4 Hz. to reach to very high magnitudes without converging locally to an orbit as shown in Fig. 3.13. Therefore, it is concluded that the Hopf bifurcation is subcritical, verifying the analytic finding obtained by computing the first Lyapunov coefficient. The response of generator load angle for $\mu=0.52$ is also shown in Fig. 3.14. Similar to the response of the generator rotor angular speed, the load angle response is in the form of oscillations with increasing magnitude.

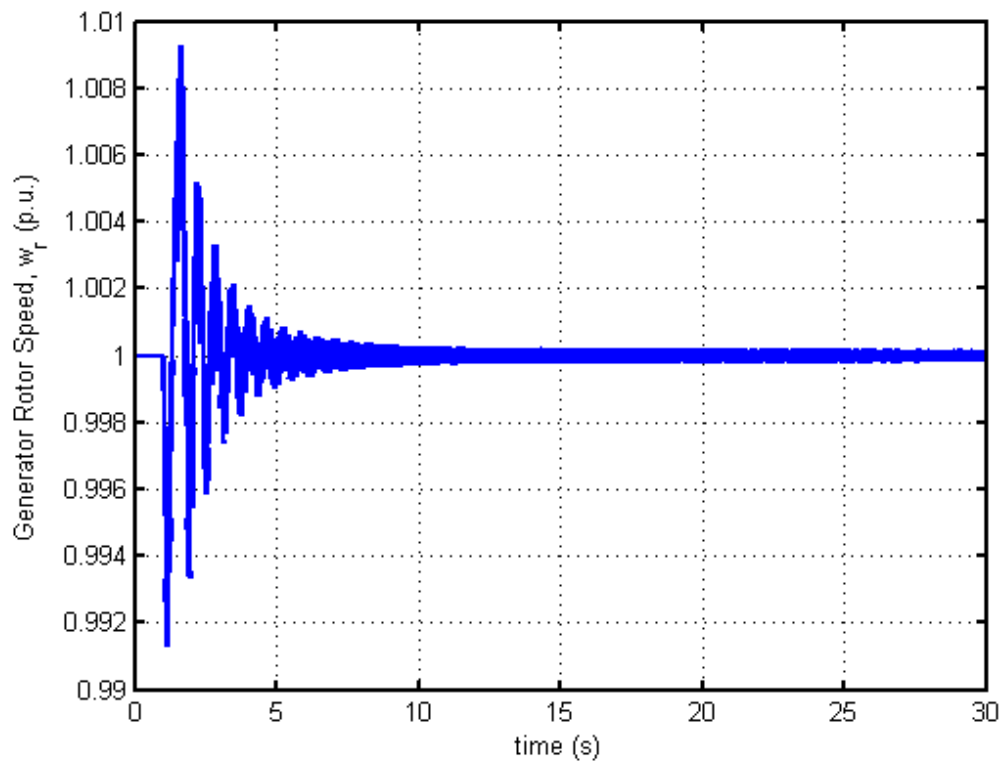


Figure 3.11 : Generator rotor speed (ω_r) response ($\mu = \mu_{H1}=0.5184$)

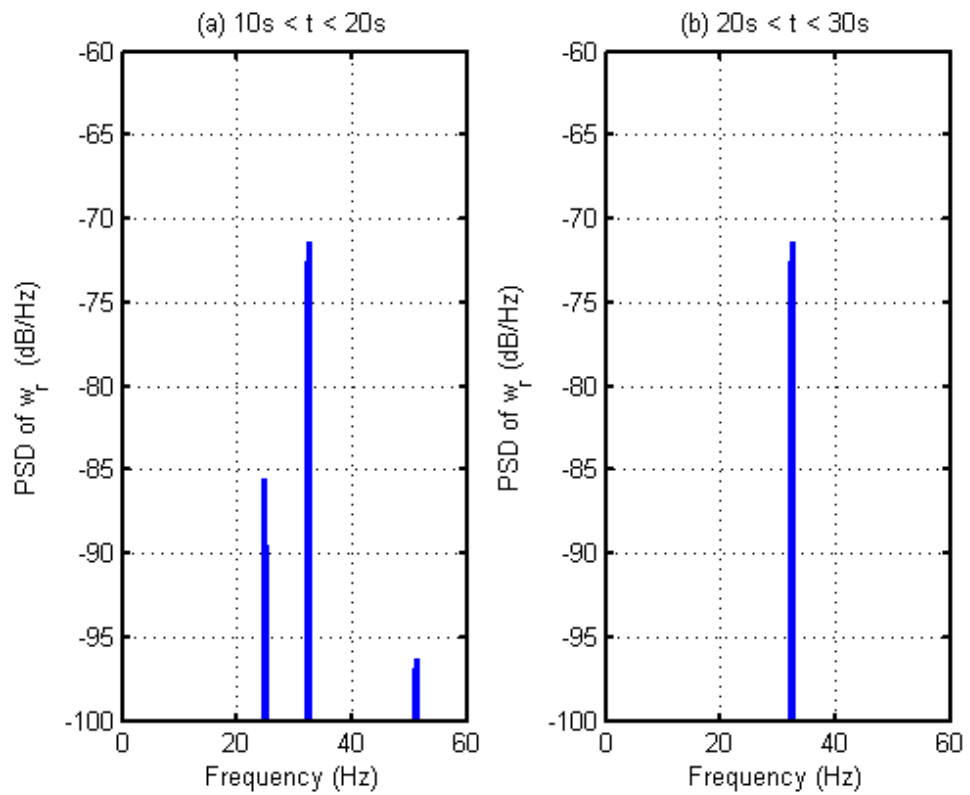


Figure 3.12 : PSD estimation of the generator rotor speed, (a) $10s < t < 20s$ and (b) $20s < t < 30s$

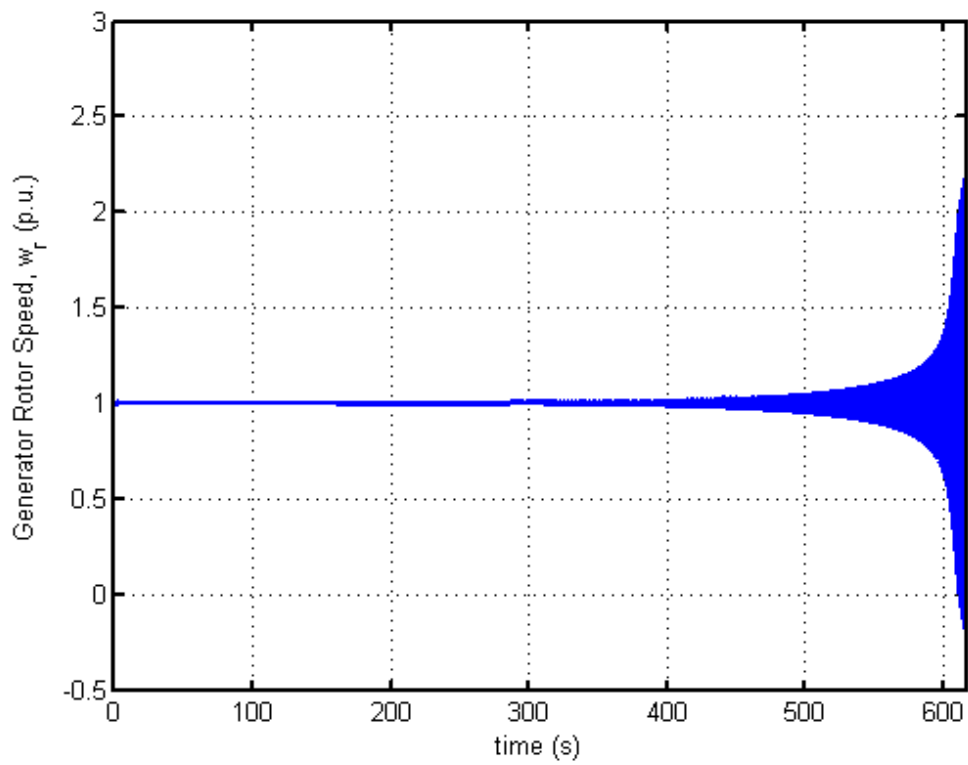


Figure 3.13 : Generator rotor speed (ω_r) response, $\mu=0.52$ ($\mu_H=0.5184$).

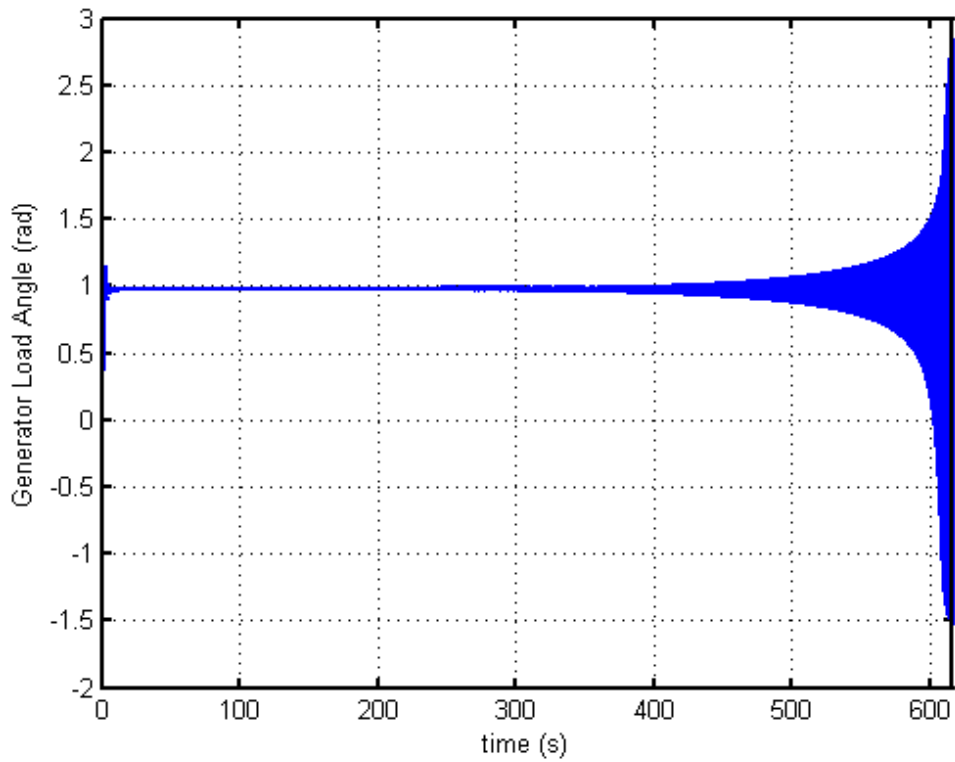


Figure 3.14 : Generator load angle ($\mu=0.52$) (Subcritical Hopf bifurcation)

It is important to note that in a real system the generator would lose synchronism and normally disconnect from the grid by the activation of protective relaying devices (e.g. out-of-step, over-speed protection) following a disturbance at the values of μ at which the SMIB power system is not stable.

Various forms of dynamic behaviors such as torus bifurcation, cyclic fold and bluesky catastrophe may occur in the instability region of the nonlinear model. Fig. 3.15 shows the generator rotor speed response exhibiting a Torus bifurcation at $\mu=0.55$. The emphasis in this Dissertation is given to determining the type of Hopf bifurcation, through which the stability of equilibrium condition is lost, by computing the first Lyapunov coefficient analytically.

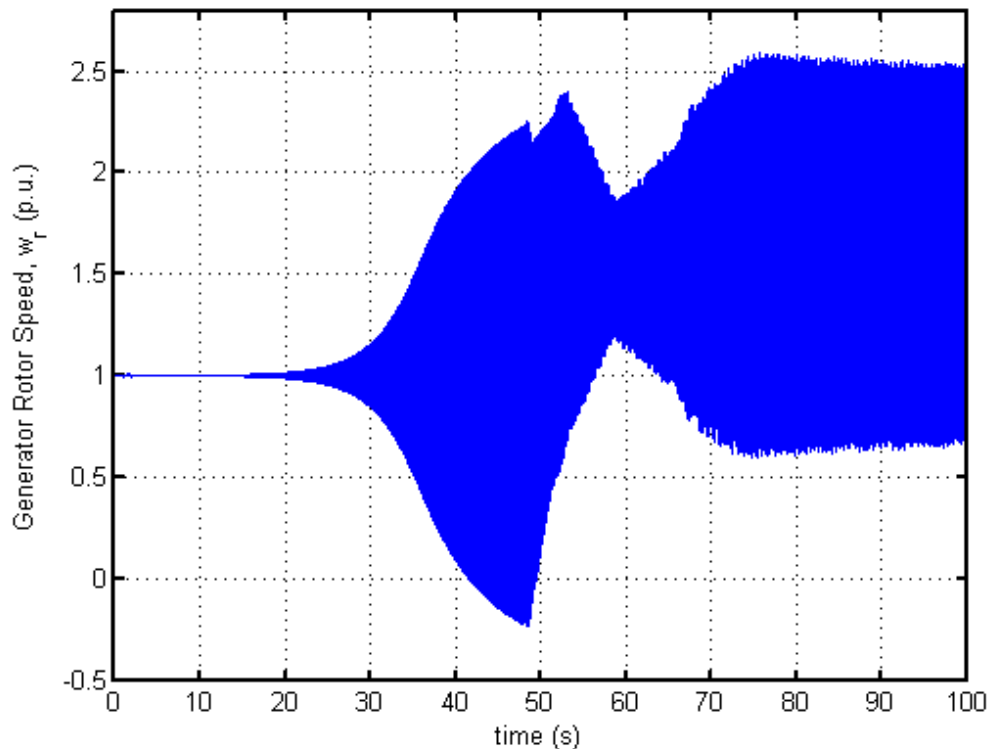


Figure 3.15 : Generator rotor speed response ($\mu=0.55$)

Depicting the subcritical Hopf bifurcation in the first torsional mode is not possible because of the second torsional mode which is already unstable at the point of Hopf bifurcation for this mode.

Fig 3.16 and Fig 3.17 depict the significant difference in the dynamic response of the generator rotor angular speed for $\mu=0.80$ and $\mu=0.82$, respectively.

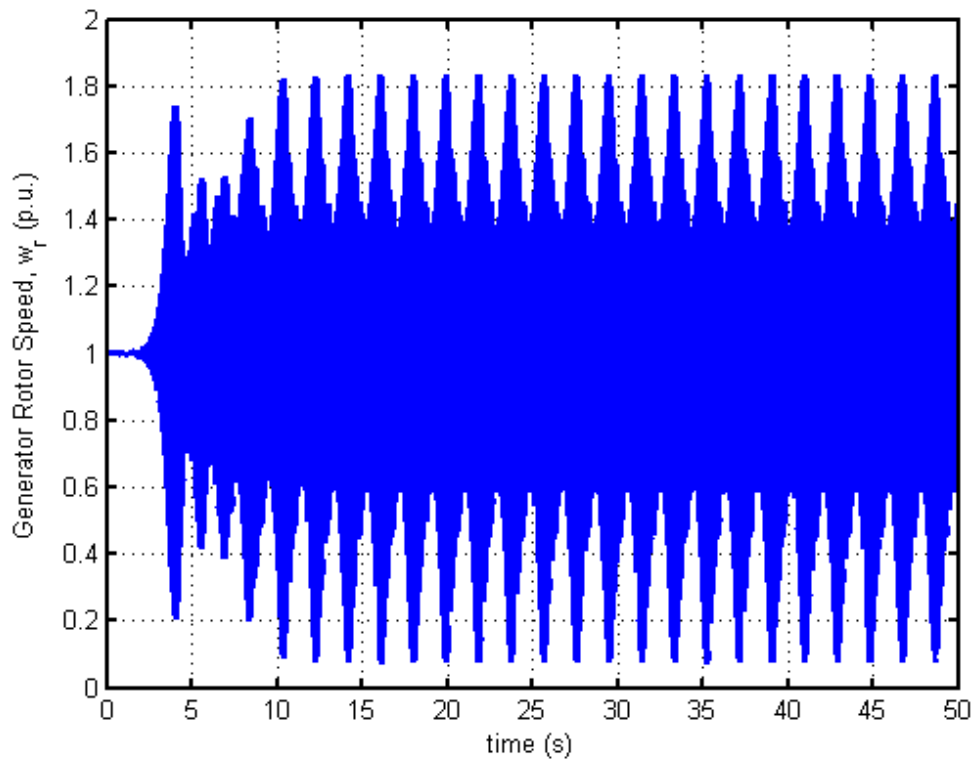


Figure 3.16 : Generator rotor speed response ($\mu=0.80$)

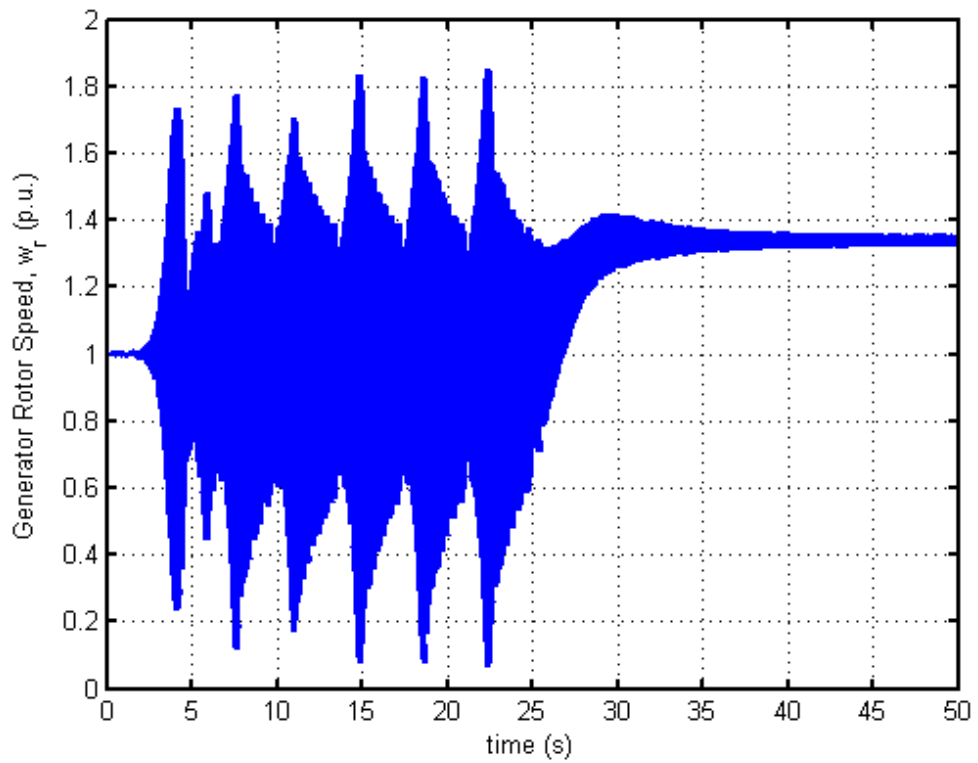


Figure 3.17 : Generator rotor speed response ($\mu=0.82$)

3.6 Parameter Dependency of the First Lyapunov Coefficient

In addition to the series compensation factor, the other control parameters T_m , V_0 and E_{fd} affect the dynamic behavior of the power system under study. In this section, the impact of these parameters on the bifurcation point and the first Lyapunov coefficient thereby on the type of Hopf bifurcations is discussed. Changes in the characteristic of the dynamic responses depending on the control parameters and the first Lyapunov coefficient will also be explored. Computing the first Lyapunov coefficient has the merit of investigating the impact of one parameter on the type of Hopf bifurcation thoroughly.

Furthermore, comparatively very small values of the computed first Lyapunov coefficients ($<2 \times 10^{-5}$) in Section 1.4 may raise a validation requirement that variations in the first Lyapunov coefficient be consistent. By investigating the parameter dependency, the accuracy of the computed first Lyapunov coefficient can also be verified.

It follows from Fig. 3.18 that increasing the mechanical torque input causes the Hopf bifurcation to occur at slightly higher series compensation levels. The first Lyapunov coefficient also increases with T_m , as depicted in Fig. 3.19. The second torsional mode $l_1(0)$ crosses zero at $T_m=0.62$ p.u.

The impact of T_m on the first Lyapunov coefficient is stronger in the second torsional mode compared to the first torsional mode. It is important to note that the supercritical Hopf bifurcation occurs in the first torsional mode at the values of the electromechanical torque input less than 0.62 p.u. The first torsional mode is unstable at these values. Therefore, validation of this analytic finding is not possible via time domain simulations.

From Fig. 3.20, one can conclude that the impact of the network voltage level on the Hopf bifurcation point is almost negligible. On the other hand, the variation of the second torsional mode $l_1(0)$ with V_0 is more significant, as shown in Fig. 3.21. The type of Hopf bifurcation for both the first torsional mode and the second torsional mode remains the same as the value of the network voltage is changed from 0.95 p.u. to 1.05 p.u.

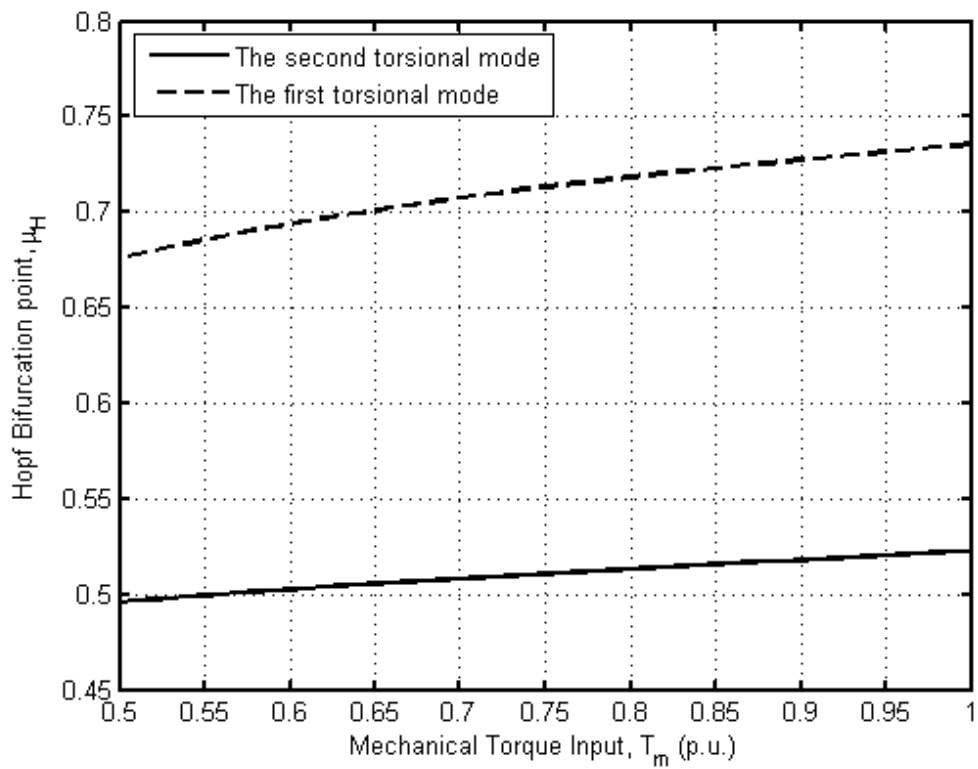


Figure 3.18 : Hopf Bifurcation points for varying values of T_m

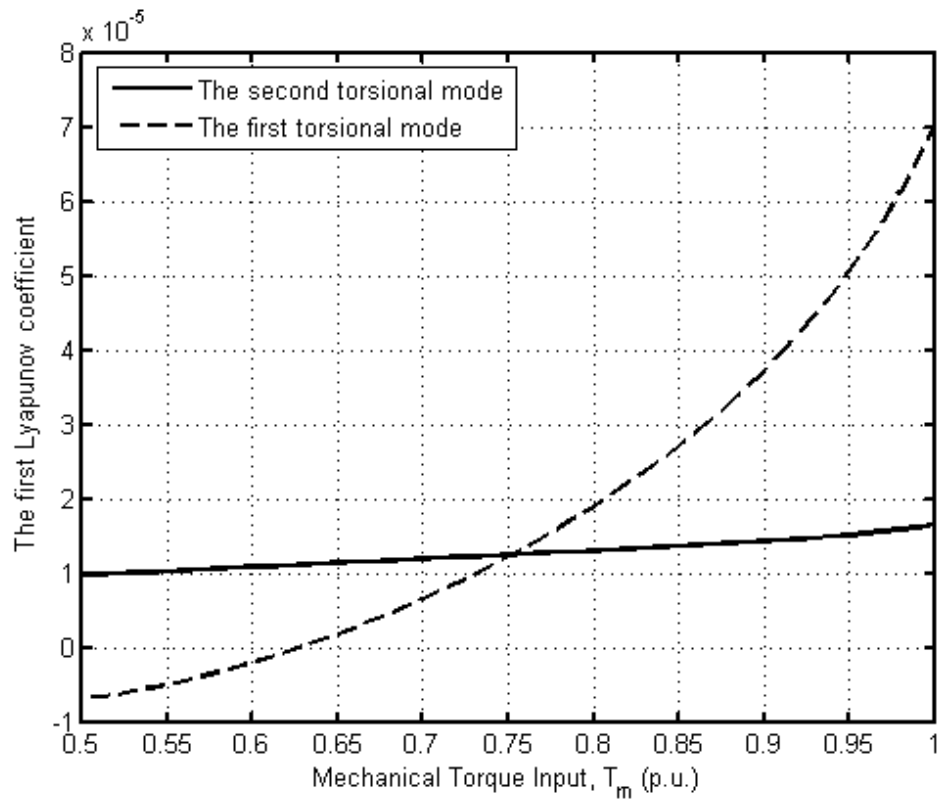


Figure 3.19 : The first Lyapunov coefficients for varying values of T_m

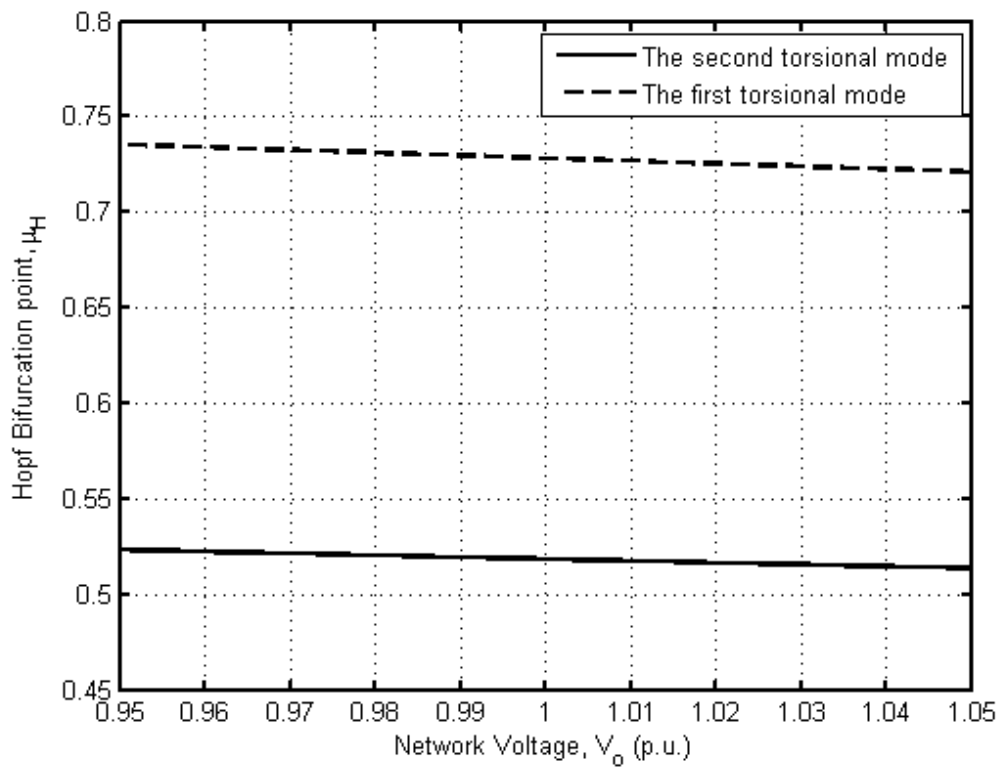


Figure 3.20 : Hopf Bifurcation points for varying values of V_0

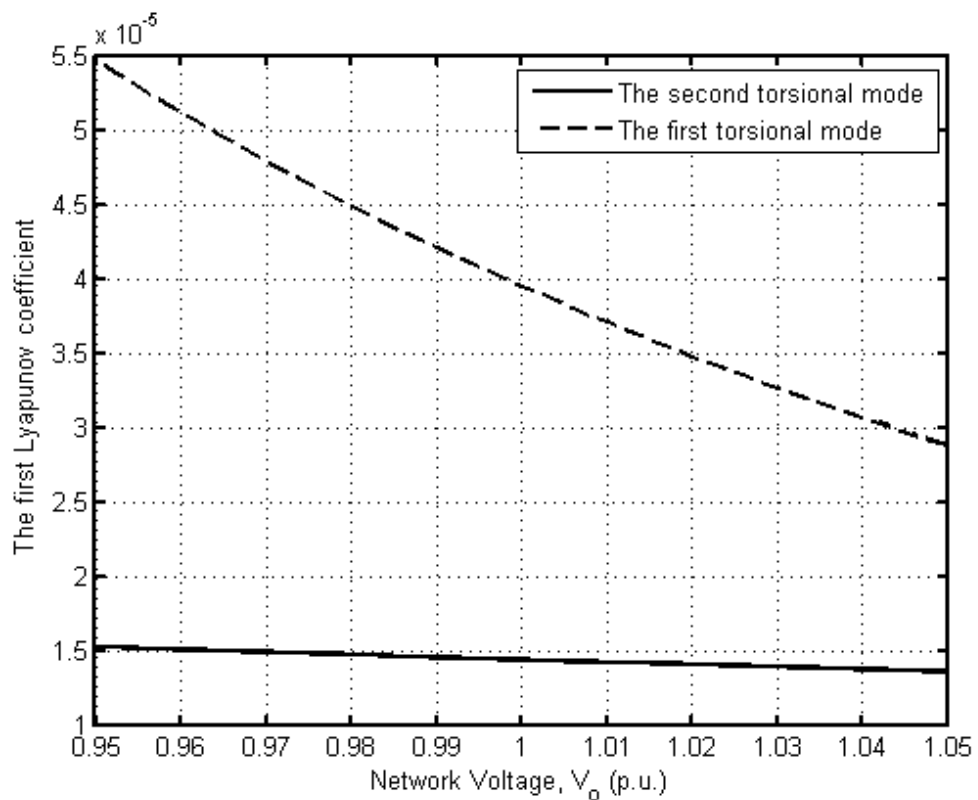


Figure 3.21 : The first Lyapunov coefficients for varying values of V_0

The impact of the field voltage on the Hopf bifurcation point and the first Lyapunov coefficient is in a way similar to that of the network voltage level. The Hopf bifurcation points slightly change as E_{fd} is increased from 2 p.u. to 3 p.u. as shown in Fig. 3.22. Moreover, from Fig. 3.23, the first Lyapunov coefficient of the second torsional mode is negative for $E_{fd} < 2.72$ p.u.

It is interesting to see that the impact of the control parameters on the first Lyapunov coefficient is consistent. Though very small, the changes in the computed $l_1(0)$ depending on an increase or decrease in one of the control parameters exhibit a regular pattern. Hence, the accuracy of the computation procedure for the first Lyapunov coefficient is considered to be adequate.

The analysis results show that the first Lyapunov coefficients remain positive and/or near zero for a wide range of the control parameters governing the dynamics of the system under study. Consequently, the regular pattern in the change of the first Lyapunov coefficients depending on a control parameter verifies the accuracy of the computation method.

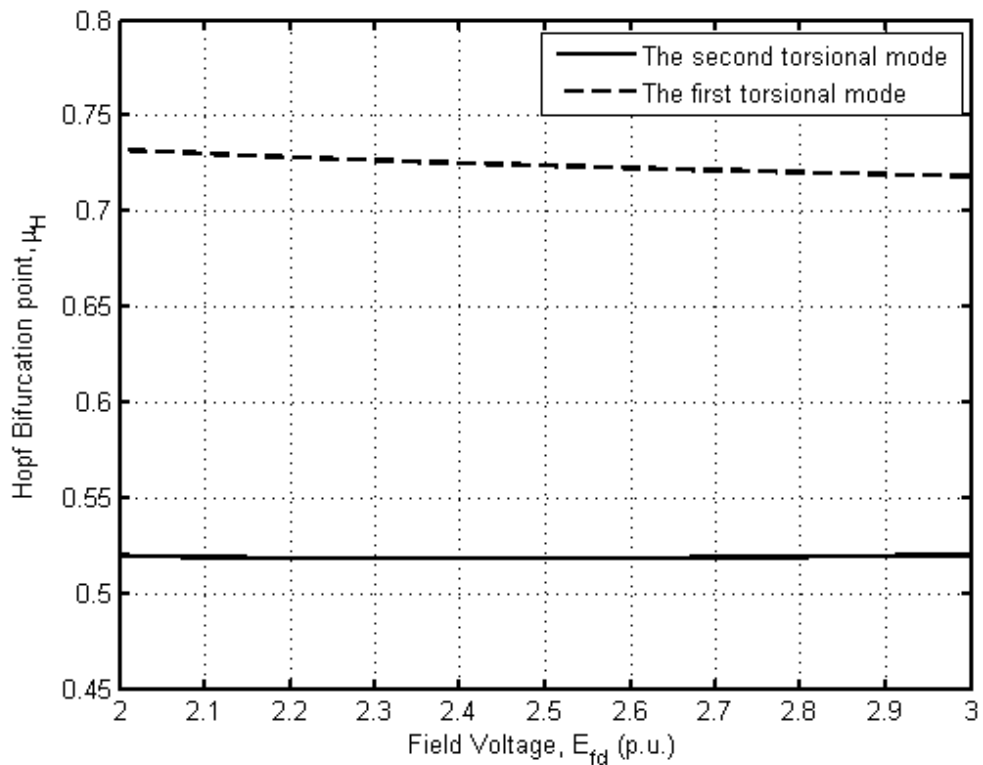


Figure 3.22 : Hopf Bifurcation points for varying values of E_{fd}

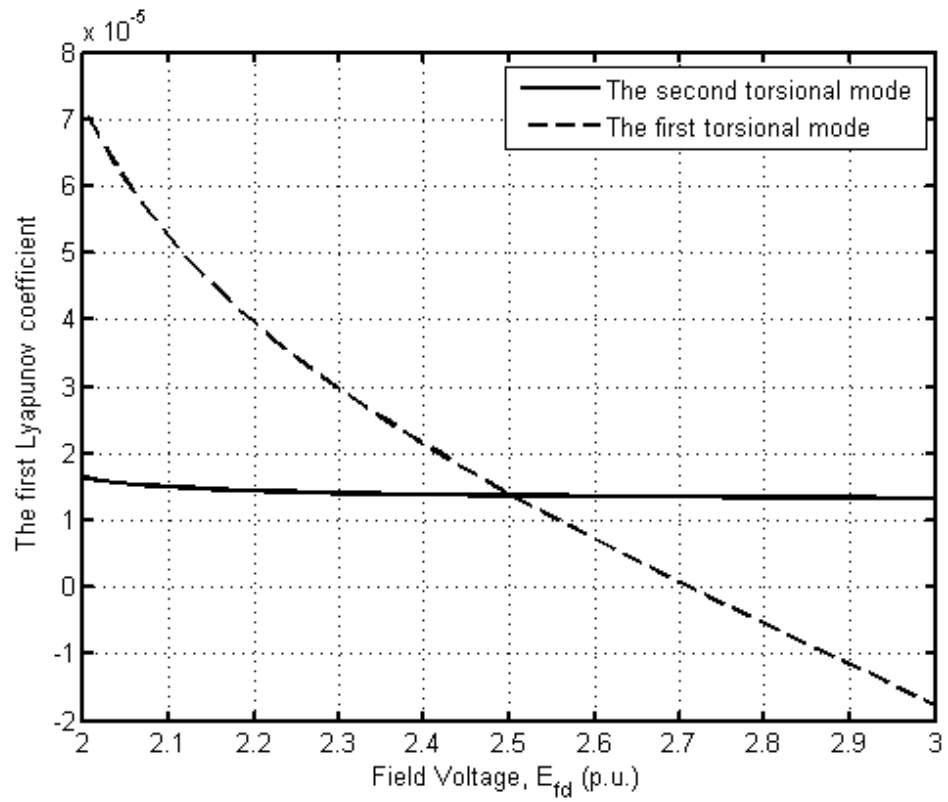


Figure 3.23 : The first Lyapunov coefficients for varying values of E_{fd}

4. SSR WITH AUTOMATIC VOLTAGE REGULATOR

In this chapter, we include an automatic voltage regulator (AVR) into the SMIB power system model analyzed in Chapter 3. The primary function of an AVR is to regulate the generator terminal voltage. In addition, AVR contributes to transient stability enhancement and regulation of reactive power flow from and to the generator. New oscillatory modes appear in the model due to the AVR but these modes are usually stable. The emphasis in this chapter is given to analyzing the impact of the AVR on the Hopf bifurcation point and the first Lyapunov coefficient which is used to identify the type of Hopf bifurcations (i.e. supercritical or subcritical) occurring in the SMIB power system under study.

4.1 Excitation System with AVR

Automatic Voltage Regulator (AVR) of type DC1A described in [64] are included into the excitation system in the model. The exciter saturation effects are neglected and the limiters are not taken into account. It is also possible to add a power system stabilizer (PSS) to the model. PSS can provide additional damping for the oscillations with frequency well below the torsional oscillation mode frequencies, which are the primary focus in this dissertation. Therefore, PSS is not included into the model.

Fig.4.1 shows the block diagram of the excitation system with AVR.

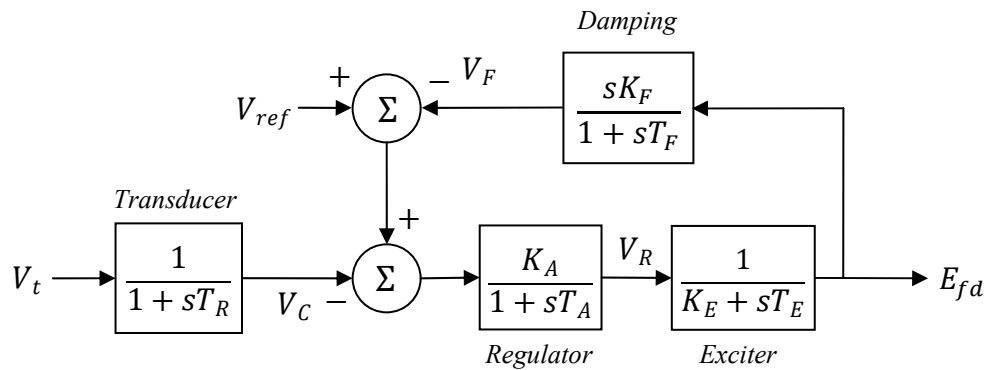


Figure 4.1 : Block diagram of the excitation system with AVR

Defining $\mathbf{V}_{exc}=[V_C V_F V_R E_{fd}]^T$, $\mathbf{V}_{exc} \in \mathbb{R}^4$, the state equations describing the dynamics of the excitation system with AVR can be written as follows:

$$\frac{d\mathbf{V}_{exc}}{dt}=\mathbf{P} \mathbf{V}_{exc}+\mathbf{Q} \quad (4.1)$$

where

$$\mathbf{P}=\begin{bmatrix} -\frac{1}{T_R} & 0 & 0 & 0 \\ 0 & -\frac{1}{T_F} & \frac{K_F}{T_F T_E} & -\frac{K_F K_E}{T_F T_E} \\ -\frac{K_A}{T_A} & -\frac{K_A}{T_A} & -\frac{1}{T_A} & 0 \\ 0 & 0 & \frac{1}{T_E} & -\frac{K_E}{T_E} \end{bmatrix} \quad (4.2)$$

$$\mathbf{Q}=\left[\frac{V_t}{T_R} \quad 0 \quad \left(\frac{K_A}{T_A} V_{ref}\right) \quad 0\right]^T \quad (4.3)$$

V_t in (4.3) is the generator terminal voltage. Neglecting the transients, it can be expressed as:

$$V_t=\sqrt{\left((-r_a i_d+X_q i_q)^2+\left(-r_a i_q-X_d i_d+X_{afd} i_{fd}\right)^2\right)} \quad (4.4)$$

Parameters of the excitation System with AVR are given below.

Regulator : $K_A=250$, $T_A=0.002s$

Exciter : $K_E=1$, $T_E=0.02s$

Damping : $K_F=0.03$, $T_F=1s$

Transducer : $T_R=0.020 s$

4.2 Complete Mathematical Model with AVR

We define the state vector $\mathbf{x}=[\mathbf{i}_g^T \mathbf{V}_c^T \mathbf{R}_s^T \mathbf{V}_{exc}^T]^T$, $\mathbf{x} \in \mathbb{R}^{19}$ and combine (3.19), (3.20), (3.32) and (4.1) as follows:

$$\dot{\mathbf{x}}=\begin{bmatrix} \mathbf{B}^{-1} \omega_b (\mathbf{C} \mathbf{i}_g+\mathbf{D}) \\ \omega_b (\mathbf{E} \mathbf{i}_g+\mathbf{F} \mathbf{V}_c) \\ \mathbf{G} \mathbf{R}_s+\mathbf{H} \\ \mathbf{P} \mathbf{V}_{exc}+\mathbf{Q} \end{bmatrix} \quad (4.5)$$

There are 19 state variables in the complete mathematical model: $i_d, i_q, i_f, i_{kd}, i_{kd}, e_{cd}, e_{cq}, \omega_1, \theta_1, \omega_2, \theta_2, \omega_r, \delta_r, \omega_4, \theta_4, V_C, V_F, V_R$ and E_{fd} . The control parameters vector consists of five variables: AVR gain (K_A), AVR Reference Voltage (V_{ref}), the series compensation factor (μ), mechanical torque input to the generator (T_m) and the network voltage level (V_0).

4.3 Bifurcation Analysis

We use the series compensation factor ($\mu = X_c/X_{L1}$) as the bifurcation parameter and carry out the bifurcation analysis by monitoring the real parts of the eigenvalues of the Jacobian matrix at system equilibrium solutions for the values of μ from 0 to 1. The other five control parameters are kept constant at set values ($T_m=0.91, K_A=250, V_0=1.0$ and $V_{ref}=1.0953$).

4.3.1 Equilibrium Solutions

In order to obtain the equilibrium solutions for the SMIB power system with AVR, firstly the initial values of the state variables $\mathbf{i}_g, \mathbf{e}_c$ and \mathbf{R}_s for the known values of T_m, V_0 and $E_{fd}(\mu=0)$ are determined as described in Section 3.3.1. Then, the generator terminal voltage (V_t) is calculated using (4.4). Then, the initial values of the excitation system state variables can be found as follows.

$$V_{C0} = V_t \quad (4.6)$$

$$V_{R0} = K_E E_{fd} \quad (4.7)$$

$$V_{F0} = 0 \quad (4.8)$$

The AVR reference voltage is computed as

$$V_{ref} = V_{C0} + E_{fd} / K_A \quad (4.9)$$

Accordingly, the equilibrium points of the set of ODEs in (4.5) are calculated for the values of μ from 0 to 1 at incremental steps of 0.001. At each step, the equilibrium solution obtained at the previous step is used as the initial values for the solution of the ODEs and equilibrium points are calculated for the current value of μ .

4.3.2 Stability of Equilibrium Solutions in SMIB Power System with AVR

The stability region of the equilibrium points is determined by computing the eigenvalues of the Jacobian matrix. The real parts of all eigenvalues are less than zero in a stable system. As shown in Fig. 4.2, Hopf bifurcations occur at $\mu = 0.51968$ and $\mu = 0.73448$.

Comparison of Fig 4.2 and Fig. 3.6 reveals that the generator rotor angle is less prone to variations in the series compensation factor in the model with AVR.

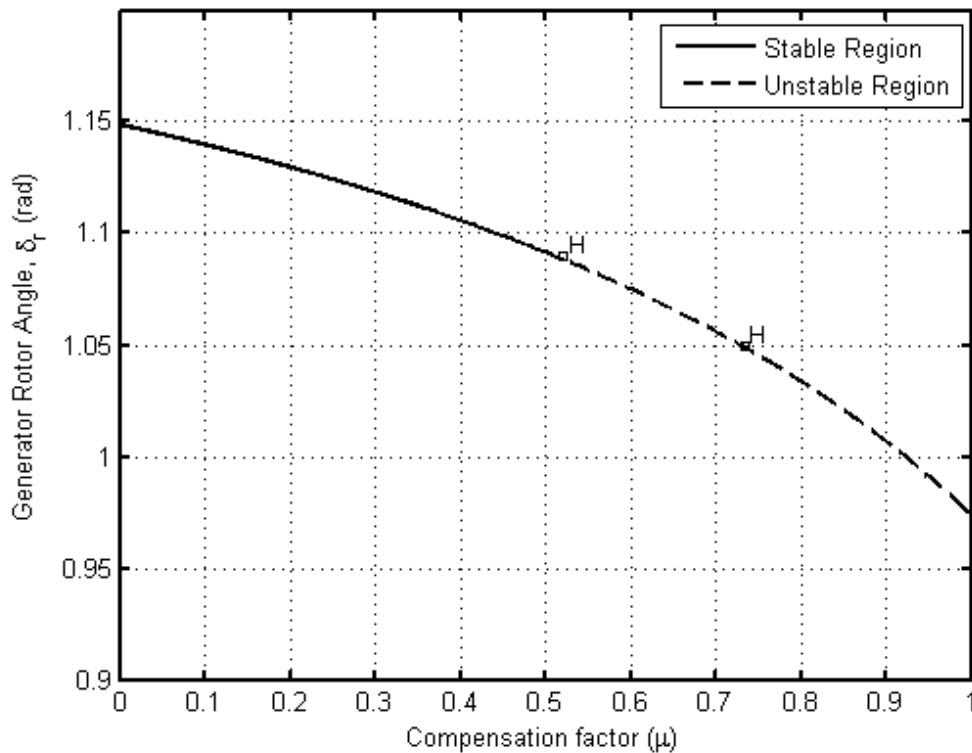


Figure 4.2 : Generator rotor angle ($T_m=0.91$, $K_A=250$, $V_0=1.0$ and $V_{ref}=1.0953$)

4.3.3 Oscillatory Modes

Fig. 4.3 shows the oscillatory modes of the SMIB power system model with AVR. In addition to the oscillatory modes identified in Chapter 3, two more oscillatory modes appear with frequencies 58.8 Hz and 6.1 Hz in the model due to the AVR.

As the series compensation factor increases, the subsynchronous electrical mode frequency decreases and interacts with all three torsional modes and one AVR oscillator mode resulting in movement of the real part of the corresponding eigenvalues towards to the zero-axis, as shown in Fig. 4.4.

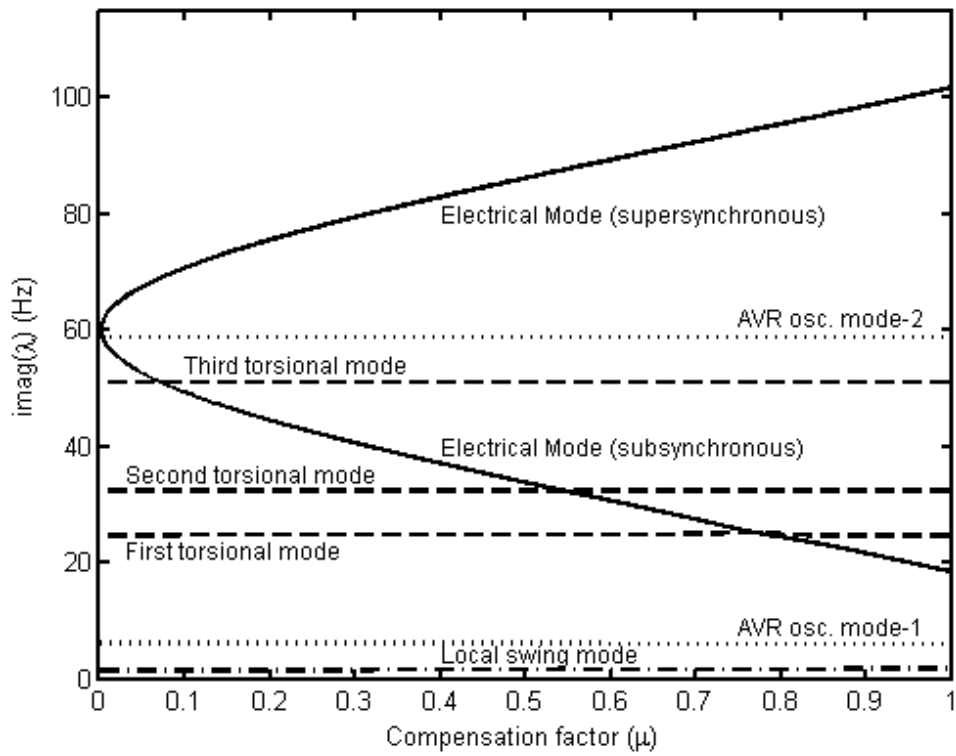


Figure 4.3 : Oscillation modes of the model with AVR

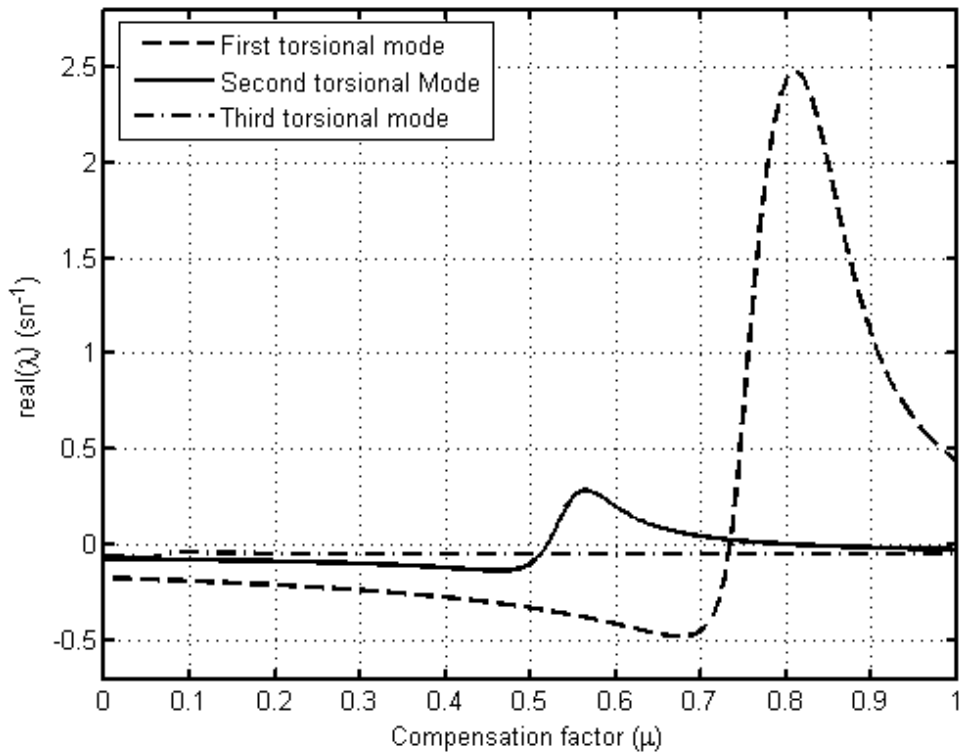


Figure 4.4 : Real parts of the torsional mode eigenvalues of the model with AVR

The subsynchronous electrical mode interacts with the third torsional mode at $\mu = 0.0701$ but the system stability is preserved. The real part of the second torsional mode eigenvalue crosses the zero-axis at $\mu = 0.5197$, as a result of interaction with the subsynchronous electrical mode and the system stability of equilibrium is lost through a Hopf bifurcation. Although the second torsional mode regains stability at $\mu = 0.8152$, the overall system stability is not regained because of the Hopf bifurcation occurring at $\mu = 0.7345$ in the first torsional mode.

Table 4.1 shows the eigenvalues of the SMIB power system with AVR at Hopf bifurcation points $\mu=0.5197$ and $\mu=0.7345$.

Table 4.1: Computed Eigenvalues for $\mu=0.5197$ and $\mu=0.7345$

| Eigen- value Number | $\mu=0.5197$ | | | $\mu=0.7345$ | | |
|---------------------------|---------------------------------|------------------------------|---------------------------|------------------------------------|------------------------------|---------------------------|
| | Real Part (s ⁻¹) | Imaginary Part (Rad/s) | Imaginary Part (Hz) | Real Part (s ⁻¹) | Imaginary Part (Rad/s) | Imaginary Part (Hz) |
| 1, 2 | -10.416 | ± 545.105 | 86.756 | -10.942 | 586.908 | 93.409 |
| 3, 4 | -277.539 | ± 369.418 | 58.795 | -277.545 | 369.432 | 58.797 |
| 5, 6 | -0.049 | ± 321.037 | 51.095 | -0.049 | 321.037 | 51.095 |
| 7, 8 | -8.083 | ± 208.057 | 33.113 | 0.026 | 203.359 | 32.366 |
| 9, 10 | 0.000 | ± 203.766 | 32.430 | -8.085 | 164.799 | 26.229 |
| 11, 12 | -0.344 | ± 155.596 | 24.764 | 0.000 | 157.451 | 25.059 |
| 13, 14 | -36.154 | ± 38.110 | 6.065 | -36.460 | 37.835 | 6.022 |
| 15, 16 | -1.225 | ± 9.785 | 1.557 | -1.502 | 10.204 | 1.624 |
| 17 | -6.860 | | | -6.961 | | |
| 18, 19 | -1.206 | ± 0.605 | 0.096 | -1.157 | ± 0.626 | 0.100 |

The complex vectors p and q satisfying (2.11) and (2.12) are given in Table 4.2. Using (2.13), the first Lyapunov coefficients at the Hopf bifurcation points $\mu_{H1} = 0.5197$ and $\mu_{H2} = 0.7345$ have been computed as -0.00015794 and -0.0026534, respectively. The negative sign of the first Lyapunov coefficients show that the type of Hopf bifurcation for both torsional modes is supercritical. The inclusion of AVR into the model under study results in the occurrence of supercritical Hopf bifurcations. For this reason, stable limit cycles are born out of the Hopf bifurcation points. On the contrary, the Hopf bifurcations are found subcritical in the model without AVR analyzed in Chapter 3. It is important to note that these findings are only valid in the local region of the Hopf bifurcation points. Various forms of bifurcations and nonlinear events may occur in the range of control parameter values, at which the dynamic system is not stable.

Table 4.2: Complex vectors p and q for $\mu=0.5197$ and $\mu=0.7345$

| $\mu=0.5197$ | | $\mu=0.7345$ | |
|---------------------|---------------------|---------------------|---------------------|
| Complex vector, p | Complex vector, q | Complex vector, p | Complex vector, q |
| -0.0052155981 | 1.5569366376 | 0.0020481012 | -7.2271383787 |
| -0.0289729037 | 0.4322003947 | 0.0284354742 | -6.6267268033 |
| -0.0024188405 | -1.2728005072 | 0.0009511072 | 6.2863643145 |
| -0.0275732938 | -0.3435249499 | 0.0271372379 | 5.4887412153 |
| -0.0027977159 | -1.2686517206 | 0.0013189771 | 6.2185692067 |
| -0.0101503441 | 0.2935219446 | 0.0132869309 | -2.7952478788 |
| 0.0011202924 | -0.9206675224 | 0.0000230088 | 2.5323445866 |
| -0.0043774193 | -9.5709197507 | -0.0019167871 | -28.3724877331 |
| -0.0191686049 | -13.4237484893 | -0.0059309603 | -20.4140472347 |
| 0.0012575492 | 16.9313157157 | -0.0004440404 | -41.1793620921 |
| 0.0054730428 | 23.9042259342 | -0.0013799266 | -29.4859646914 |
| -0.0010155458 | -7.4693154549 | 0.0013960282 | 72.9799536651 |
| -0.0043292280 | -11.1881568559 | 0.0043208010 | 54.8104882592 |
| -0.0017132946 | -0.0987440877 | 0.0018443686 | 0.7563486171 |
| -0.0072968791 | -0.1427577312 | 0.0057060071 | 0.5442932572 |
| -0.0056400788 | -0.0018091071 | 0.0066857968 | -0.0362531816 |
| 0.0017781911 | -0.0037297520 | -0.0028974343 | -0.0121242362 |
| 0.9708259733 | -0.0000122822 | -0.9551202873 | 0.0001124581 |
| 0.0581754304 | -0.0000359538 | -0.0948499864 | 0.0014424640 |

4.3.4 Time Domain Simulations

In order to verify the bifurcation analysis results, time domain simulations have been carried out in MATLAB-Simulink. The embedded M-file consisting of the set of ODEs obtained in (4.5) has been incorporated in the Simulink model. Fig. 4.6 shows the generator rotor speed response to a disturbance of 0.46 p.u. pulse torque on the synchronous generator shaft at $t=1s$ for a duration of 0.5s at the Hopf bifurcation point ($\mu_H = 0.5197$). Following the disturbance, the generator rotor speed oscillates at decaying magnitudes until the appearance of a limit cycle of small magnitude.

The second torsional mode has a pair of purely imaginary eigenvalues (i.e. zero real parts) at the Hopf bifurcation point, $\mu_H = 0.5197$. Hence, no decay or increase in the magnitude of oscillations in the second torsional mode with frequency is observed on the PSD estimation, even though the other two oscillatory modes disappear substantially within 20s following the disturbance, as shown in Fig. 4.6.

The simulation is repeated at a slightly higher compensation factor ($\mu=0.525$) and the generator rotor speed and load angle responses are shown in Figs. 4.7-8. The oscillations of small magnitude appear following the disturbance as in the case with $\mu=0.5197$. It is evident from Fig. 4.9 that the dynamic responses converge to a limit cycle.

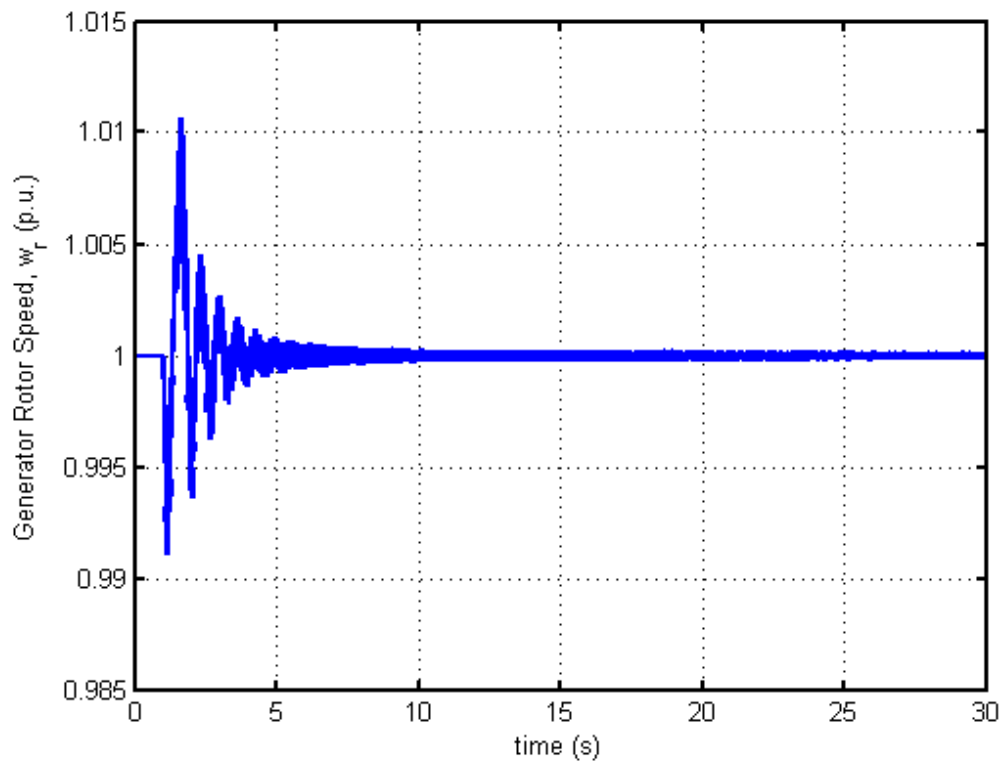


Figure 4.5 : Generator rotor speed response ($\mu=\mu_{H1}=0.5197$)

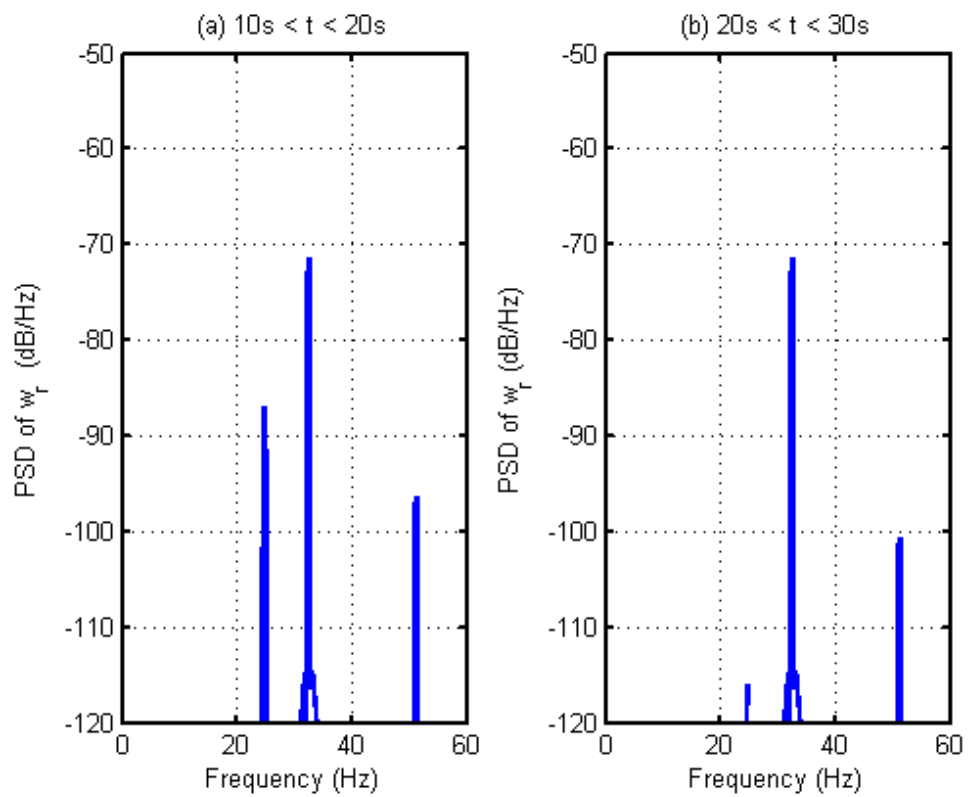


Figure 4.6 : PSD of the generator rotor speed, (a) $10s < t < 20s$ and (b) $20s < t < 30s$

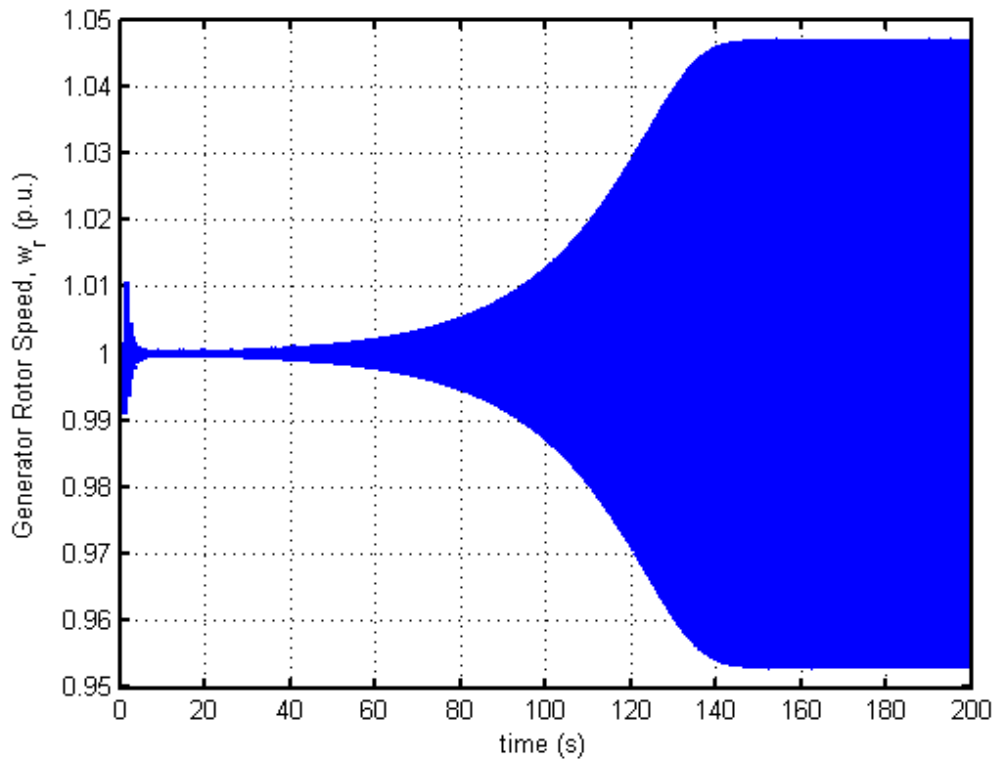


Figure 4.7 : Generator rotor speed ($\mu = 0.525$) (Supercritical Hopf bifurcation)

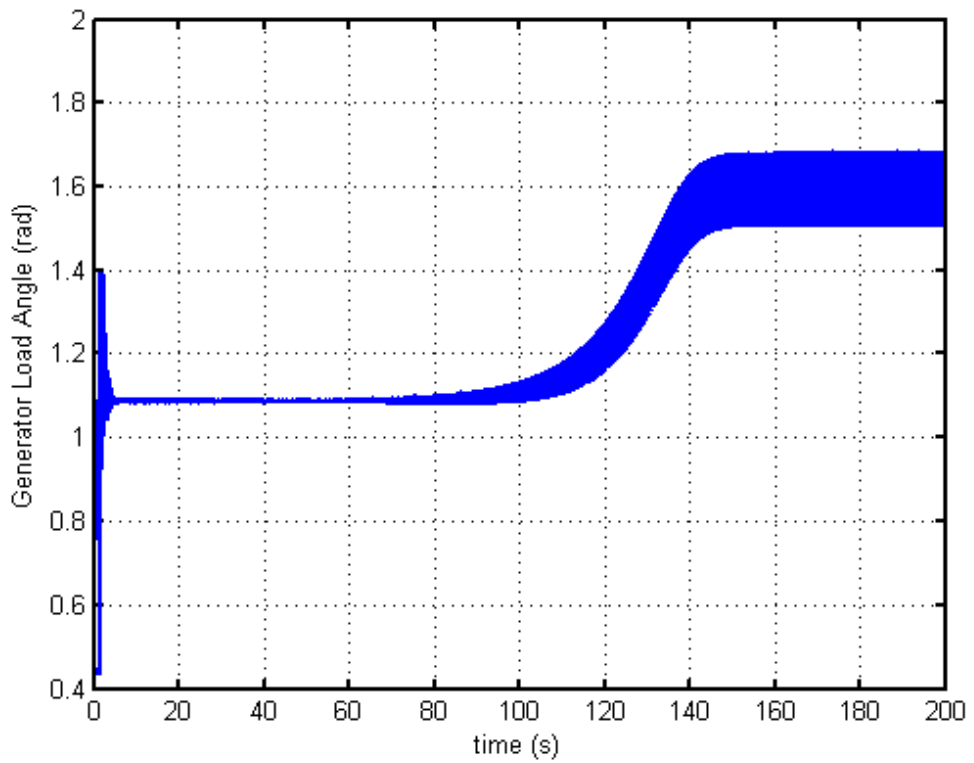


Figure 4.8 : Generator load angle ($\mu = 0.525$) (Supercritical Hopf bifurcation)

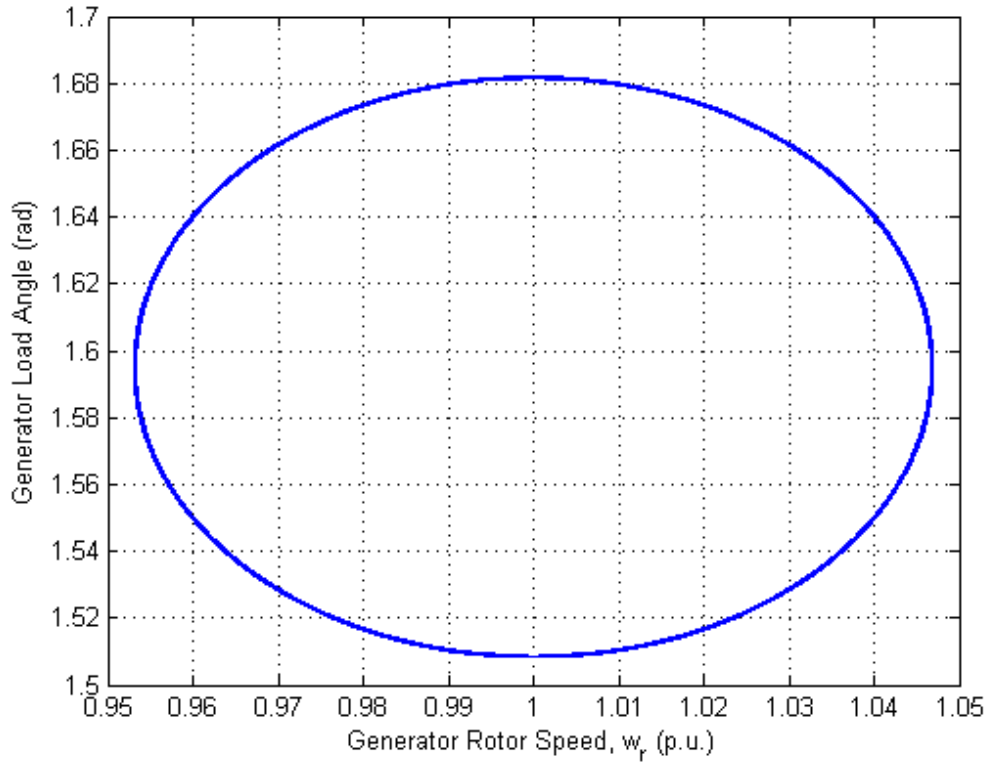


Figure 4.9: Two-dimensional projections of the phase portrait onto the ω_r - δ_r plane from $t=190s$ to $t=200s$ ($\mu = 0.525$) (Supercritical Hopf bifurcation)

Analytic finding that the Hopf bifurcation is supercritical has been verified by time domain simulations. It is important to emphasize that various forms of bifurcations can occur in the region at which the system is not stable.

4.3.5 Impact of the AVR Gain on $l_1(0)$

We analyze the impact of the AVR gain (K_A) on the Hopf bifurcation point and the first Lyapunov coefficient. Taking the series compensation factor as the bifurcation parameter, the bifurcation analysis is carried out for the values of K_A between 50 and 450. The Hopf bifurcation point and the first Lyapunov coefficient are evaluated accordingly. The other three control parameters are kept constant ($T_m=0.91$, $V_\theta=1.0$ and $V_{iset}=1.0869$).

Variation of the Hopf bifurcation point with the AVR gain is almost negligible, as shown in Fig. 4.10. On the other hand, the first Lyapunov coefficients increase with the AVR gain. Fig 4.11 shows that significant increase in the first Lyapunov coefficient occurs when the AVR gain is changed from 50 to 150. In the remaining range from 150 to 450, however, the increase is gradual.

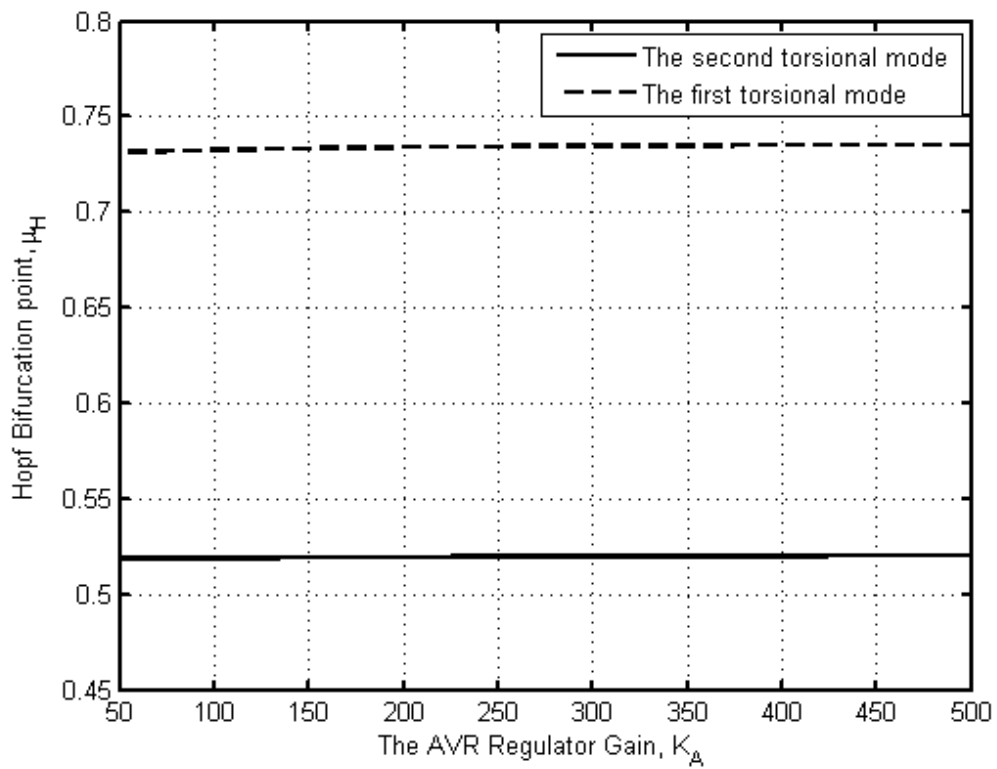


Figure 4.10 : Variation of Hopf bifurcation point with the AVR Gain

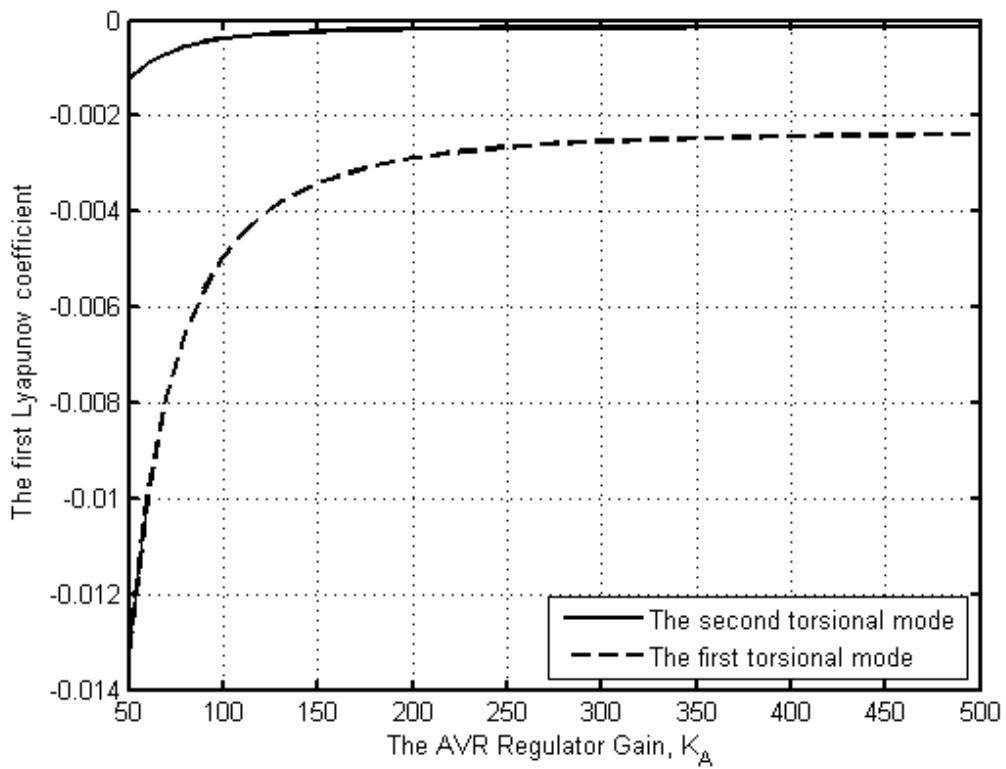


Figure 4.11 : Variation of the first Lyapunov coefficients with AVR gain, K_A

5. DELAYED FEEDBACK CONTROLLER

This chapter introduces a novel controller based on the delayed feedback control theory to stabilize unstable torsional oscillations on the turbine-generator shaft system due to the SSR. Also known as Time-Delay Auto Synchronization (TDAS), the delayed feedback control scheme makes use of the current and time delayed values of an observable state variable in a dynamic system to obtain a stabilizing signal.

Over the last decade, the TDAS control method has been successfully implemented in quite diverse experimental systems to stabilize both unstable periodic orbits and unstable steady states. From the view point of optimization requirements, the time delay (τ) and the DFC gain (K_{DFC}) are the only parameters to be optimally set in the proposed controller. It is found that the optimum value of the DFC time delay is related to the imaginary parts of the unstable mode eigenvalues.

The Delayed Feedback Controller (DFC) developed in this Dissertation is combined into the SMIB power system model through the excitation system with AVR and uses the generator rotor angular speed signal as the only input.

5.1 Delayed Feedback Controller

The block diagram of the DFC is shown in Fig. 5.1. The DFC uses the generator rotor angular speed as the sole input signal. The difference between τ -time delayed input signal and its current value is multiplied by a gain to obtain the stabilizing output signal (V_S).

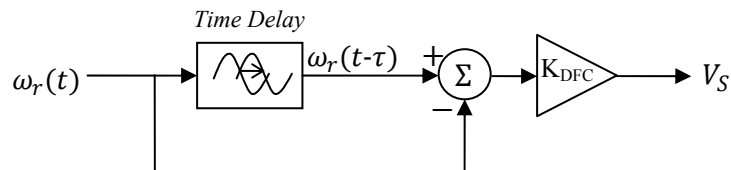


Figure 5.1 : Delayed Feedback Controller (DFC)

The output signal V_S is then added to the AVR block as shown in Fig. 5.2.

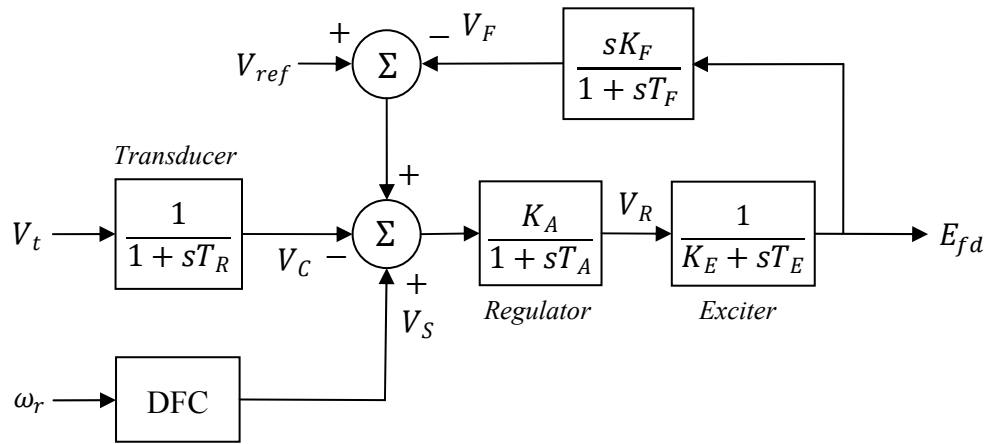


Figure 5.2 : Excitation System with AVR and DFC

The expression for V_S can be written as

$$V_S(t) = K_{DFC} (\omega_r(t-\tau) - \omega_r(t)) \quad (5.1)$$

Due to the intricate nature of the delayed nonlinear differential equations, an analytic approach to study the DFC effect on the model dynamic stability is extremely complex.

5.2 The DFC Performance

The effectiveness of the DFC is investigated by time domain simulations using the software MATLAB-Simulink. A negative pulse torque disturbance identical to the one in Chapters 3 and 4 is applied on the generator operating at steady state for the purpose of exciting the natural oscillation modes in the model.

Fig. 5.3 shows the generator rotor speed response without DFC at 55% series compensation. The unstable torsional oscillations increase in magnitude until a sudden drop after $t \approx 27s$. The dynamic response is in the form of sudden drop following the growing oscillations in the unstable modes for the series compensation levels at which the system is unstable.

With $T_m=0.91$, $K_A=250$, $V_0=1.0$ and $V_{ref}=1.0953$, the generator rotor angular speed response is obtained for the cases with the controller at for $\mu=0.55$, $\mu=0.75$ and $\mu=0.85$ at all three of which the nonlinear dynamic system is not stable. Figs. 5.4 to 5.16 show the generator rotor speed responses with DFC.

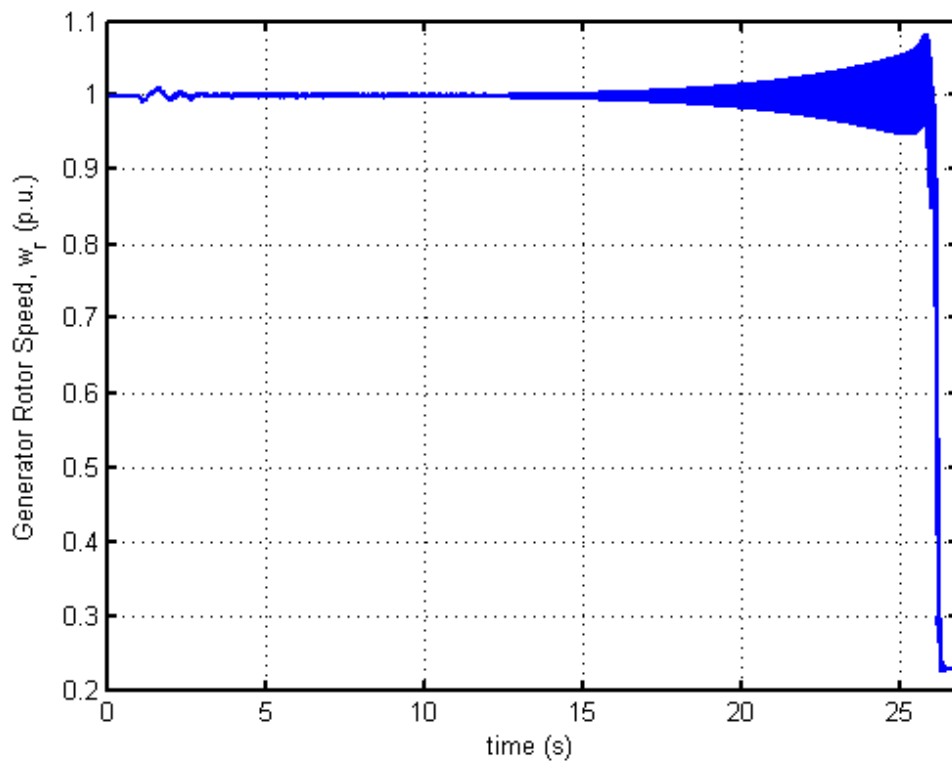


Figure 5.3 : Generator rotor speed response without the DFC ($\mu=0.55$)

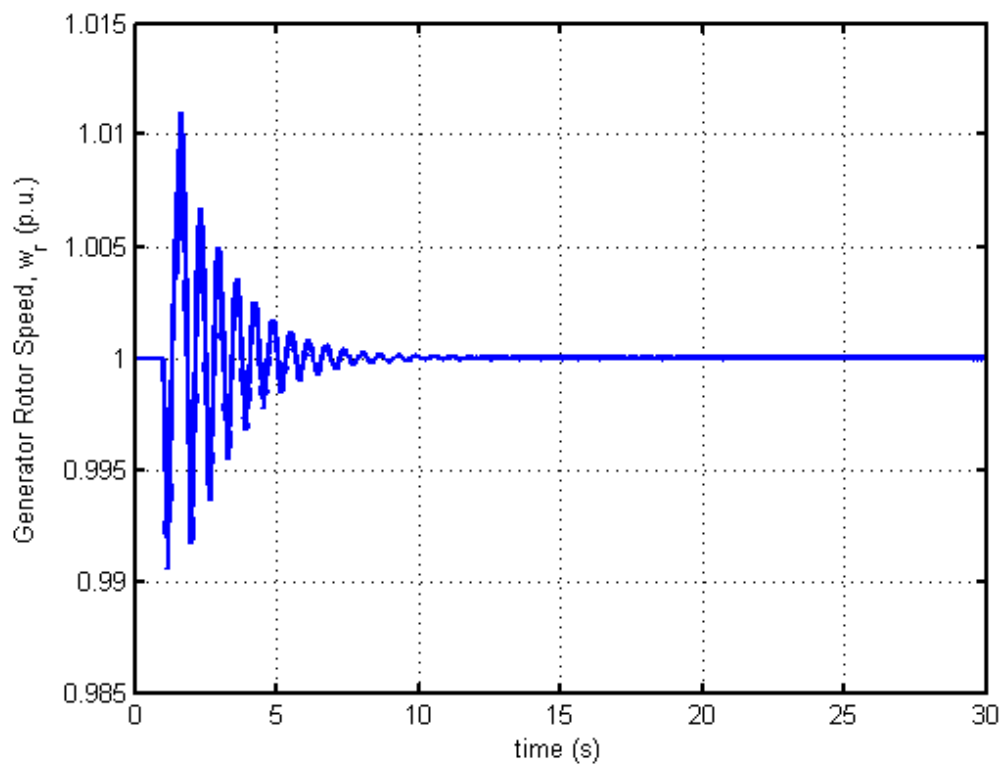


Figure 5.4 : Generator rotor speed response with DFC ($\mu=0.55$, $\tau = 0.0185s$, $K_{DFC}=76$)

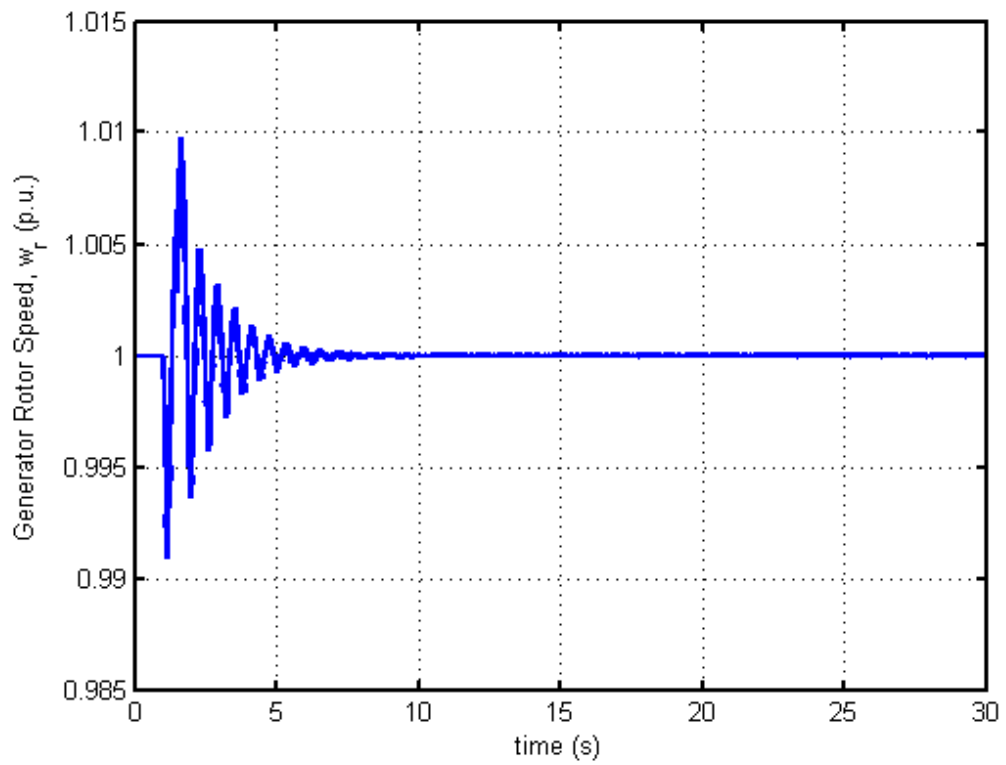


Figure 5.5 : Generator rotor speed with the DFC ($\mu=0.75$, $\tau = 0.0175s$)

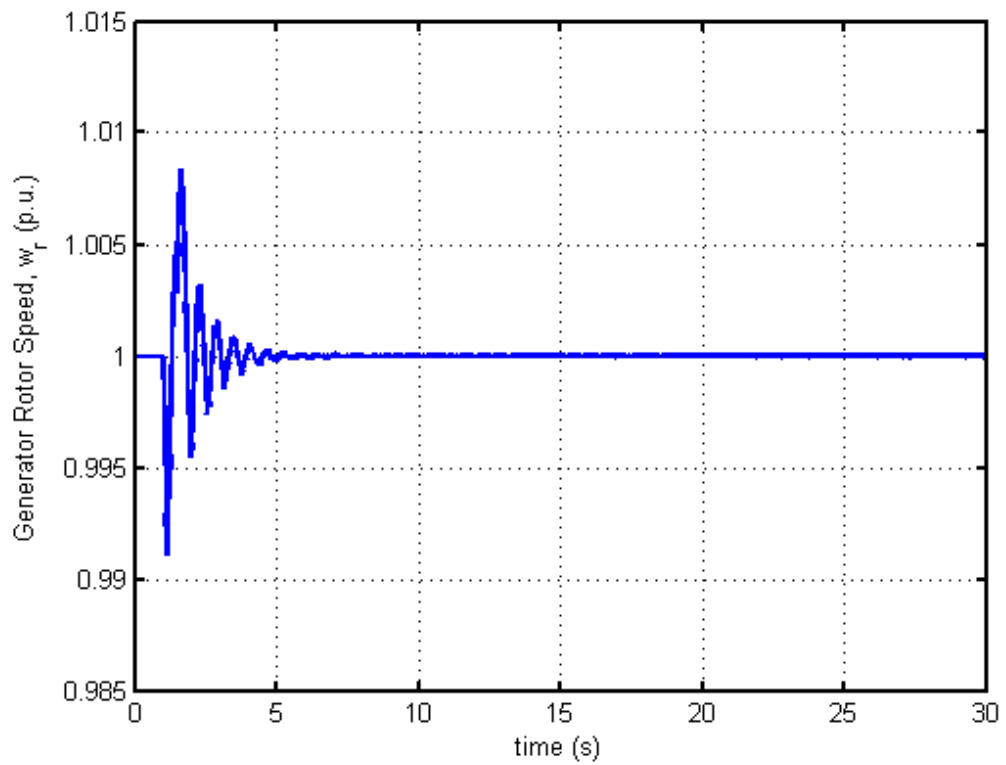


Figure 5.6 : Generator rotor speed with the DFC ($\mu=0.85$, $\tau=0.0135s$)

It is evident from the time domain simulations that the designed controller gives superior results. Consequently, provided that the control parameters are set correctly, the controller effectively damps the unstable torsional oscillations due to SSR in the model.

Figs. 5.7 to 5.9 show the output of DFC. Due to the local mode oscillations following the disturbance, DFC output remains high until the local mode oscillations decay and disappear. Blocking the controller output along the period during which the magnitude of the local mode oscillations remains higher than a certain limit or filtering out the low frequency components in the input signal of the controller can improve the controller performance by preventing the controller action for the stable modes.

It is important to note that the generator terminal voltage is also affected by DFC since the controller is combined with AVR. Terminal voltage regulating function of AVR is critical from the view point of transient stability and operational reliability. Therefore, the impact of DFC on the regulating duty of AVR is also investigated. It is evident from Figs. 5.10 to 5.12 that the generator terminal voltage is successfully maintained at its set value following the initial oscillations.

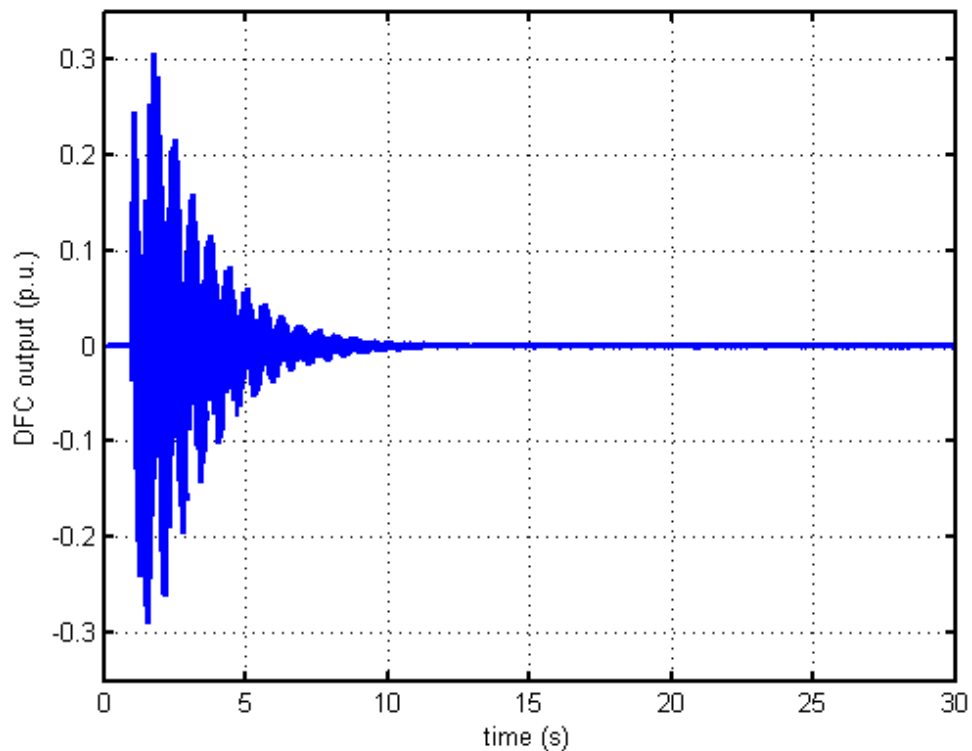


Figure 5.7 : The DFC output ($\mu=0.55$, $\tau=0.0185s$, $K_{DFC}=76$)

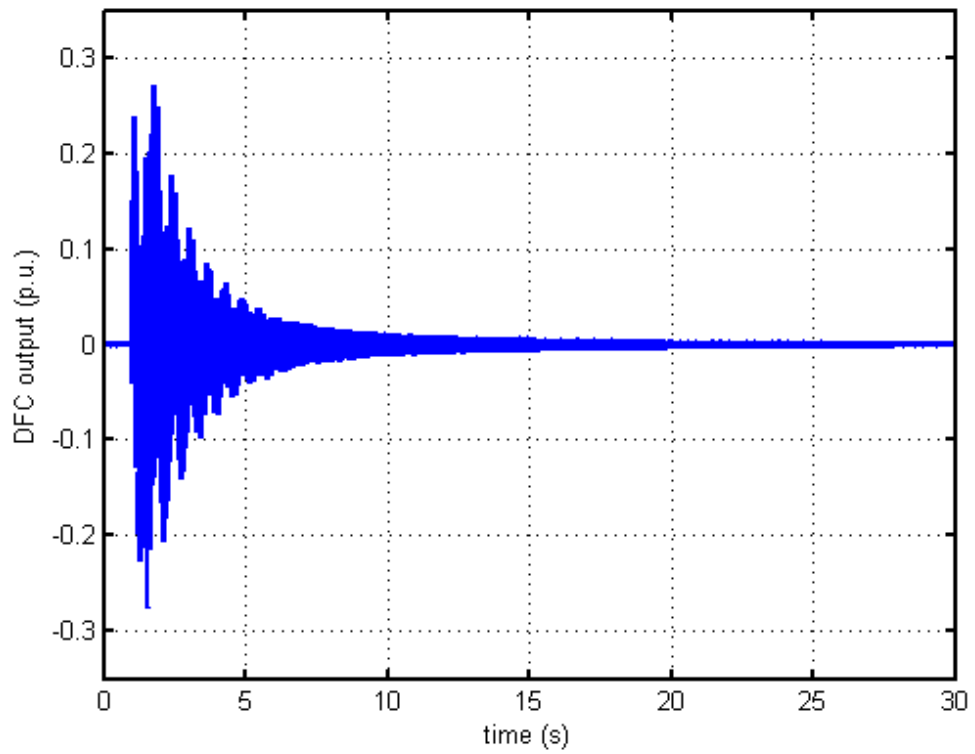


Figure 5.8 : The DFC output ($\mu=0.75$, $\tau = 0.0175s$, $K_{DFC}=76$)

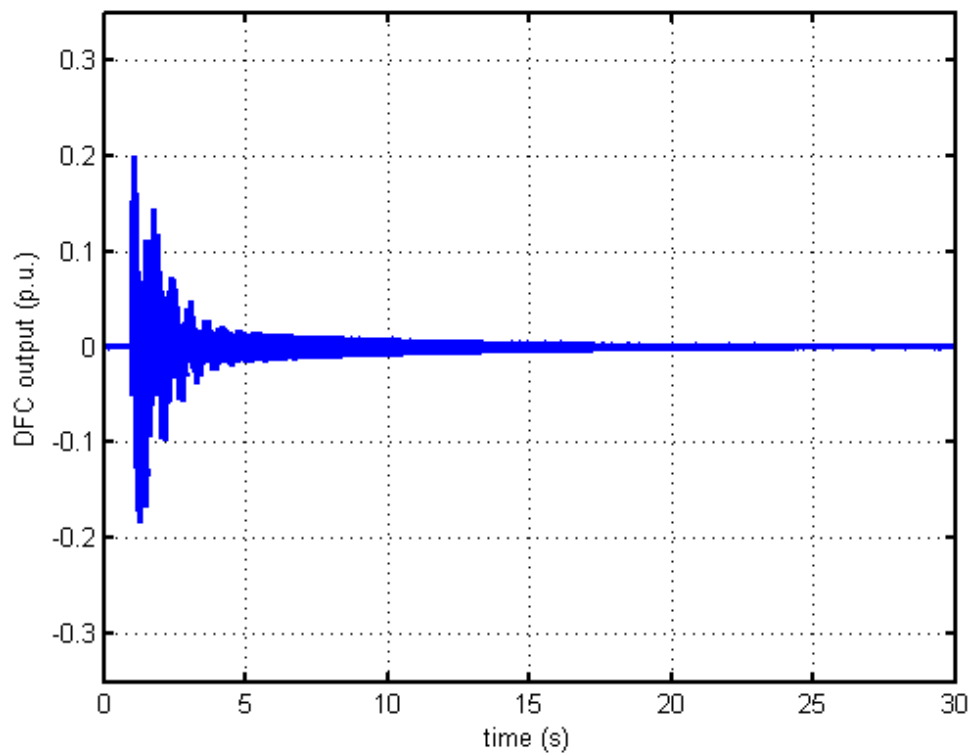


Figure 5.9 : The DFC output ($\mu=0.85$, $\tau = 0.0135s$, $K_{DFC}=76$)

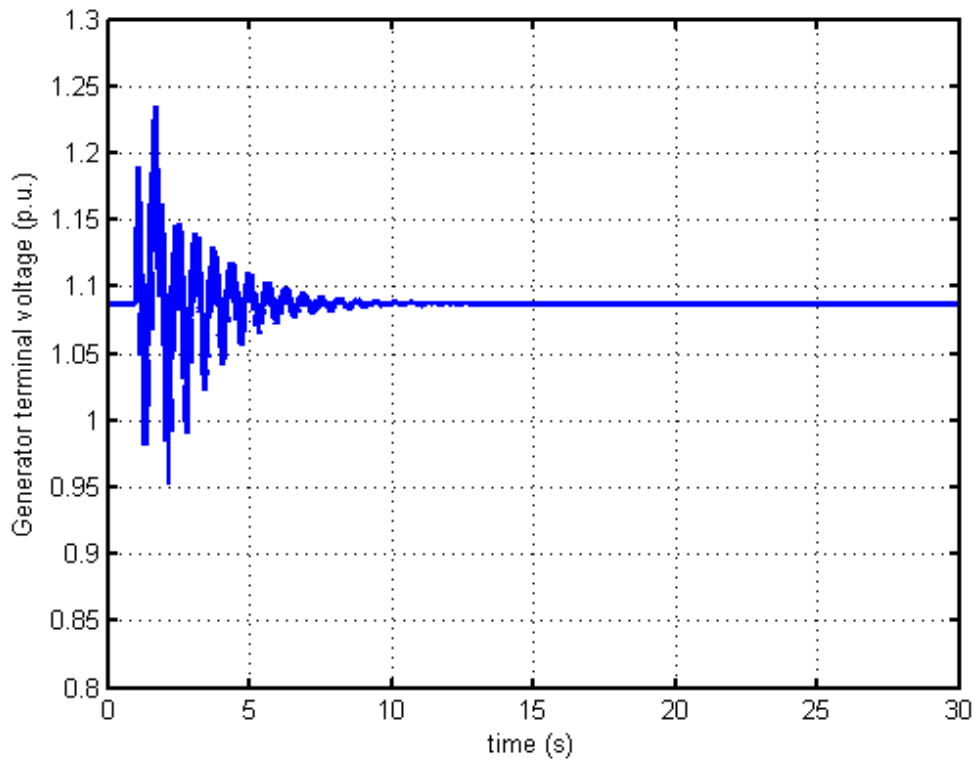


Figure 5.10 : Generator terminal voltage with the DFC ($\mu=0.55$, $\tau=0.0185s$)

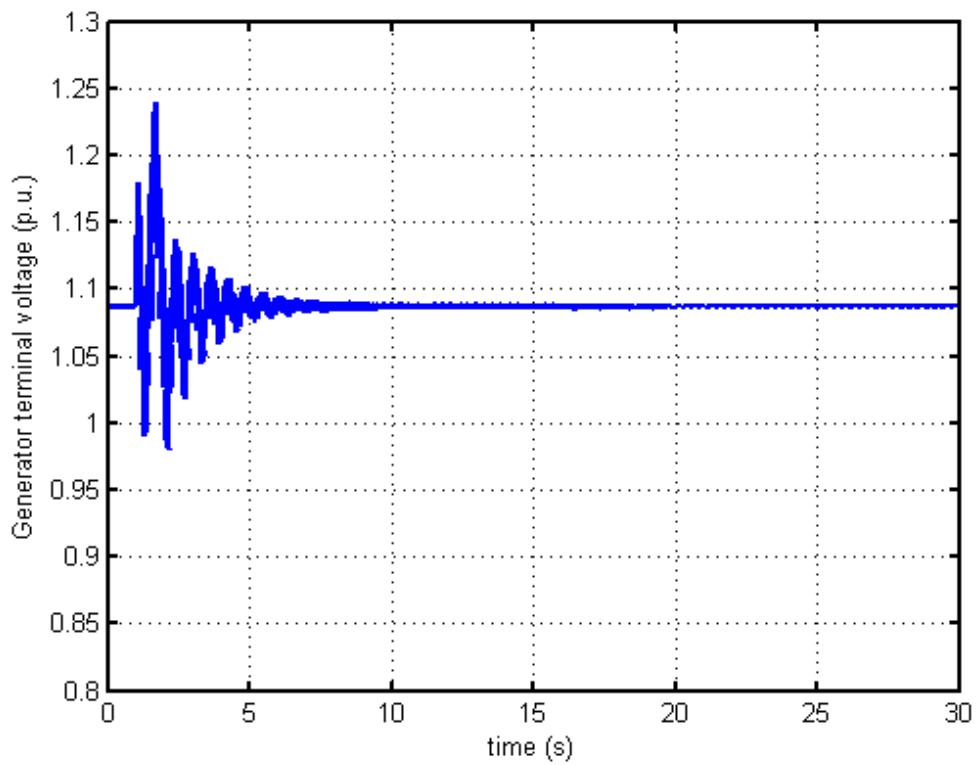


Figure 5.11 : Generator voltage with DFC ($\mu=0.75$, $\tau=0.0175s$, $K_{DFC}=76$)

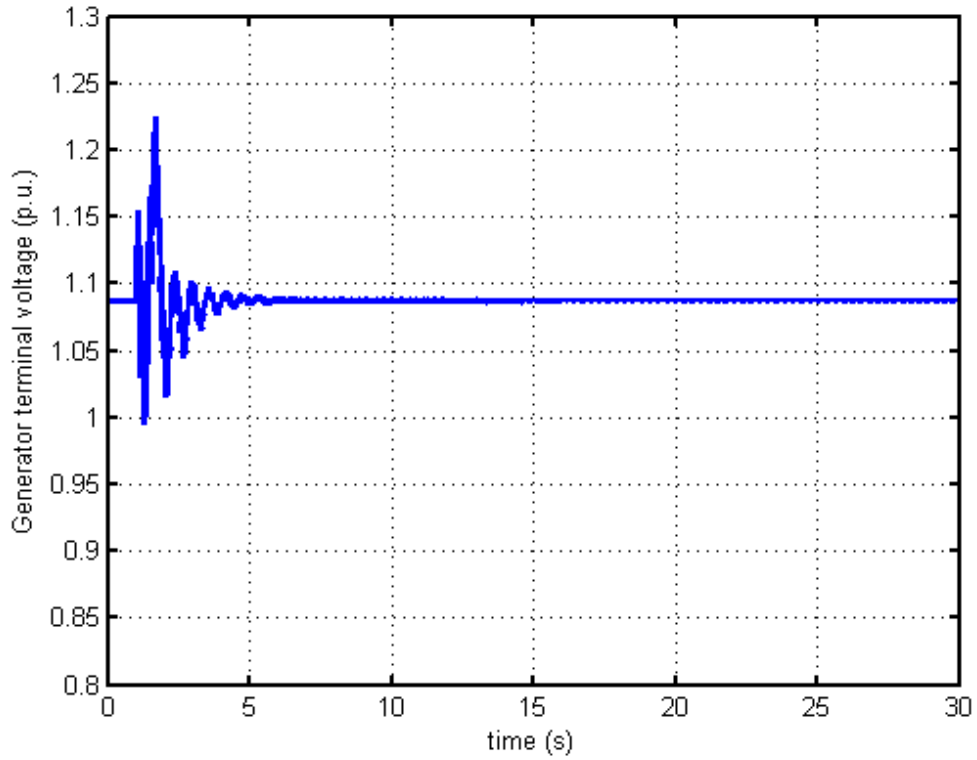


Figure 5.12 : Generator voltage with the DFC ($\tau=0.0135s$, $K_{DFC}=76$)

It is important to emphasize that the DFC effectiveness in stabilizing the unstable torsional oscillations due to SSR depends on the optimal setting of the control parameters τ and K_{DFC} . Furthermore, applying a high pass filter to the input signal ω_r can improve the overall dynamic response by eliminating the effect of the local swing mode oscillation which is stable on the controller output and therefore no damping improvement is needed for the purpose of preventing the turbine-shaft fatigue.

5.3 Optimization of the DFC Parameters

In the absence of a convenient method to obtain the DFC control parameters analytically, the Optimization Performance Index (OPI) based on the evaluation of time domain simulations is defined as follows:

$$OPI(\tau, K_{DFC}) = \max(\omega_r(t)) - \min(\omega_r(t)) \quad 5.2$$

over a time interval from $t=13s$ to $t=15s$. The selection of other time intervals is also possible as long as the OPI variations are significant along the time range and the initial stable oscillations disappear substantially before the start of the selected time

interval. Difference between the maximum and minimum values of the generator rotor speed at the specified time interval is a measure of the stabilizing performance of the DFC with the set control parameters.

The optimization procedure involves performing time domain simulations and determining the OPI for various values of τ . The optimum DFC time delay is the value at which the minimum OPI is achieved. Upon determining the optimum time delay for the controller, in a similar manner, the time domain simulations are carried out for a certain range of K_{DFC} . The optimum value of K_{DFC} is the gain with which the minimum OPI is obtained. The procedure also allows assessing the control parameter sensitivity of the DFC.

With $T_m=0.91$, $K_A=250$, $V_0=1.0$ and $V_{ref}=1.0953$, the generator rotor is subjected to the identical disturbance as in Section 5.2 in order to excite the system natural oscillation modes. Figs. 5.15 to 5.17 show the OPI values for a range of the DFC time delay at three levels of the series compensation factor, $\mu=0.55$, $\mu=0.75$ and $\mu=0.85$ for which the optimum DFC time delays are found 0.185s, 0.175s and 0.135 for $K_{DFC}=76$, respectively.

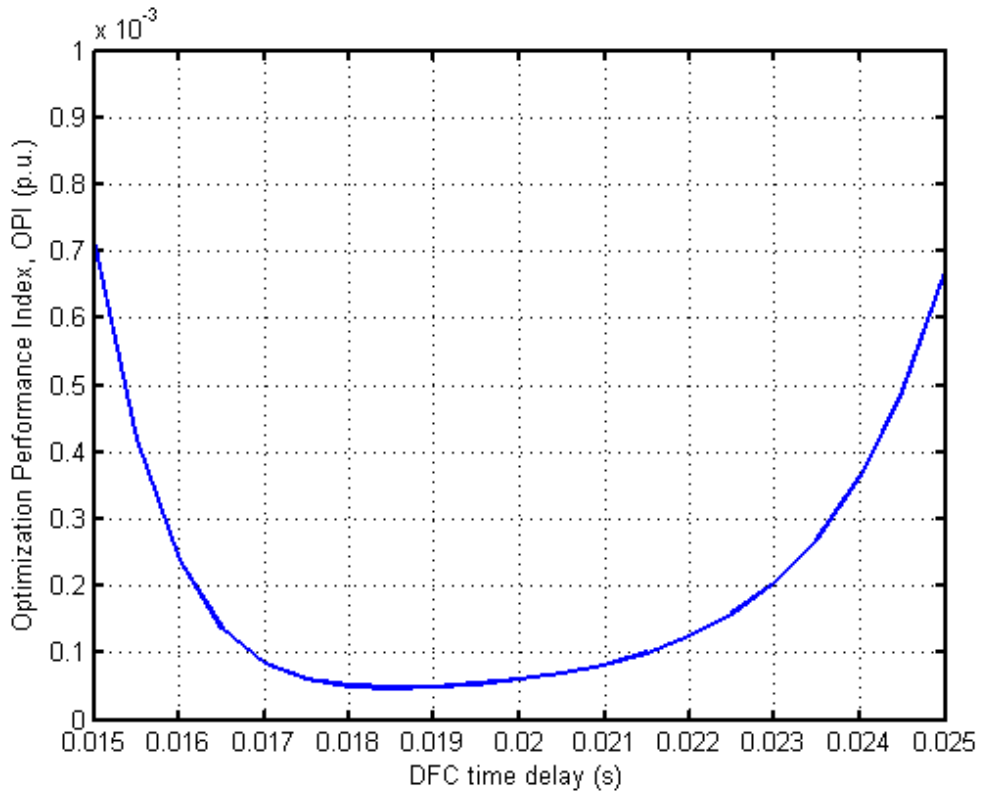


Figure 5.13 : OPI vs DFC time delay. $\tau_{opt}=0.0185s$ ($\mu=0.55$, $K_{DFC}=76$)

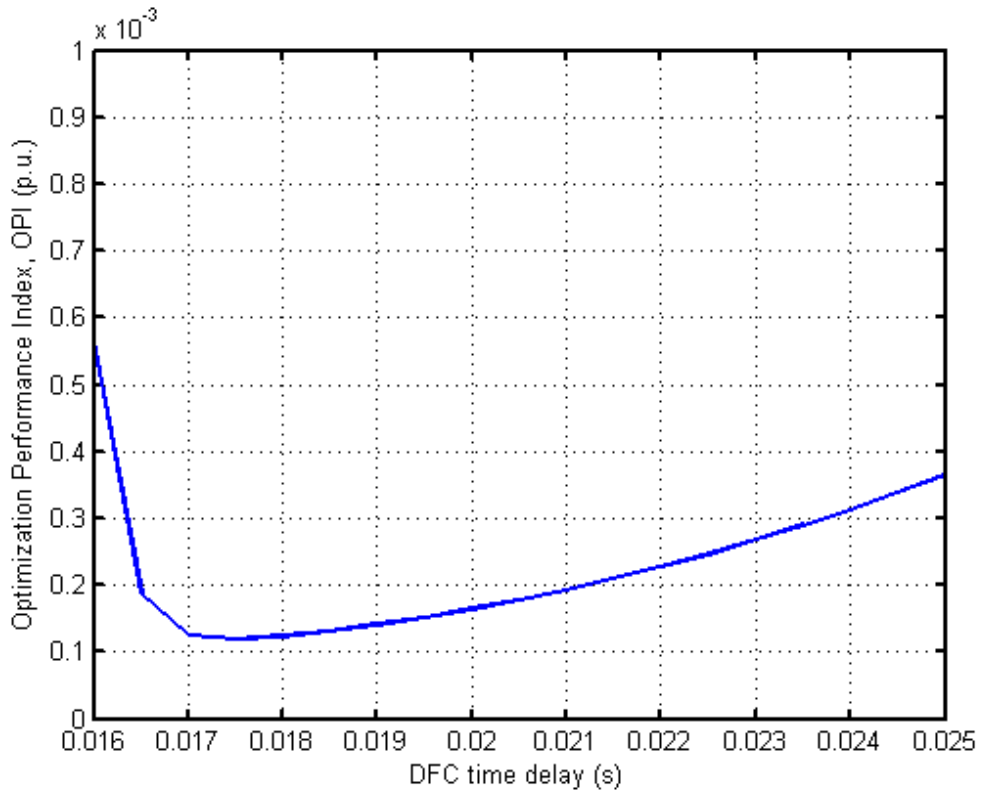


Figure 5.14 : OPI vs DFC time delay. $\tau_{opt}=0.0175s$ ($\mu=0.75$, $K_{DFC}=76$)

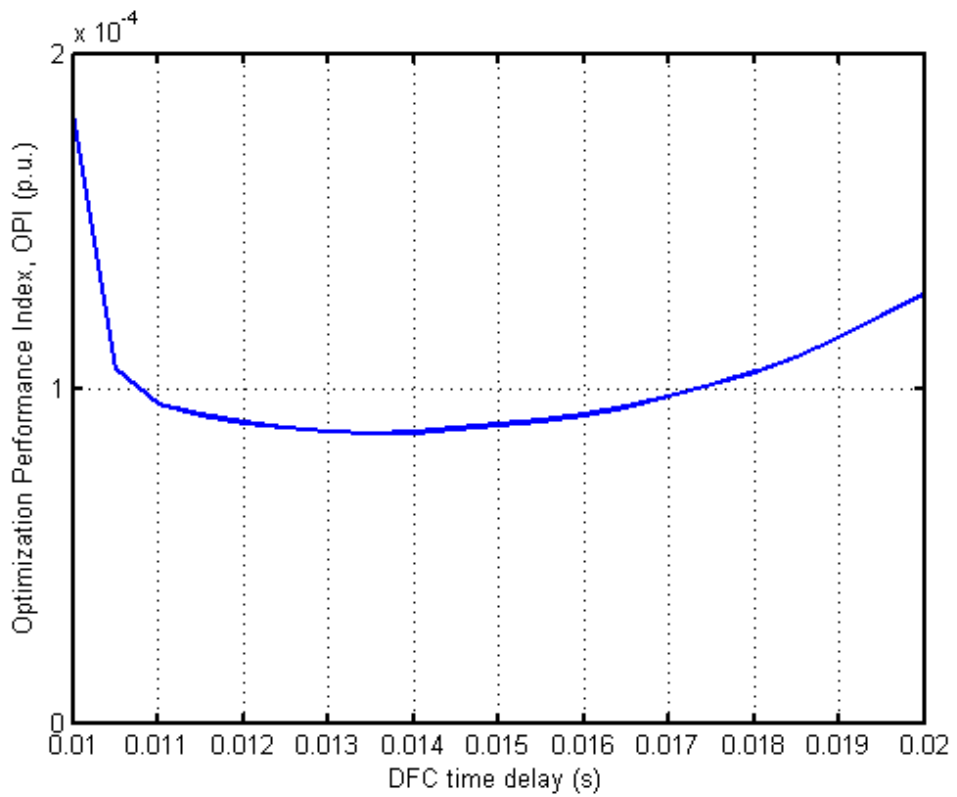


Figure 5.15 : OPI vs DFC time delay. $\tau_{opt}=0.0135s$ ($\mu=0.85$, $K_{DFC}=76$)

Figs. 5.15 to 5.17 show the evaluated OPI values that result in good performance of

the controller for a range of the DFC time delay at three levels of the series compensation factor, $\mu=0.55$, $\mu=0.75$ and $\mu=0.85$ for which the optimum DFC time delays of 0.185s, 0.175s and 0.135 for respectively. It is concluded that setting K_{DFC} parameter to a value between 70 and 80 results in an effective DFC performance as long as τ is optimally set.

The time delay values of the controller giving the optimum performance based on the evaluated OPI for the values of the series compensation levels through which the dynamic system is unstable due to the Hopf bifurcations occurring in the first and the second torsional modes are shown in Fig. 5.21.

It is interesting to observe that setting the time delay to 0.018 for the series compensation levels at which the second torsional mode is unstable results in an acceptable performance. As for the series compensation levels through which the first torsional mode is unstable, setting the time delay to 0.014 ensures that the controller provides damping the unstable torsional oscillations adequately.

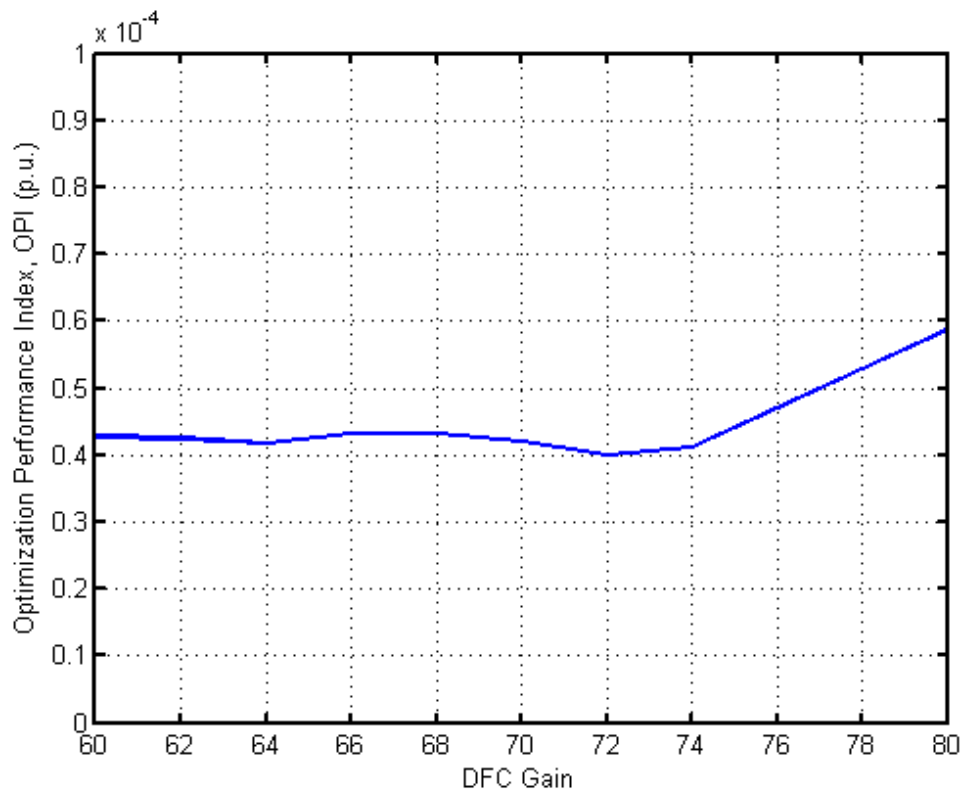


Figure 5.16 : OPI vs DFC gain ($\mu=0.55$, $\tau=0.0185s$)

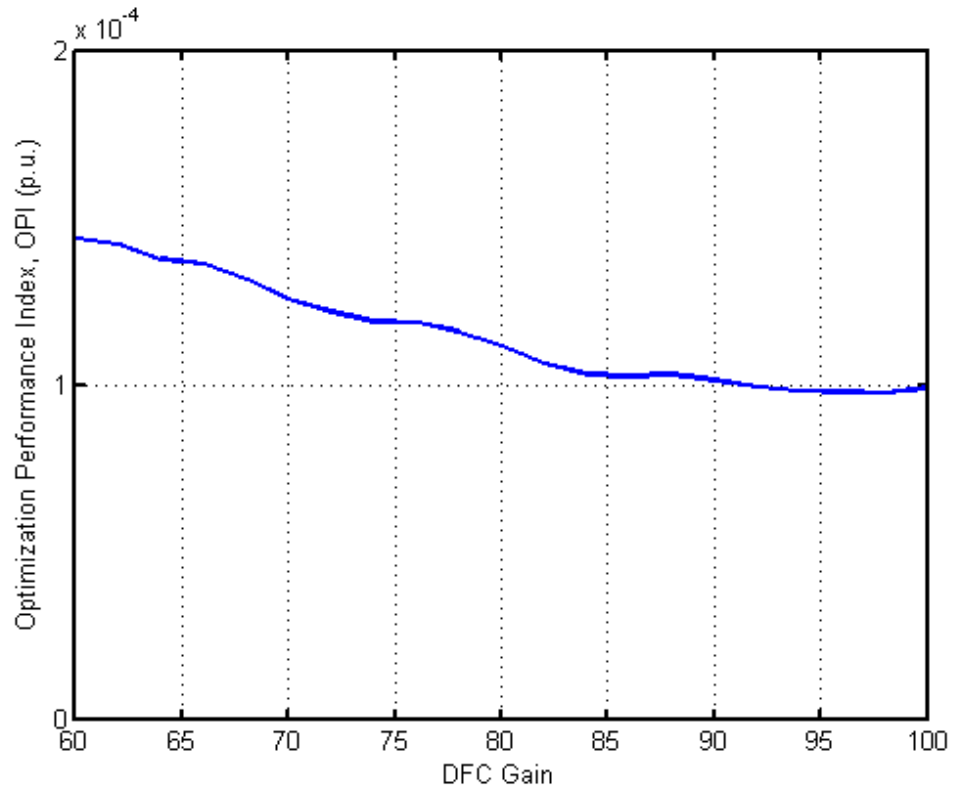


Figure 5.17 : OPI vs DFC gain ($\mu=0.75, \tau=0.0175s$)

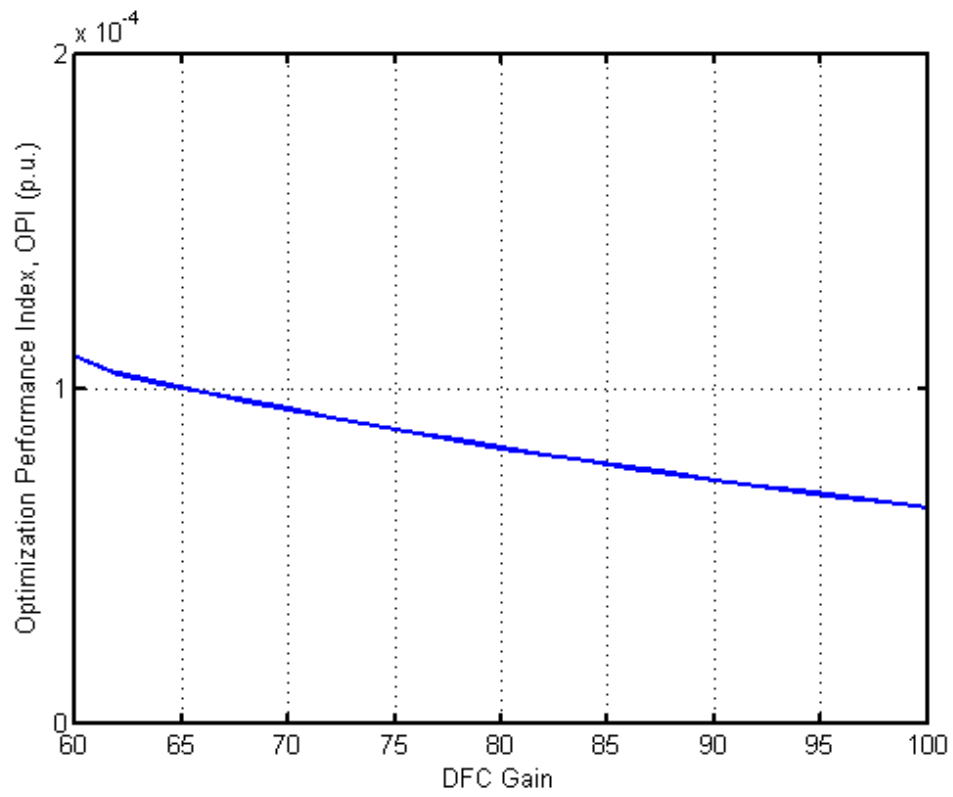


Figure 5.18 : OPI vs DFC gain ($\mu=0.85, \tau=0.0135s$)

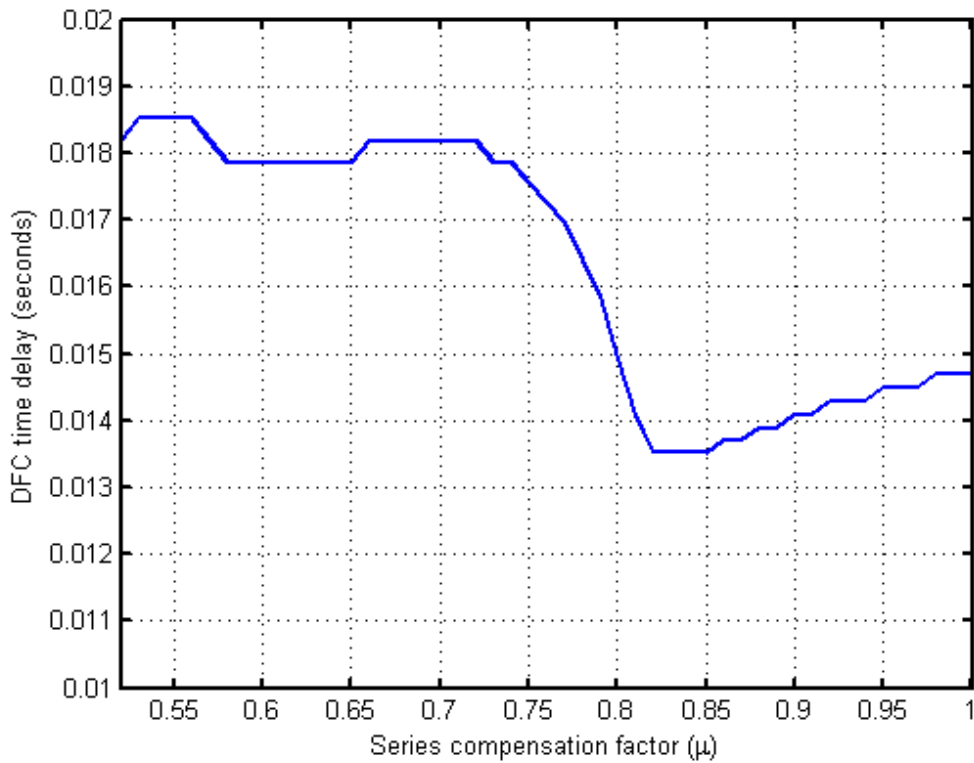


Figure 5.19 : DFC time delay optimum values ($T_m=0.91$, $V_{ref}=1.0953$, $K_{DFC}=76$)

5.4 DFC Performance at Different Operating Conditions

The optimum values of the DFC parameters which are effective at one operating condition may not yield the same performance at other operating conditions. The correct setting of the DFC time delay parameter is important to ensure an effective controller performance. With fixed series compensation factor, the optimum value of the DFC time delay varies depending on the operating conditions such as the loading level (i.e. mechanical torque input) of the generator and the AVR reference voltage.

5.4.1 DFC Optimum Time Delay Depending on the Loading Level

Fig 5.22 and Fig 5.23 show the generator rotor speed responses for $T_m=0.60$ and $T_m=0.75$, respectively. The AVR reference voltage is adjusted to regulate the generator terminal voltage at 1.09 p.u. Employing the optimization procedure described in 1.3, the optimum value of τ for $T_m=0.60$ has been computed as 0.022s. Repeating the procedure for $T_m=0.75$ gives an optimum value of 0.20s. In each case, the disturbance torque applied on the generator shaft is 50% of T_m .

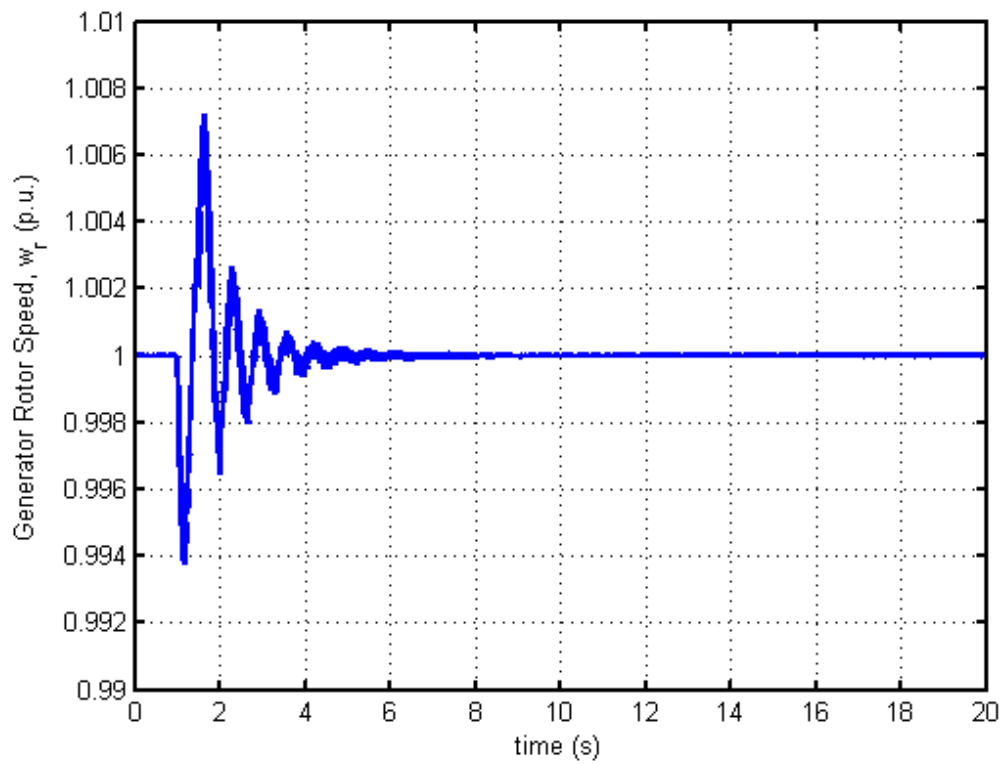


Figure 5.20 : Generator rotor speed ($\mu=0.55, T_m=0.60, V_{ref}=1.09, \tau = 0.022s$)

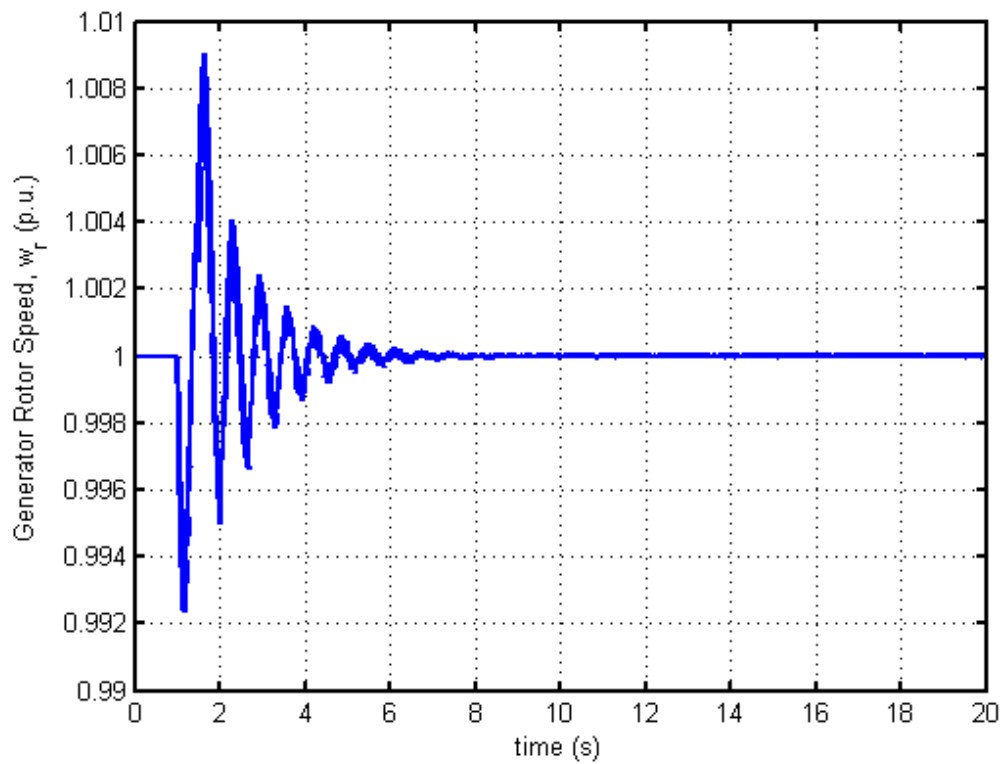


Figure 5.21 : Generator rotor speed ($\mu=0.55, T_m=0.75, V_{ref}=1.09, \tau = 0.020s$)

5.4.2 DFC Optimum Time Delay Depending on the AVR Reference Voltage

The AVR regulates the generator terminal voltage by comparing the actual terminal voltage with the AVR reference voltage set value (V_{ref}). The optimum τ also varies with V_{ref} . In Section 4.3, the optimum τ was evaluated as 0.0185s for $V_{ref}=1.0953$ p.u. ($\mu=0.55$, $T_m=0.91$). The generator terminal voltage was regulated at 1.0871 p.u. In order to assess the effectiveness of the DFC with $\tau=0.0185$ s at a lower generator terminal voltage regulated at 1.0577 p.u. ($V_{ref}=1.0657$ p.u.), an external torque of 50% of T_m is applied and the generator rotor speed response is obtained as shown in Fig. 5.24.

Evaluation the OPI values reveals that the optimum τ is 0.0160s for $V_{ref}=1.0657$ and it is smaller than the optimum τ computed for $V_{ref}=1.0953$. Fig. 5.25 shows the generator rotor speed response with $\tau=0.0160$ s. The DFC performances for both cases are almost the same and the equilibrium condition is reached. Extending the DFC parameters optimization to evaluate the DFC gain (K_{DFC}), the optimum K_{DFC} has been found as 45. With both parameters optimized, the DFC yields a slightly better performance, as shown in Fig. 5.26.

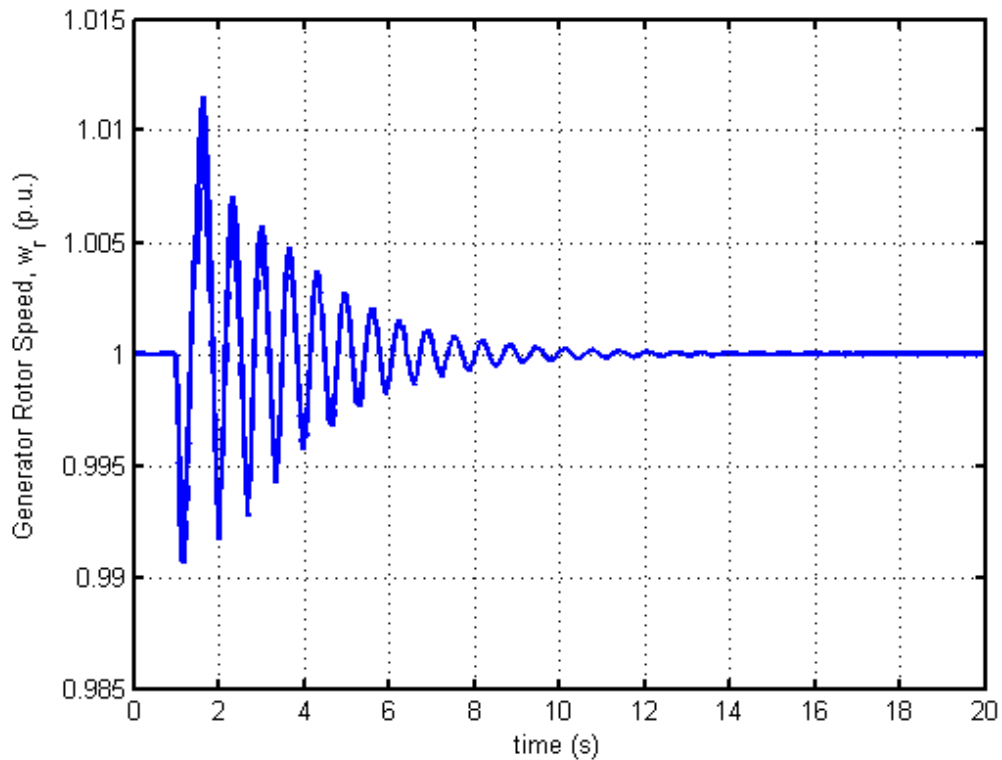


Figure 5.22 : Generator rotor speed ($\mu=0.55$, $T_m=0.91$, $V_{ref}=1.0657$, $\tau = 0.0185$ s)

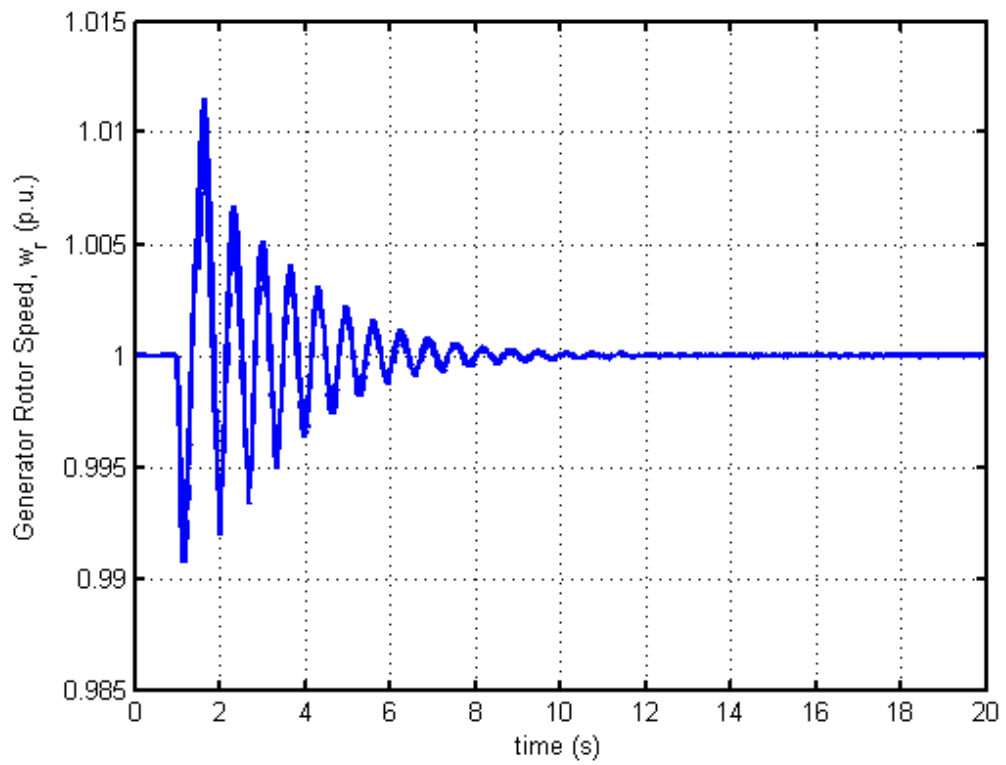


Figure 5.23 : Generator rotor speed ($\mu=0.55$, $V_{ref}=1.0657$, $\tau=0.0160s$, $K_{DFC}=76$)

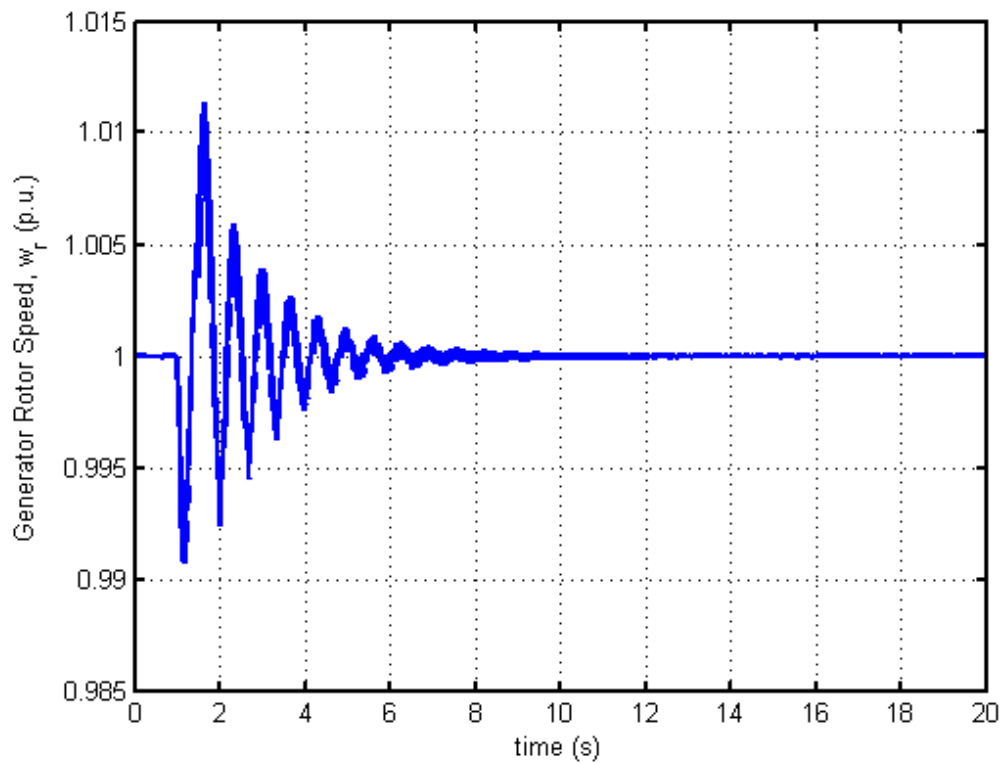


Figure 5.24 : Generator rotor speed ($\mu=0.55$, $V_{ref}=1.0657$, $\tau=0.0160s$, $K_{DFC}=45$)

The nonlinear state feedback controller proposed by Harb and Widyan [28] requires two state signals to obtain a control signal, which is computed by subtracting ω_1^3 (the first-turbine generator section) from ω_r^3 . Although the nonlinear controller stabilizes the operating point at all realistic series compensation levels, the damping of torsional oscillations takes much longer when compared with the DFC, which requires the measurement of only one state signal (ω_r). The fast damping of the torsional oscillations prevents high cycle fatigue formation on the shaft.

As a result, it is required that both control parameters of the DFC (i.e. τ and K_{DFC}) are optimized in order to obtain an effective performance from the controller. The DFC optimum set values depend upon the operating parameters such as the series compensation, the mechanical torque input to the generator and the AVR reference voltage.

In order to overcome the difficulties with the requirement to compute the DFC parameters optimally for each operating condition, an adaptive approach which involves changing the DFC parameters based on the on-line performance evaluation of the damping performance can be implemented.

6. THE EFFECT OF LIMITERS ON THE DFC PERFORMANCE

In this chapter, the limiters will be included in the AVR and the delayed feedback controller and their effect on the controller performance will be investigated. The function of AVR limiter is to limit the output of the regulator so that the exciter and synchronous generator operate within design limits. The DFC limiters are applied to prevent the stabilizing control signal from blocking voltage regulation function of the AVR.

6.1 AVR and DFC with Limiters

The block diagram of the excitation system with AVR and DFC with limiters is shown in Fig. 6.1. The regulator output limiter keeps V_R within the limits V_{RMAX} and V_{RMIN} . The DFC output limiter acts to limit stabilizing control signal (V_S) within the limits V_{SMAX} and V_{SMIN} .

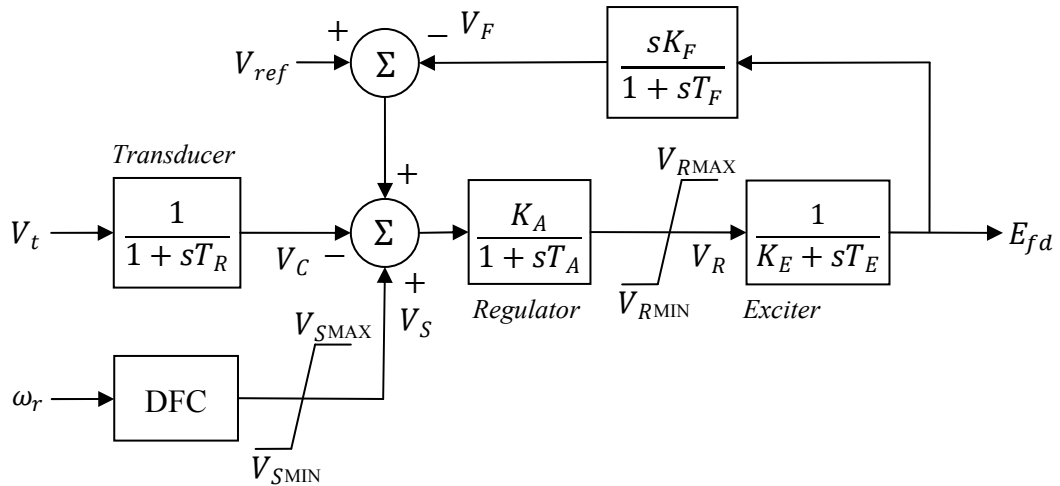


Figure 6.1 : AVR and DFC with limiters

The settings of the limiters are given below:

$$V_{RMAX} = 7.3 \text{ p.u.} \quad V_{RMIN} = -7.3 \text{ p.u.}$$

$$V_{SMAX} = 0.15 \text{ p.u.} \quad V_{SMIN} = -0.15 \text{ p.u.}$$

6.2 The DFC Performance with Limiters

The effect of the limiters on the DFC performance is studied for the cases $\mu=0.55$, $\mu=0.75$ and $\mu=0.85$. The presence of limiters prevents the DFC and the AVR output from reaching to unrealistic values. Therefore, the representation of the power system under study is more accurate. With $T_m=0.91$, $V_0=1.0$ and $V_{ref}=1.0953$, the synchronous generator rotor is subjected to the identical torque disturbance of 0.46 p.u. at $t=1s$ in order to excite the natural oscillation modes, as in Chapter 5.

Figs 6.2 and 6.3 show the generator rotor speed response and the load angle for $\mu=0.55$, respectively. It is evident that both state variables remain within the acceptable limits and the effectiveness of the DFC is not altered significantly with the introduction of the limiters at the series compensation level of 0.55. As shown in Fig. 6.4, the DFC and AVR limiters become active for several seconds following the disturbance. During the short time interval that the DFC and AVR outputs are limited, the stabilizing performance of the delayed feedback controller is not effective. The generator terminal voltage momentarily drops to 0.97 p.u. and rises to 1.22 p.u. before it eventually reaches to near equilibrium, as shown in Fig. 6.5-b.

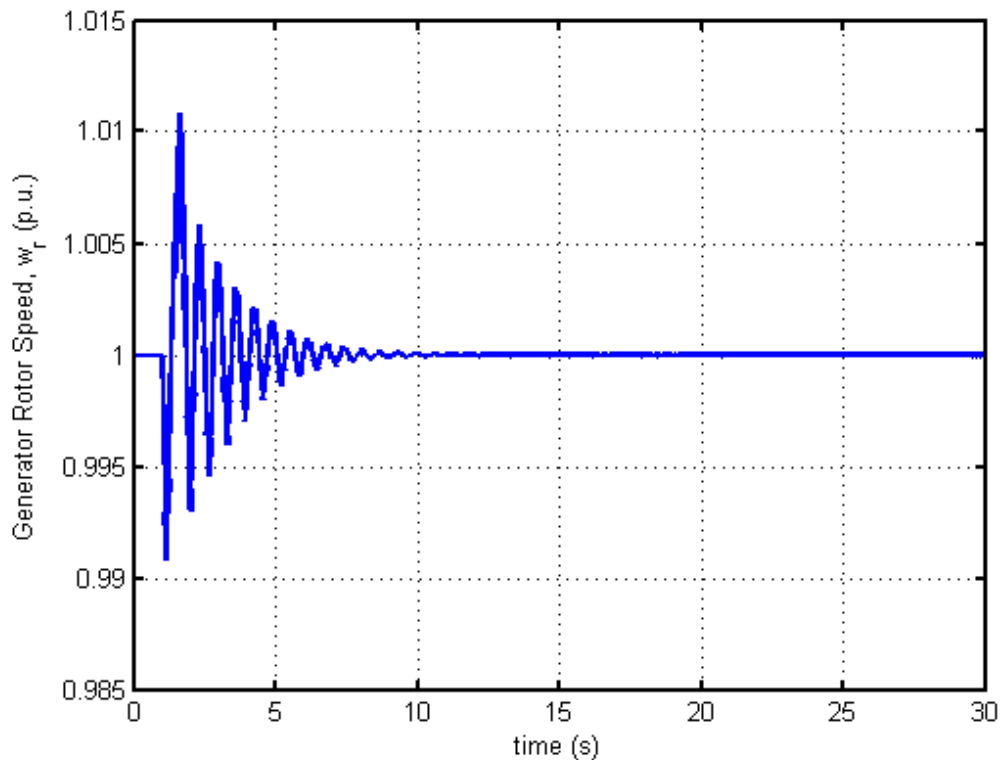


Figure 6.2 : Generator rotor speed with DFC and AVR limiters ($\mu=0.55$)

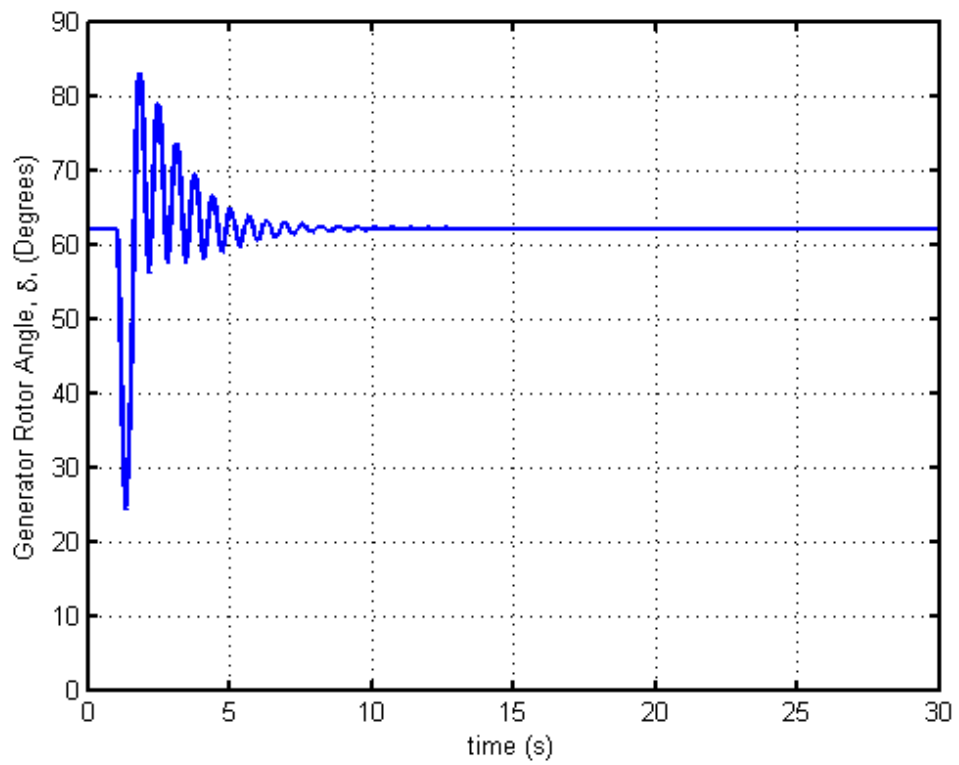


Figure 6.3 : Generator rotor angle with DFC and AVR limiters ($\mu=0.55$)

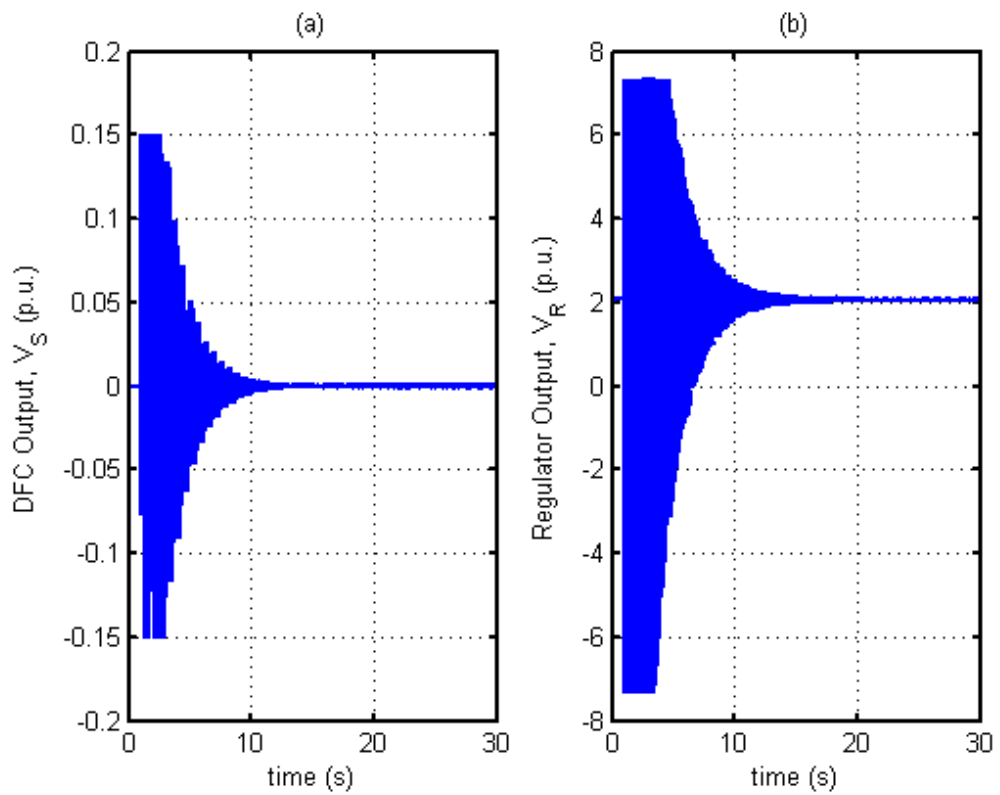


Figure 6.4 : (a) DFC output, V_S and (b) Regulator output, V_R ($\mu=0.55$)

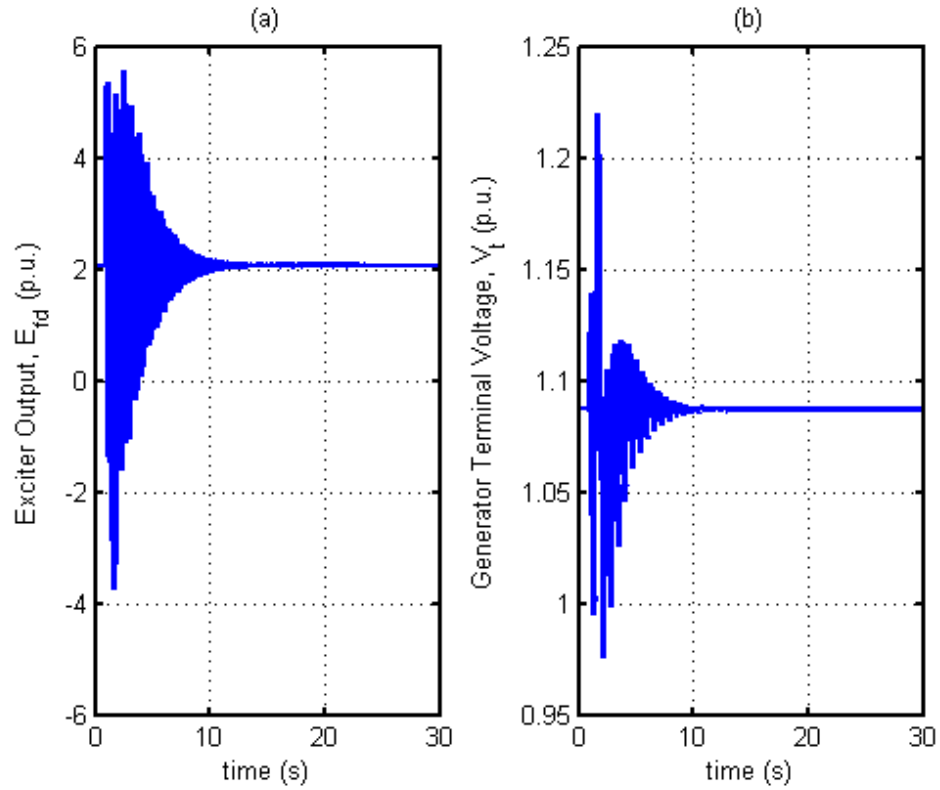


Figure 6.5 : (a) Exciter output, E_{fd} and (b) Terminal voltage, V_t ($\mu=0.55$)

Similarly, the case with $\mu=0.75$ yields an effective controller performance with the DFC and AVR limiters. Fig. 6.6 shows that the generator rotor speed reaches to equilibrium without experiencing unstable oscillations. The load angle also remains within the transient stability range, as shown in Fig. 6.7.

The DFC and AVR limiters cut in shortly after the disturbance as in the case with $\mu=0.55$. As a result of the rapid decay in the local swing mode oscillations, the regulator limiter cuts out at $t \approx 3$ s. The DFC limiter becomes active relatively shorter than the regulator limiter, as shown in Fig. 6.8.

Different from the case $\mu=0.55$, the DFC and AVR outputs continue to oscillate at decaying magnitudes even though the state variables reach near equilibrium at $t \approx 8$ s. Moreover, Fig. 6.9 shows that the generator terminal voltage experiences minimum and maximum instantaneous values of 0.97 p.u. and 1.23 p.u., respectively.

Consequently, the inclusion of DFC and AVR limiters do not cause a significant reduction on the effectiveness of the controller and it can effectively damp the unstable torsional oscillations due to SSR even at a practically high level of series compensation.

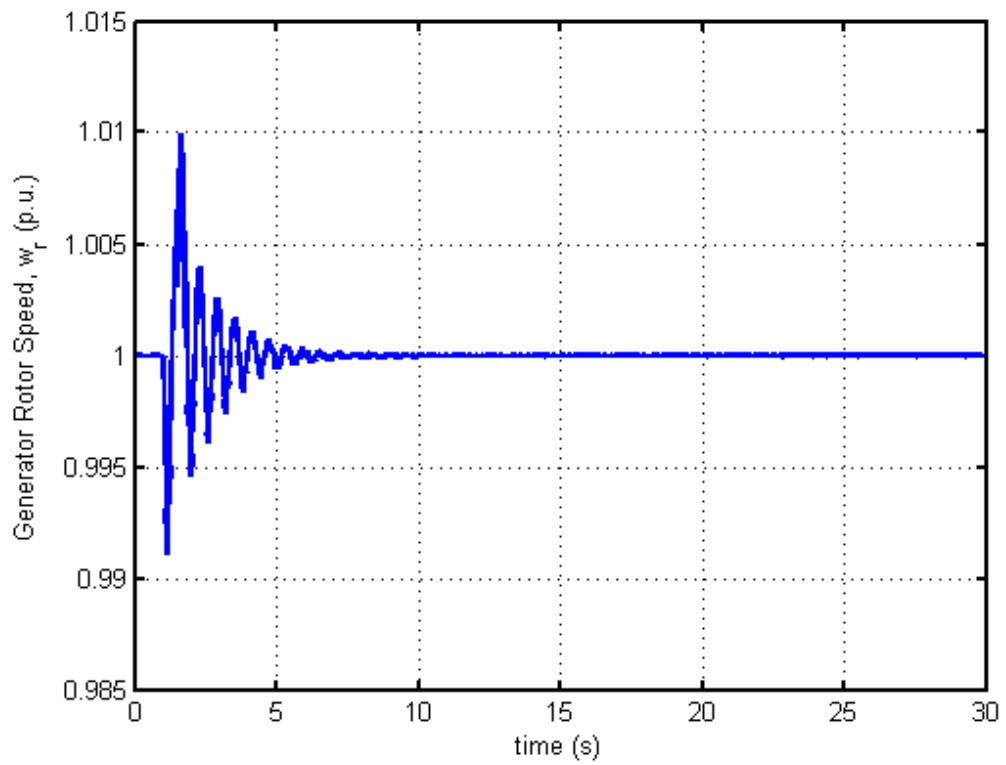


Figure 6.6 : Generator rotor speed with DFC and AVR limiters ($\mu=0.75$)

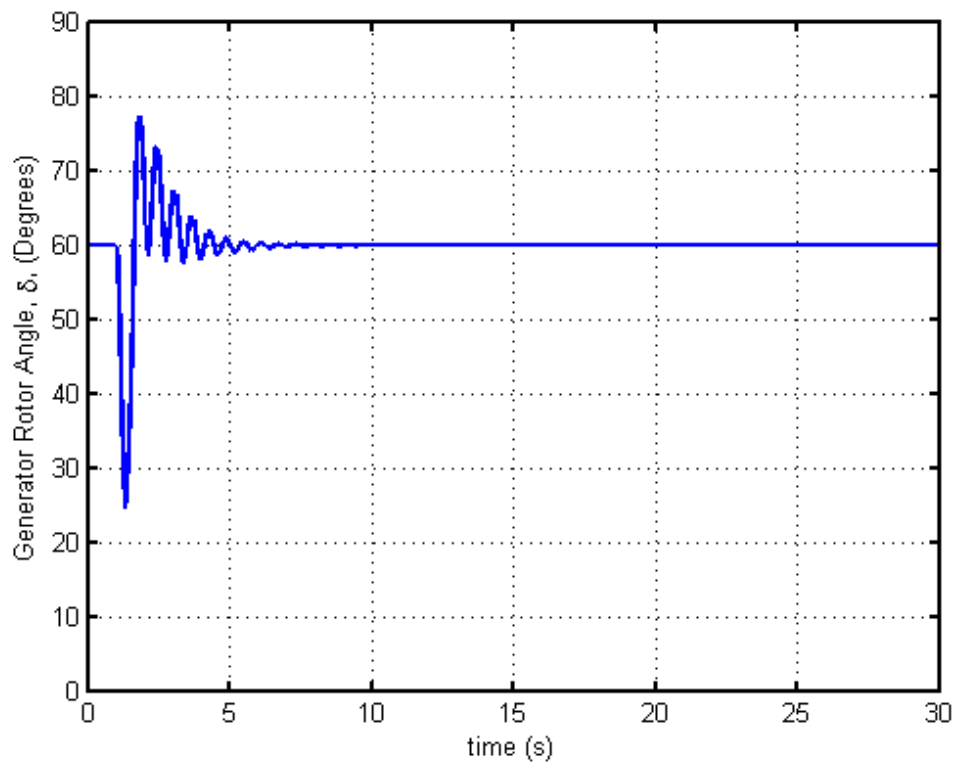


Figure 6.7 : Generator rotor angle with DFC and AVR limiters ($\mu=0.75$)

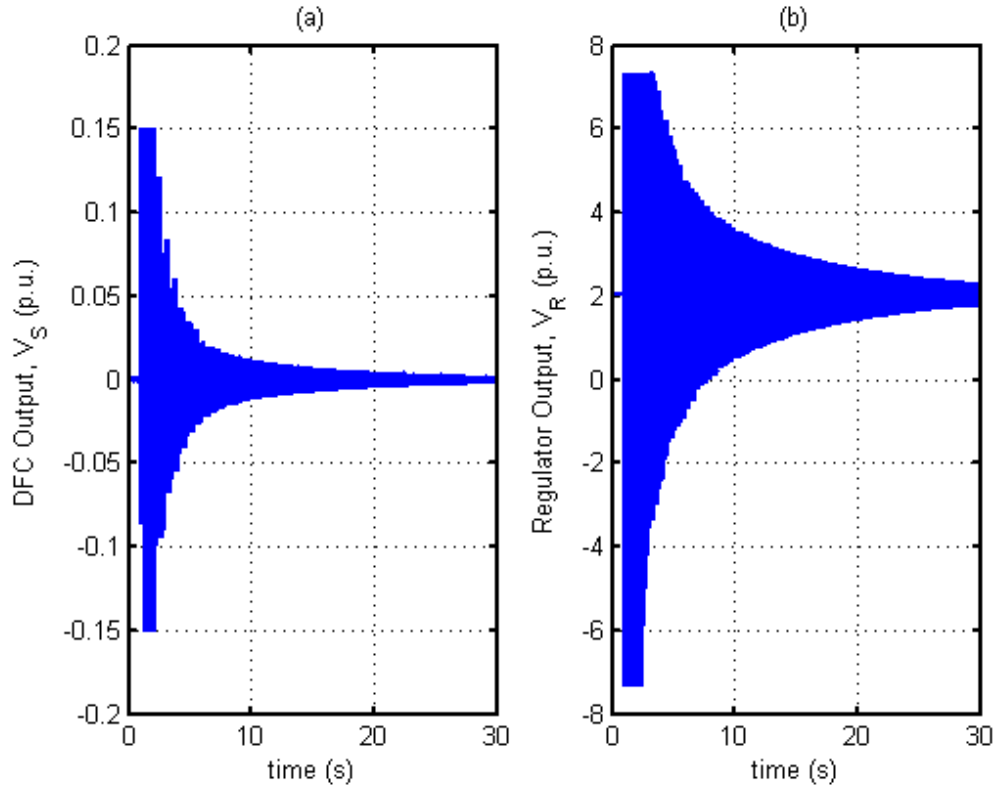


Figure 6.8 : (a) DFC output, V_S and (b) Regulator output, V_R ($\mu=0.75$)

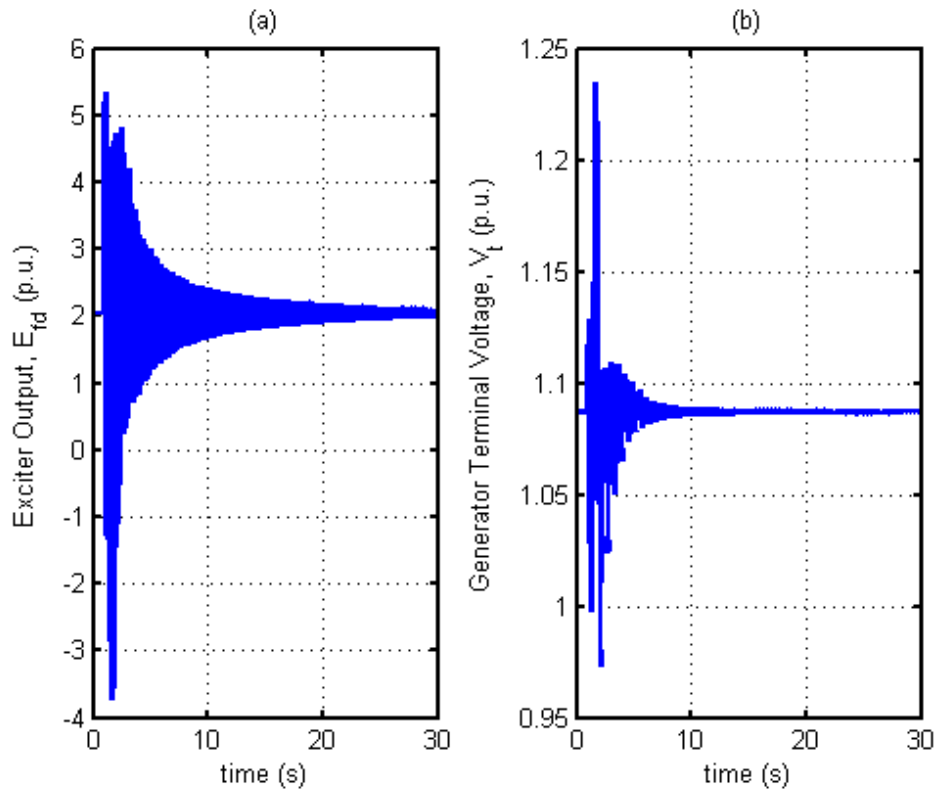


Figure 6.9 : (a) Exciter output, E_{fd} and (b) Terminal voltage, V_t ($\mu=0.75$)

The DFC with limiters does not yield effective performance in stabilizing the subsynchronous oscillations for the case with $\mu=0.85$. Fig. 6.10 shows that the magnitude of generator rotor speed oscillations increases following the disturbance and equilibrium condition is not reached. The reason for ineffective controller performance is that the DFC and AVR limiters become active following the disturbance as shown in Fig. 6.11.

It is thought that the eigenvalue real part of the unstable mode (σ_{uns}) plays an important role on the effectiveness of the DFC. The greater σ_{uns} results in faster increase in the magnitude of the unstable oscillations. In the cases at which the DFC effectively stabilized the unstable modes, $\mu=0.55$ ($\sigma_{\text{uns}}=0.25 \text{ s}^{-1}$) and $\mu=0.75$ ($\sigma_{\text{uns1}}=0.67 \text{ s}^{-1}$ and $\sigma_{\text{uns2}}=0.02 \text{ s}^{-1}$), the value of σ_{uns} is relatively small when compared with the case at which the DFC is not effective, $\mu=0.85$ ($\sigma_{\text{uns}}=1.99 \text{ s}^{-1}$). From the view point of practical operating limits for series capacitors, the compensation factor usually lies between 0.20 and 0.70 [65]. Therefore, the effectiveness of the DFC performance at series compensation levels lower than 80% is considered to be adequate.

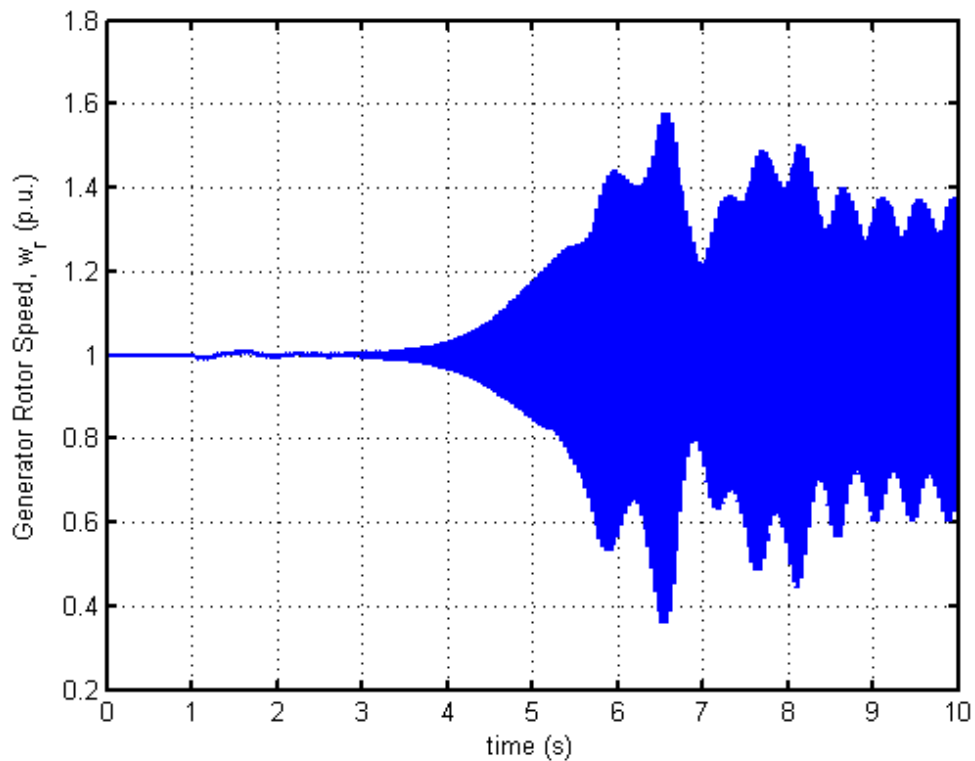


Figure 6.10 : Generator rotor speed with DFC and AVR limiters ($\mu=0.85$)

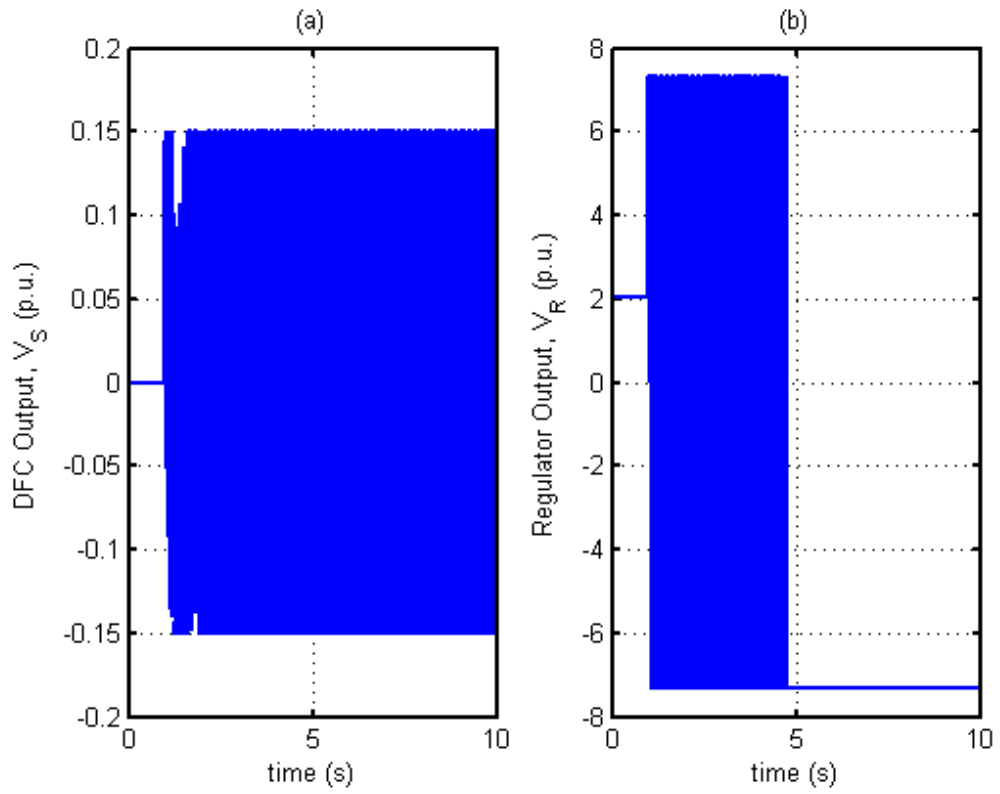


Figure 6.11 : (a) DFC output, V_S and (b) Regulator output, V_R ($\mu=0.85$)

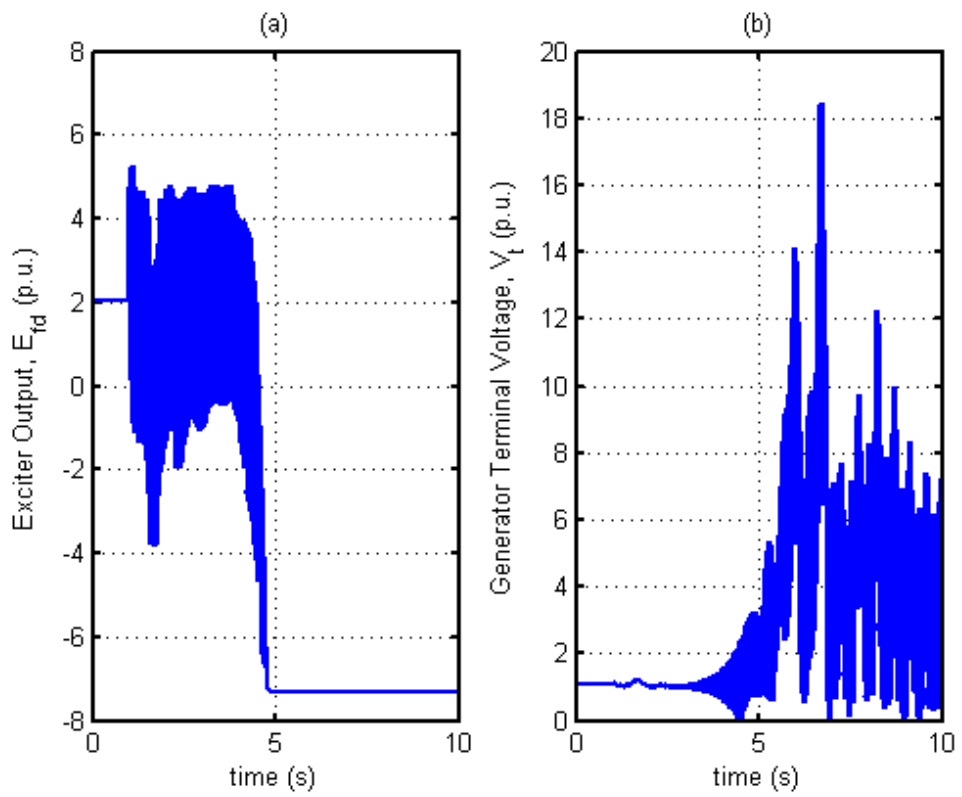


Figure 6.12 : (a) Exciter output and (b) Generator terminal voltage ($\mu=0.85$)

7. CONCLUSION

In this dissertation, Hopf bifurcations in the first system of the IEEE Second Benchmark Model for SSR studies have been analyzed using the bifurcation theory. Damper windings of the synchronous generator have been included in the nonlinear model. The first-order nonlinear autonomous ODEs were obtained to represent the dynamics of the dynamic model. The existence of Hopf bifurcations in the model has been verified. Instead of employing the Floquet theory, we have computed the first Lyapunov coefficients analytically in order to determine whether the Hopf bifurcations are subcritical or supercritical. The compensation factor has been used as the bifurcation parameter.

In the case with constant field voltage, the type of Hopf bifurcations occurring in the nonlinear model is found subcritical. On the other hand, supercritical Hopf bifurcation occurs in the model with AVR. The effects of variations in the mechanical torque input to the generator, network voltage, field current and the AVR gain on the type of Hopf bifurcation and the Hopf bifurcation point have also been investigated. The Hopf bifurcation points Time domain simulations in MATLAB-Simulink have been presented to demonstrate the validity of analytic findings.

In addition, a novel controller based on the delayed feedback control theory for damping the unstable torsional oscillations caused by SSR has been developed. The proposed TDAS controller uses the synchronous generator rotor angular speed signal, an accessible state variable, as the only input. Time domain simulations show that the TDAS controller successfully stabilizes the unstable torsional oscillations provided that the time delay and gain parameters are optimized. An optimization performance index has been defined and the optimum parameters for the time delay and the gain of the TDAS controller have been evaluated. Despite the inclusion of AVR and DFC limiters results in ineffective stabilizing performance at very high compensation levels, the designed controller yields effective performance within the practical range of series compensation levels.

In summary, the following conclusions are made:

- In the IEEE SBM for SSR studies, the Hopf bifurcations occurring in the first and the second torsional mode are subcritical if the excitation system supplies constant field voltage.
- The inclusion of Automatic Voltage Regulator into the excitation system results in supercritical Hopf bifurcations.
- The operating parameters other than the series compensation factor have also impact on the Hopf bifurcation point and the type of Hopf bifurcation.
- The proposed TDAS controller based on the delayed feedback control theory is effective for damping the unstable torsional oscillations due to SSR in the studied model.
- The optimum time delay parameter of the TDAS controller depends on the imaginary part of the eigenvalue of the unstable mode.
- At the practical levels of the series compensation factor (i.e. 0.20-0.75), the proposed TDAS controller yields effective performance even if the AVR limiters are included into the model.
- As the eigenvalue real part of the unstable mode increases, the effectiveness of the TDAS controller decreases.

The major contributions in this dissertation are as follows:

1. Use of the first Lyapunov coefficient in order to determine the type of the Hopf bifurcations in a power system experiencing SSR.
2. Development of a novel controller based on the delayed feedback control theory for the purpose of stabilizing the unstable torsional oscillations due to SSR. The proposed TDAS controller yields an effective performance.
3. Development of an optimization performance index for the evaluation of optimum parameters of the TDAS controller.

The future study based on the contributions in this dissertation should concentrate on the following areas:

1. Improvement of the evaluation procedure for the optimum control parameters of the TDAS controller.
2. Adaptive determination of the TDAS controller optimum parameters depending on various operating conditions.
3. Application of the TDAS controller to the other models for SSR studies (e.g. IEEE First Benchmark Model) and to the power systems with various configurations.
4. Investigation of effectiveness of the TDAS controller in damping local mode oscillations as an alternative to Power System Stabilizers.
5. Application of the TDAS controller to provide additional damping for torsional oscillation modes for mitigating fatigue deformation.
6. Development of an analytic framework to explain the effectiveness of the TDAS controller and identify methods for optimal tuning of the control parameters

REFERENCES

- [1] **IEEE Committee Report**, 1992. Reader's Guide to Subsynchronous Resonance, *IEEE Trans. on Power Systems*, **7**, No. 1, 150-157.
- [2] **Balance J. W. and Goldberg S.**, 1973. Subsynchronous Resonance in Series Compensated Transmission Lines, *IEEE Trans. On PAS*, **92**, 1649-1658.
- [3] **Walker D. N., Bowler C. E., Jackson R. L., and Hodges D. A.**, 1975. Results of Subsynchronous Resonance Test at Mohave, *IEEE Trans. on PAS*, **94**, 1878-1889.
- [4] **Farmer R. G., Katz E. and Schwalb A. L.**, 1977. Navajo Project on Subsynchronous Resonance Analysis and Solutions, *IEEE Trans. on PAS*, **96**, 1226-1232.
- [5] **IEEE Power System Engineering Committee Report**, 1985. Terms, Definitions & Symbols for Subsynchronous Oscillations", *IEEE Trans. on PAS*, **104**, 1326-1334.
- [6] **Kabiri K., Dommel H. W. and Henschel S.**, 2001. A simplified System for Subsynchronous Resonance Studies, *International Conference on Power Systems Transients*, Rio de Janeiro, Brazil, June 24-28.
- [7] **Joyce J. S., Kulig T. and Lambrecht D.**, 1978. Torsional Fatigue of Turbine-Generator Shafts Caused by Different Electrical System Faults and Switching Operations, *IEEE Trans. on Power Apparatus and Systems*, **97**, 1965-1977.
- [8] **IEEE SSR Working Group**, 1977. First Benchmark Model for Computer Simulation of Subsynchronous Resonance, *IEEE Trans. on Power Apparatus and Systems*, **96**, 1565-1572.
- [9] **IEEE SSR Working Group**, 1985. Second Benchmark Model for Computer Simulation of Subsynchronous Resonance, *IEEE Trans. Power Apparatus and Systems*, **104**, 1057-1066.

- [10] **Kilgore L. A., Ramey D. G. and Hall M. C.,** 1977. Simplified transmission and generation system analysis procedures for subsynchronous resonance, *IEEE Transactions on Power Apparatus and Systems*, **96**, 1840-1846.
- [11] **Agrawal B. L. and Farmer R. G.,** 1979. Use of frequency scanning technique for subsynchronous resonance analysis, *IEEE Transactions on Power Apparatus and Systems*, **98**, 341-349.
- [12] **Iravani M. and Edris A.A.,** 1995, Eigen analysis of series compensation schemes reducing the potential subsynchronous resonance, *IEEE Trans., PWRS-10, no.2*, 876-883.
- [13] **Gross G., Imparato C. F. and Look P. M.,** 1982. A tool for the comprehensive analysis of power system dynamic stability, *IEEE Transactions on Power Apparatus and Systems*, **101, no. 1**, 226-234.
- [14] **Canay I. M.,** 1982. A novel approach to the torsional interaction and electrical damping of synchronous machine, part I: Theory, *IEEE Trans. Power Apparatus and Systems*, **101, no. 10**, 3630-3638.
- [15] **Canay I. M.,** 1982. A novel approach to the torsional interaction and electrical damping of synchronous machine, part II: Application to an arbitrary network, *IEEE Trans. Power Apparatus and Systems*, **101, no. 10**, 3639-3647.
- [16] **Lei X., Buchholz B., Lerch E., Povh D. and Retzmann D.,** 2000. A Comprehensive simulation program for subsynchronous resonance analysis, *IEEE PES Summer Meeting*, Seattle, USA, July 16-20, 695-700.
- [17] **Gross G. and Hall M. C.,** 1978. Synchronous Machine and Torsional Dynamics Simulation in the Computation of Electromagnetic Transients, *IEEE Transactions on Power Apparatus and Systems*, **97**, 1074-1085.
- [18] **Zhu W., Mohler R. R., Spee R., Mittelstadt W. A. and Maratukulam,** 1995. An EMTP Study of SSR Mitigation Using the Thyristor Controlled Series Capacitor, *IEEE Transactions on Power Delivery*, **10, No. 3**, 1479-1485.
- [19] **Hingorani N. G.,** 1981. A New Scheme for Subsynchronous Resonance, *IEEE Transactions on Power Systems*, **7, no. 1**, 150-157.

- [20] **Zhao X. and Chen C.**, 1999. Damping Subsynchronous Resonance Using an Improved NGH SSR Damping Scheme, *IEEE PES Summer Meeting*, Edmonton, Canada, Jul 18-22, 780-785.
- [21] **Keshavan, B.K. and Prabhu, N.**, 2001. Damping of subsynchronous oscillations using STATCOM - a FACTS device, *IEEE T&D Conference and Exposition*, Atlanta, USA, Oct 28-Nov 2, 1-7.
- [22] **Padiyar K. R. And Prabhu N.**, 2008. Design and Performance Evaluation of Subsynchronous Damping Controller with STATCOM, *IEEE Transactions on Power Delivery*, **21**, no. 1, 1398-1405.
- [23] **Wang L. And Hsu Y. Y.**, 1988. Damping of Subsynchronous Resonance Using Excitation Controllers and Static VAR Compensators: A Comparative Study, *IEEE Transactions on Energy Conversion*, **3**, no. 1, 6-13.
- [24] **Yan A. and Yu Y.**, 1982. Multi-Mode Stabilization of Torsional Oscillations Using Output Feedback Excitation Control, *IEEE Trans. on PAS*, **101**, 1245-1253.
- [25] **Hsu Y. Y. and Wu C. J.**, 1988. Design of PID Static VAR Controllers for the Damping of Subsynchronous Oscillations, *IEEE Transactions on Energy Conversion*, **3**, no. 2, 210-216.
- [26] **Wang L. and Tseng H. Y.**, 1999. Suppression of Common-Mode Torsional Oscillations of Nonidentical Turbine-Generators Using SMES, *IEEE PES Winter Meeting*, New York, USA, Jan 31-Feb 4, **1**, 117-122.
- [27] **Wang L.**, 1991. Damping of torsional oscillations using excitation control of synchronous generator: the IEEE Second Benchmark Model Investigation, *IEEE Trans. on Energy Conversion*, **6**, No. 1, 47-54.
- [28] **Harb A. M. and Widyan M. S.**, 2002. Controlling Chaos and Bifurcation of Subsynchronous Resonance in Power System, *Nonlinear Analysis: Modeling and Control*, **7**, no. 2, 15-36.
- [29] **Abed E. H. and Varaiya P.**, 1984. Nonlinear Oscillations in Power Systems, *International Journal of Electric Power and Energy Systems*, **6**, no. 1, 373-343.
- [30] **Wang H. O., Abed E. H., and Hamdan A. M. A.**, 1994. Bifurcations, chaos, and crises in voltage collapse of a model power system, *IEEE Transactions on Circuits and Systems – I: Fundamental Theory and Applications*, **41**, 294-302.

- [31] **Rajagopalan C., Sauer P. W., and Pai M. A.**, 1989. Analysis of voltage control systems exhibiting Hopf bifurcation, *IEEE Proceedings of the 28th Conference on Decision and Control*, Tampa, USA, Dec 13-15, pp. 332-335.
- [32] **Ajjarapu V. and Lee B.**, 1992. Bifurcation theory and its application to nonlinear dynamical phenomena in an electrical power system, *IEEE Transactions on Power Systems*, **7**, 424-431.
- [33] **Lerm A. A. P. and Silva A. S.**, 2004. Avoiding Hopf Bifurcations in Power Systems via Set-Points Tuning, *IEEE Transactions of Power Systems*, **19**, no. 2, 1076-1084.
- [34] **Wang S., Crouch P. and Armbruster D.**, 1996. Bifurcation Analysis of Oscillations in Electric Power Systems, *IEEE 35th Conference on Decision and Control*, Kobe, Japan, Dec 11-13, **4**, pp. 3864-3869.
- [35] **Zhu W., Mohler R. R., Spee R., Mittelstadt E. A. and Maratukulam D.**, 1995. Hopf Bifurcations in a SMIB Power System with SSR, *IEEE Transactions on Power Systems*, **11**, no. 3, 1579-1584.
- [36] **Iravani M. R. and Semlyen A.**, 1992. Hopf Bifurcations in Torsional Dynamics, *IEEE Transactions of Power Systems*, **7**, no. 1, 28-36.
- [37] **Harb A. M.**, 1996. Application of Bifurcation Theory to Subsynchronous Resonance in Power Systems, *Ph.D. dissertation*, Dept. Electrical Eng., Virginia Polytechnic Institute and State Univ., Blacksburg.
- [38] **Harb A. M.**, 2000. On the Effect of Machine Saturation on SSR in Power Systems, *Electric Machines and Power Systems*, **28**, 1019-1035.
- [39] **Mitani Y., Tsuji K., Varghese M., Wu F. and Varaiya P.**, 1998. Bifurcations Associated with Sub-Synchronous Resonance, *IEEE Transactions on Power Systems*, **13**, no. 1, 139-144.
- [40] **Kuznetsov Y. A.**, 2004. Elements of Applied Bifurcation Theory, Springer-Verlag, New York.
- [41] **Guckenheimer J. and Kuznetsov Y. A.**, 2008. Bautin bifurcation [Online]. Available: http://www.scholarpedia.org/article/Bautin_bifurcation
- [42] **Kucukefe Y. and Kaypmaz A.**, 2008. Hopf bifurcations in the IEEE Second Benchmark Model for SSR Studies, *16th Power Systems Computations Conference*, Glasgow, United Kingdom, July 14-18.

- [43] **Pyragas K.**, 1992. Continuous control of chaos by self-controlling feedback, *Physics Letters A*, **170**, 421-428.
- [44] **Pyragas K., Pyragas V. and Benner H.**, 2004. Delayed feedback control of dynamical systems at a subcritical Hopf bifurcation, *Physical Review E*, **70**, 056222.
- [45] **Ahlborn A. and Parlitz U.**, 2004. Stabilizing Unstable Steady States using Multiple Delay Feedback Control, *Physical Review Letters*, **93**, 264101.
- [46] **Dahms T., Hövel P. and Schöll E.**, 2007. Control of unstable steady states by extended time-delayed feedback, *Physical Review E*, **76**, 056201.
- [47] **Hikihara T. and Kawagoshi T.**, 1996. An experimental study on stabilization of unstable periodic motion in magneto-elastic chaos, *Physics Letters A*, **211**, 29-36.
- [48] **Guderian A., Munster A. F., Kraus M. and Schneider F. W.**, 1998, Electrochemical Chaos Control in a Chemical Reaction: Experiment and Simulation, *Journal of Physical Chemistry A*, **102**, 5059-5064.
- [49] **Krodkiewski J. M. and Faragher J. S.**, 2000, Stabilisation of motion of helicopter blades using delay feedback – Modelling, computer simulation and experimental verification, *Journal of Sound and Vibration*, **234**, 591-610.
- [50] **Hall K., Christini D. J., Tremblay M., Collins J. J., Glass L. and Billette J.**, 1997, Dynamic control of cardiac alternans, *Physical Review Letters*, **78**, 4518-4521.
- [51] **Olgac N., Sipahi R., and Ergenc A. F.**, 2004. Feedback time delay as a stabilizing tool in trajectory tracking, analysis and Experiments, *Proceedings of the 2004 American Control Conference*, Boston, USA, June 30 – July 2, pp. 5443-5448.
- [52] **Olgac N. and Holm-Hansen B.**, 1995. Design considerations for Delayed-Resonator Vibration Absorbers, *J Eng Mech-ASCE*, **121**, no. 1, 80-89.
- [53] **Drazin P. G.**, 1992. *Nonlinear Systems*, Cambridge University Press, Cambridge.
- [54] **Seydel R.**, 1994. *Practical Bifurcation and Stability Analysis, From Equilibrium to Chaos*, Springer-Verlag, New York.

- [55] **Kale J. K. and Koçak H.**, 1991. Dynamics and Bifurcations, Springer-Verlag, New York.
- [56] **Hamzi B., Kang W. and Krener A. J.**, 2005. The Controlled Center Dynamics, *Multiscale Model. Simul.*, **3**, no. 4, 838-852
- [57] **Sotomayor J., Mello L. F. and Braga D. C.**, 2007. Bifurcation analysis of the Watt governor system, *Computational & Applied Mathematics*, **26**, 19-44
- [58] **Govaerts W. and Kuznetsov A.**, 2007. Continuation Software in Matlab: MatCont, [Online], Available: <http://www.matcont.ugent.be>
- [59] **Anderson P. M., Agrawal B. L. and Van Ness J. E.**, 1990. Subsynchronous Resonance in Power Systems, IEEE Press, New York.
- [60] **Yu Y.**, 1983. Electric Power System Dynamics, Academic Press, New York.
- [61] **Krause P. C.**, 1986. Analysis of Electric Machinery, McGraw-Hill, New York
- [62] **Harb A. M. and Widyan M.S.**, 2004, Chaos and bifurcation control of SSR in the IEEE second benchmark model, *Chaos Solitons and Fractals*, **21**, 537-552.
- [63] **Kundur P.**, 1994. Power System Stability and Control, McGraw-Hill, New York.
- [64] **IEEE Standard 421.5**, 1992. *Recommended Practice for Excitation System Models for Power System Stability Studies*, New York.
- [65] **Grünbaum R., Halvarsson B. and Wilk-Wilczynski A.**, 1999, FACTS and HVDC LIGHT for Power System Interconnections, *Power Delivery Conference*, Madrid, Spain, September 1999.

APPENDICES

APPENDIX A.1 : Calculation of p and q Complex Vectors, Extracted from [58]

APPENDIX A.1

Calculation of p and q Complex Vectors

Define \mathbf{V}_q and \mathbf{D}_q as the eigenvectors matrix and the eigenvalue matrix of the Jacobian matrix ($\mathbf{J}_{n \times n}$) at the Hopf bifurcation point so that $\mathbf{J} * \mathbf{V}_q = \mathbf{V}_q * \mathbf{D}_q$. Matrix \mathbf{V}_q is the modal matrix - its columns are the eigenvectors of \mathbf{J} . Matrix \mathbf{D}_q is the canonical form of \mathbf{J} - a diagonal matrix with \mathbf{J} 's eigenvalues on the main diagonal.

Let i_{Hq} denote the eigenvalue index with $real(\lambda_{iHq}) = 0$ and $imag(\lambda_{iHq})$ of the eigenvalues of \mathbf{J} . Orthogonal-triangular decomposition of the real and imaginary vector of $\mathbf{V}_{j,iHq}$, where $j=1,2,\dots,n$, gives the unitary matrix \mathbf{Q}_q .

Define also \mathbf{V}_p and \mathbf{D}_p as the eigenvectors matrix and the eigenvalue matrix of $\mathbf{J}^T_{n \times n}$ at the Hopf bifurcation point so that $\mathbf{J}^T \mathbf{V}_p = \mathbf{V}_p \mathbf{D}_p$. Matrix \mathbf{V}_p is the modal matrix - its columns are the eigenvectors of \mathbf{J}^T . Matrix \mathbf{D}_p is the canonical form of \mathbf{J}^T - a diagonal matrix with \mathbf{J}^T 's eigenvalues on the main diagonal.

Let i_{Hp} denote the eigenvalue index with $real(\lambda_{iHp}) = 0$ and $imag(\lambda_{iHp}) = w_0$, $w_0 > 0$, of the eigenvalues of \mathbf{J}^T . Orthogonal-triangular decomposition of the real and imaginary vector of $\mathbf{V}_{j,iHp}$, where $j=1,2,\dots,n$, gives the unitary matrix \mathbf{Q}_p .

$$\mathbf{R} = \mathbf{J} * \mathbf{J} + w_0^2 * \mathbf{I}_{2 \times 2} \quad (\text{A.1})$$

$$\mathbf{V} = \begin{bmatrix} \mathbf{R} & \mathbf{Q}_p \\ \mathbf{Q}_q^T & \mathbf{0}_{2 \times 2} \end{bmatrix}^{-1} \begin{bmatrix} \mathbf{0}_{n \times 2} & \mathbf{I}_{2 \times 2} \end{bmatrix} \quad (\text{A.2})$$

$$\mathbf{W} = \begin{bmatrix} \mathbf{R} & \mathbf{Q}_p \\ \mathbf{Q}_q^T & \mathbf{0}_{2 \times 2} \end{bmatrix}^{T^{-1}} \begin{bmatrix} \mathbf{0}_{n \times 2} & \mathbf{I}_{2 \times 2} \end{bmatrix} \quad (\text{A.3})$$

$$\mathbf{A}_q = \mathbf{V}_{1:n,1}^T * \mathbf{J} * \mathbf{V}_{1:n,2} - i\omega_0 \mathbf{V}_{1:n,1}^T * \mathbf{V}_{1:n,2} \quad (\text{A.4})$$

$$\mathbf{B}_q = -\mathbf{V}_{1:n,1}^T * \mathbf{J} * \mathbf{V}_{1:n,2} + i\omega_0 \mathbf{V}_{1:n,1}^T * \mathbf{V}_{1:n,2} \quad (\text{A.5})$$

$$\mathbf{A}_p = \mathbf{W}_{1:n,1}^T * \mathbf{J}^T * \mathbf{W}_{1:n,2} + i\omega_0 \mathbf{W}_{1:n,1}^T * \mathbf{W}_{1:n,2} \quad (\text{A.6})$$

$$\mathbf{B}_p = -\mathbf{W}_{1:n,1}^T * \mathbf{J}^T * \mathbf{W}_{1:n,2} - i\omega_0 \mathbf{W}_{1:n,1}^T * \mathbf{W}_{1:n,2} \quad (\text{A.7})$$

$$\mathbf{q}_0 = \mathbf{A}_q * \mathbf{V}_{1:n,1} + \mathbf{B}_q * \mathbf{V}_{1:n,2} \quad (\text{A.8})$$

$$\mathbf{p}_0 = \mathbf{A}_p * \mathbf{W}_{1:n,1} + \mathbf{B}_p * \mathbf{W}_{1:n,2} \quad (\text{A.9})$$

Finally, normalization of \mathbf{q}_0 and \mathbf{p}_0 gives p and q :

$$\mathbf{q} = \frac{\mathbf{q}_0}{(\sum_i^n (q_{0i})^2)^{1/2}} \quad (\text{A.10})$$

$$\mathbf{p} = \frac{\mathbf{p}_0}{(\mathbf{q}^T * \mathbf{p}_0)} \quad (\text{A.11})$$

CURRICULUM VITAE



Full name: Yaşar KÜÇÜKEFE
Place and date of birth: 23.08.1971
Permanent Address: Emlak Konutları, Sardunya-1 Apt. Daire:23 Çorlu-
Tekirdağ

**Universities and
Colleges attended:** Middle East Technical University
Balıkesir Cumhuriyet Lisesi

Publications:

- **Kucukefe Y.** and Kaypmaz A., 2008: Hopf bifurcations in the IEEE Second Benchmark Model for SSR Studies, *16th Power Systems Computations Conference*, July 14-18, 2008 Glasgow, United Kingdom.
- **Kucukefe Y.** and Kaypmaz A., 2008: Bir Tam Taşıt Modelinin Zaman Gecikmeli Geribesleme Kontrolü ile Aktif Süspansiyonu, *Otomatik Kontrol Türk Milli Komitesi, Otomatik Kontrol Ulusal Toplantısı*, November 13-15, 2008 İstanbul, Turkey.
- **Kucukefe Y.** and Kaypmaz A., 2009: Delayed Feedback Control as Applied to Active Suspension of a Ground Vehicle, *IEEE Region-8 EUROCON Conference*, May 18-23, 2009 St. Petersburg, Russia.